

https://dspace.org/

The effect of various chemical modifications on the physicomechanical properties of 3D bioprinted scaffolds for tissue engineering

Parak, Azraa

2020

https://hdl.handle.net/10539/30424

Parak, Azraa (2019) The effect of various chemical modifications on the physicomechanical properties of 3-D bioprinted scaffolds for tissue engineering, University of the Witwatersrand, Johannesburg, <http://hdl.handle.net/10539/30424>

Downloaded from a DSpace repository. https://dspace.org/

THE EFFECT OF VARIOUS CHEMICAL MODIFICATIONS ON THE PHYSICOMECHANICAL PROPERTIES OF 3D BIOPRINTED SCAFFOLDS FOR TISSUE ENGINEERING

AZRAA PARAK

A dissertation submitted to the Faculty of Health Sciences,
University of the Witwatersrand,
in fulfillment of the requirements for the degree of
Master of Pharmacy

Supervisor:
Professor Viness Pillay
University of the Witwatersrand
Department of Pharmacy and Pharmacology
South Africa

Co-Supervisors:
Professor Yahya.E Choonara; University of the Witwatersrand,
Department of Pharmacy and Pharmacology, South Africa

Associate Professor Lisa.C du Toit: University of the Witwatersrand,
Department of Pharmacy and Pharmacology, South Africa

Associate Professor Pradeep Kumar: University of the Witwatersrand,
Department of Pharmacy and Pharmacology, South Africa

Johannesburg, 2019

DECLARATION

I, Azraa Parak, declare that this dissertation is my own work. It is being submitted for the degree of Master of Pharmacy in the Faculty of Health Sciences in the University of the Witwatersrand, Johannesburg.

It has not been submitted before for any degree or examination at this or any other University.

……

This…….day of ……. 2019

RESEARCH OUTPUTS

Azraa Parak, Priyamvada Pradeep, Lisa C. du Toit, Pradeep Kumar, Yahya E. Choonara, Viness Pillay, *Functionalizing bioinks for 3D bioprinting applications*, Drug Discovery Today, 2019, 24:1, 198-205.

ANIMAL ETHICS DECLARATION

I hereby confirm that the following study entitled "**Evaluation of the *in vivo* biodegradability of 3D printed biomaterial scaffolds in a rat model**" had received the approval from the Animal Research Ethics Committee of the University of the Witwatersrand with ethics clearance number 2018/09/44/B (Appendix).

ABSTRACT

The realm of tissue engineering has been modernized by 3D bioprinting. The efficacy of 3D bioprinting is limited, however, by the lack of available biomaterials which fulfill all the criteria required to be printed adequately (bioinks) and still produce constructs that align themselves with necessary scaffold requirements for use are engineered tissue. Its efficacy is thus also limited - in terms of clinical applicability - by the suboptimal properties of printed constructs, when compared to their biological counterparts. This project aimed to overcome these challenges by conceptualizing post-processing of 3D bioprinted structures in the form of post-printing chemical modifications which have been proposed to alter the mechanical properties of already printed structures. This could potentially improve the applicability of already available bioinks which are ideal for 3D printing processes, but lack adequate mechanical properties. The resultant alteration of these mechanical properties improves upon the concept of 'customizable scaffolds' and would allow for tunable mechanical properties of already available bioinks and their subsequently printed constructs. This idea of customizable scaffolds would potentially combat the lack of ideal bioinks, as printable bioinks could now be tuned for a variety of clinical applications. We also assess the efficacy of a novel bioink combination in the printing process and quantify the properties of its printed construct. Poly (3-hydroxybutyric acid-co-3-hydroxyvaleric acid) (PHBV) was used in combination with Cellulose Acetate Phthalate (CAP) as a bioink. Propylene carbonate and glycerol were incorporated into the formulation and evaluated for their effects as plasticizers. We then evaluated the effects of chemical surface modifications - in the form of aminolysis and hydrolysis - on mechanical properties, in order to introduce a new concept of post-printing modification as a method of inducing and/or exploiting desirable properties in printed constructs. Characterization of the bioink as well as the scaffolds were undertaken via Fourier Transform Infrared Spectroscopy, Differential Scanning Calorimetry, Scanning Electron Microscopy, and biomechanical testing. In vivo studies were performed to assess the biocompatibility and biodegradation of the produced and modified scaffolds, as well as the tissue response to these scaffolds. The scaffold was successfully printed and characterized, with the addition of propylene carbonate improving the printing process and improving the Young's modulus of the construct as well as its degradation behaviour, and with the chemical modifications successfully altering the mechanical properties of the scaffolds, thus proving that constructs can be tailored post-printing in order to alter various properties and subsequently improve the variability in potential clinical applications. This investigation ultimately highlighted the success of post-processing in the form of chemical modifications to alter mechanical properties of already printed constructs, as well as evaluated the success of PHBV/CAP as a novel bioink combination.

ACKNOWLEDGMENTS

In the name of the Almighty, the most Beneficent, the most Merciful.

Without faith and guidance, none of this would have been possible.

To my mother, Soraiya Moola, for being my pillar of strength in the hardest of times, and my most vivacious cheerleader in the best of times. Thank you for always encouraging me to strive for more, and for always leading by example. To my father, Suleman Parak, for teaching me the value of hard work and perseverance. Thank-you both for your sacrifices, your unconditional love, and your unwavering support. I will never truly be able to express my gratitude.

To my brother, Uzayr Parak, for never allowing me to see giving up as an option. Thank you for your guidance, your unwavering faith that I would succeed, and for believing in me. You have, and always will be, my role model. To my new sister, Tasneem Mahomed, thank-you for your kind words, encouragement and unfailing support.

I would like to express my gratitude to Professor Viness Pillay, Professor Yahya Choonara, Professor Pradeep Kumar, Professor Lisa du Toit, and Dr. Thashree Marimuthu for their guidance, encouragement and useful critique to this research work.

To my incredible colleagues; for the laughter, the ‘corridor chats’, and the constant encouragement. You are all truly phenomenal people, and I am so excited to see where life takes you.

To the technical staff; Mr. Sello Ramarumo, Mr. Kleinbooi Mohlabi and Mr. Bafana Temba. Thank you for always assisting with the procurement of chemicals and technical support.

To Sister Mary Ann Costello, Sister Amelia Rammekwa, Dr Kim Jardine and rest of the team at the Central Animal Services for their invaluable assistance, and willingness to always accommodate me.

This was not an easy journey. It was filled with ups and downs, tears of both joy and frustration. But it has been worth it; I have learnt that in order to truly succeed, one cannot fear failure.

“The greatest glory of living lies not in never falling, but in rising every time you fall.”

~Nelson Mandela

DEDICATION

This work is dedicated to my parents and my brother.

All that I am today is because of you.

I love you.

Table of Contents

DECLARATION ii

RESEARCH OUTPUTS iii

ANIMAL ETHICS DECLARATION iv

ABSTRACT v

ACKNOWLEDGMENTS vi

DEDICATION viii

LIST OF FIGURES xvii

LIST OF TABLES xx

CHAPTER 1

INTRODUCTION AND BACKGROUND

1.1 Background to the Study 1

1.2 Rationale and Motivation for this Study 2

1.3 Factors to Consider in 3D Bioprinting for Tissue Engineering 4

1.3.1 Biological Considerations in Tissue Engineering 4

1.3.2 Mechanical Specifications for 3D Bioprinting 5

1.3.3 Printing Compatibility of Materials for Use in Bioprinting 7

1.4 Novelty of this Study 7

1.5 Aim and Objectives 8

Synopsis of Dissertation 9

References 10

CHAPTER 2

REVIEW OF BIOPRINTING, METHODS OF FUNCTIONALIZATION AND METHODS OF TUNABILITY

2.1 Introduction 12

2.2 Materials Used as Bioinks 14

2.2.1 Natural Polymers 16
2.2.2 Synthetic Polymers 17

2.3 3D Bioprinting for Tissue Engineering 19

2.3.1 Types of 3D bioprinting 19

2.4 Scaffolds in Tissue Engineering 22

2.5 Functionalization of Scaffolds for Optimal Properties 23

2.5.1 Functionalization for Improving Mechanical Integrity 24
2.5.2 Functionalization for Improving Printability 29
2.5.3 Functionalization for Enhancing Biocompatibility and Bioactivity 31

2.6 Methods of Tunability of 3D Printing Process 34

2.6.1 Altering Temperature 35
2.6.2 Altering Concentration 37

2.7 Concluding Remarks 39

References 40

CHAPTER 3

IDENTIFYING APPROPRIATE MATERIALS AND OPTIMISING THE BIOINK FORMULATION

3.1 Introduction 46

3.2 Evaluating Various Polymers for their Potential Use as Bioinks 46

3.2.1 Materials and Methods 46

3.2.2 Evaluation of Potential Polymers for Bioink Consideration 47

3.2.2.1 Poly (2-hydroxyethyl methacrylate) (pHEMA) 47

3.2.2.2 Poly (3-hydroxybutyric acid-co-3-hydroxyvaleric acid) (PHBV) 47

3.2.3 Effect of Combination of Polymers 48

3.2.3.1 Hydroxypropyl Cellulose (HPC) 49

3.2.3.2 Cellulose Acetate Phthalate (CAP) 49

3.2.3.3 Effects of Concentration 49

3.2.4 Effect of Plasticizers 51

3.2.4.1 Triethyl Citrate (TEC) 51

3.2.4.2 Propylene Carbonate (PC) 51

3.2.4.3 Glycerol 52

3.3 Preparation of the PHBV-CAP Bioink 52

3.3.1 Materials and Methods 53

3.3.1.1 Materials 53

3.3.1.2 Synthesis of the Novel PHBV-CAP bioink 53

3.3.1.3 Viscoelastic Assessment of the Bioinks 53

3.3.1.4 Blueprinting and Manufacture of the 3D Bioprinted Scaffolds Using the PHBV-CAP Bioink 54

3.3.1.5 Determination of the Chemical Transitions within the 3D-Bioprinted Scaffolds. 54

3.3.1.6 Thermal Characterization of the 3D-Bioprinted Scaffolds 54

3.3.1.7 Mapping of the Surface Morphology of the 3D-Bioprinted Scaffolds 55

3.3.1.8 Determination of the Mechanical Properties of the 3D-Bioprinted Scaffolds 55

3.3.1.9 Comparative Biodegradation Rate Analysis of the 3D-Bioprinted scaffolds 56

3.4 Results and Discussion 57

3.4.1 Manufacturing of the 3D Bioprinted Scaffolds using the 3D Bioplotter.....57
3.4.2 Physicomechanical Analysis of the Bioink.....59
3.4.3 Chemical Transitions of Bioprinted Scaffolds.....62
3.4.4 Thermal Characteristics of Bioprinted Scaffold as well as Native Materials.....65
3.4.5 Surface Morphology Mapping of 3D Bioprinted Scaffolds.....67
3.4.6 Mechanical Properties of 3D Bioprinted Scaffolds.....68
3.4.7 *In Vitro Degradation Behaviour of the Produced Scaffolds*.....72

3.5 Concluding Remarks.....74

References.....76

CHAPTER 4

POST-PRINTING CHEMICAL FUNCTIONALIZATION OF SCAFFOLDS AND SUBSEQUENT ANALYSIS

4.1 Introduction 79

4.2 Preliminary Formulation Design 81

4.2.1 Materials and Methods 81

4.2.1.1 Materials 81

4.2.1.2 Post-Printing Chemical Functionalization and Subsequent Biomacromolecular Attachment 81

4.2.1.3 Chemical Transitions of Chemically Modified 3D Bioprinted Scaffolds and Chemically Modified 3D Bioprinted Scaffolds with Biomacromolecular Attachment 82

4.2.1.4 Thermal Characteristics of Chemically Modified 3D Bioprinted Scaffolds 82

4.2.1.5 Mapping of Surface Morphology of Chemically Modified 3D Bioprinted Scaffolds 83

4.2.1.6 Evaluation of the Mechanical Strength of Chemically Modified 3D Bioprinted Scaffolds 83

4.2.1.7 Comparative Biodegradation Rate Analysis of the Chemically Modified 3D-Bioprinted Scaffolds 84

4.3 Results 85

4.3.1 Aminolysis Chemical Functionalization 85

4.3.1.1 Chemical Transitions Associated with Aminolysed 3D Bioprinted Scaffolds 85

4.3.1.2 Thermal Transitions Associated with Aminolysed 3D Bioprinted Scaffolds 87

4.3.1.3 Evaluation of Mechanical Properties of Aminolysed 3D Bioprinted Scaffolds 89

4.3.1.4 Mapping of Surface Morphology of Aminolysed 3D Bioprinted Scaffolds 91

4.2.1.5 Evaluation of Biodegradation Behaviour of Aminolysed 3D Bioprinted Scaffolds 92

4.3.2 Hydrolysis Functionalization 95

4.3.2.1 Chemical Transitions Associated with Hydrolysed 3D Bioprinted Scaffolds 95

4.3.2.2 Thermal Transitions Associated with Hydrolysed 3D Bioprinted Scaffolds 96

4.3.2.3 Evaluation of Mechanical Properties of Hydrolysed 3D Bioprinted Scaffolds 97

4.3.2.4 Mapping of Surface Morphology of Hydrolysed 3D Bioprinted Scaffolds 101

4.3.2.5 Evaluation of Biodegradation Behaviour of Hydrolysed 3D Bioprinted Scaffolds 102

4.3.3 Biomacromolecular Attachment 106

4.3.3.1 Chemical Transitions of Chemically Modified 3D Bioprinted Scaffolds with Biomacromolecular Attachment 106

4.4 Concluding Remarks 110

References 112

CHAPTER 5

THE *IN VIVO* ASSESSMENT OF BIODEGRADATION BEHAVIOUR AND IMMUNE RESPONSE OF THE SCAFFOLDS IN A RAT MODEL

5.1 Introduction 114

5.1.1 Selection of Appropriate Animal Model for In Vivo Studies 114

5.2 Materials and Methods 115

5.2.1 Preparation of 3D Bioprinted Scaffold for In Vivo Implantation 115

5.2.2 Surgical Protocol for Implanting Scaffolds into Rat Model 115

5.3 Results and Discussion 118

5.3.1 Surgical procedure of Implanting the Scaffolds in the Rat Model 118

5.3.2 In Vivo Analysis 118

5.3.2.1 Biodegradation Behaviour Assessed *In Vivo* 118

5.3.2.2 Tissue Immune Response of the Animal Model to the Scaffold Implantation 119

5.4 Concluding Remarks 130

References 131

CHAPTER 6

CONCLUSIONS AND RECOMMENDATIONS

6.1 Conclusions 132

6.2 Recommendations 135

LIST OF FIGURES

Figure 1.1 Schematic concept of three types of scaffold modification with various molecular attachments, employing a polycaprolactone (PCL) scaffold as an example; (a) Type 1 modification: Aminolysis of the PCL scaffold and subsequent chitosan attachment. (b) Type 2 modification: Hydrolysis of the PCL scaffold and subsequent chitosan attachment. (c) Type 3 modification: The PCL scaffold was alkynylated by aminolysis and subsequently grafted with zwitterionic PCBMA-N_3 (Adapted from (Li *et al.*, 2013, De Luca *et al.*, 2014)) 4

Figure 2.1 Various common bioprinting techniques: a) Extrusion-based bioprinting, b) droplet-based bioprinting, c) laser-based bioprinting. [Ref. (Datta *et al.*, 2018); Reproduced with permission from Elsevier B.V. Ltd. © 2018]. 20

Figure 2.2 Schematic summary of various methods of functionalization 23

Figure 2.3 Schematic illustration of a two-step crosslinking mechanism that applies concurrent crosslinking of vitamin B2-induced covalent crosslinking and thermal crosslinking [Ref. (Jang *et al*., 2016); Reproduced with permission from Elsevier B.V. Ltd. © 2016] 27

Figure 3.1 Visual depiction of the difference in fabricated scaffolds which were printed a) onto a metal platform versus b) into a petri dish filled with deionized water placed on the metal platform 58

Figure 3.2 a) Graphical depiction of the change in tan d in plasticized compared to non-plasticized scaffolds as a function of temperature b) Graphical depiction of the change in shear storage modulus in plasticized scaffolds compared to non-plasticized scaffolds as a function of temperature 60

Figure 3.3 a) FTIR spectra and chemical structures of the native materials (PHBV and CAP), b) FTIR spectra of the two plasticized PHBV-CAP (PC-PC, PC-G) as well as the non-plasticized PHBV-CAP (PC) 63

Figure 3.4 Diagrams illustrating production of proposed blends a) PHBV-CAP (PC), b) PHBV-CAP-Propylene Carbonate (PC-PC), c) PHBV-CAP-Glycerol (PC-G) 65

Figure 3.5 DSC Thermograms showing the behaviour of a) native materials b) non-plasticized scaffolds compared to the plasticized scaffold 66

Figure 3.6 SEM images of (a): PC, (b): PC-G, (c): PC-PC (magnification for all: x65) 68

Figure 3.7 A stress-strain curve comparing the tensile properties of plasticized scaffolds to the non-plasticized scaffold 69

Figure 3.8 A stress-strain curve comparing the compression properties of plasticized scaffolds to the non-plasticized scaffold 69

Figure 3.9 *In vitro* degradation behaviour of plasticized scaffolds (PC-PC, PC-G) vs. the non-plasticized scaffold (PC).....72

Figure 3.10 *In vitro* degradation rate of plasticized scaffolds (PC-PC, PC-G) vs. the non-plasticized scaffold (PC).....73

Figure 4.1 FTIR spectra showing the change in chemical structure due to the functionalization of the scaffold through aminolysis.....86

Figure 4.2 Diagram depicting the proposed reaction and chemical structure of the amine-modified scaffold.....87

Figure 4.3 DSC thermogram showing the effect of aminolysis based functionalization on the thermal transitions of the scaffold.....88

Figure 4.4 A stress-strain curve comparing the tensile properties of an amine-functionalized scaffold (PCP-NH_2) to that of PC-PC.....89

Figure 4.5 A stress-strain curve comparing the compression properties of amine-functionalized scaffolds (PCP-NH_2) when compared to the previously characterized PC-PC.....90

Figure 4.6 SEM image of scaffold post-aminolysis functionalization (mag: 65x).....91

Figure 4.7 Graphical representation of the degradation behaviour of amine-functionalized scaffolds when compared to PC-PC scaffolds.....93

Figure 4.8 Graphical representation of the degradation rate of amine-functionalized scaffolds when compared to PC-PC scaffolds, using dry mass ratio.....94

Figure 4.9 FTIR spectra showing the change in chemical structure due to the functionalization of the scaffold through hydrolysis.....95

Figure 4.10 Diagram depicting the proposed reaction and chemical structure of the hydrolysis-modified scaffold.....96

Figure 4.11 DSC thermogram showing the effect of hydrolysis-based functionalization on the thermal behaviour of the scaffold.....97

Figure 4.12 A stress-strain curve comparing the tensile properties of a hydroxy-functionalized scaffold (PCP-OH) to that of previously characterized PC-PC.....98

Figure 4.13 A stress-strain curve comparing the compression properties of hydroxy-functionalized scaffolds (PCP-OH) when compared to the previously characterized PC-PC.....99

Figure 4.14 Graphs comparing the a) tensile properties of PC-PC, PCP-NH_2 and PCP-OH, b) the compressive properties of PC-PC, PCP-NH_2 and PCP-OH.....100

Figure 4.15 SEM image showing the change in structure and morphology of the scaffold post-hydrolysis functionalization (mag: 65x).....102

Figure 4.16 Graphical comparison of the degradation behaviour of hydroxy-functionalized scaffolds to PC-PC scaffolds.....103

Figure 4.17 Graph comparing the degradation behaviours of PC-PC, PCP-NH_2 and PCP-OH104

Figure 4.18 Graphical representation of the degradation rate of hydroxy-functionalized scaffolds when compared to PC-PC scaffolds, using dry mass ratio 105

Figure 4.19 Graph comparing the degradation rate of PC-PC, PCP-NH_2 and PCP-OH.....106

Figure 4.20 FTIR spectra showing the effect of hyaluronic acid grafting onto the PCP-NH_2 backbone 107

Figure 4.21 Diagram depicting the chemical reaction and proposed structure of PCP-NH_2 modified with hyaluronic acid.....109

Figure 4.22 The effect of hyaluronic acid grafting onto the PCP-OH backbone 109

Figure 4.23 Diagram depicting the reaction and proposed chemical structure of PCP-OH modified with hyaluronic acid.....111

Figure 5.1 Flow chart showing the surgical procedure used to conduct *in vivo* studies.....119

Figure 5.2 Immunohistological images showing the two-day immune response displayed during *in vivo* studies in response to implantation of various scaffold types a) (i-iii) PCP-OH, b) (i-iii) PCP-NH_2, c) (i-iii) PC-PC (magnification for all: x10).....125

Figure 5.3 Images showing the immunohistological analysis of two scaffold types, after a two-day *in vivo* implantation period a) PCP-N H_2, b) PC-PC (magnification for both: x10).....126

Figure 5.4 Immunohistological images showing the seven-day immune response displayed during *in vivo* studies in response to implantation of various scaffold types a) (i-iii) PCP-OH, b) (i-iii) PCP-NH_2, c) (i-iii) PC-PC (magnification for all: x10).....128

Figure 5.5 Immunohistological images showing the two-day immune response towards sham surgeries which were used as a control, wherein surgical interventions were conducted, but no scaffold was implanted (magnification: x4) 129

Figure 5.6 Immunohistological images showing the seven-day immune response towards sham surgeries which were used as a control, wherein surgical interventions were conducted, but no scaffold was implanted (magnification: x4) 130

LIST OF TABLES

Table 2.1 Materials commonly used in bioinks 14

Table 2.2 Comparison of the advantages and disadvantages of commonly used bioprinting methods 21

Table 3.1 Evaluation of PHBV as a potential bioink for 3D Bioprinting 48

Table 3.2 Printability of various polymers in various concentrations 50

Table 3.3 Summary of 3D-Bioprinting parameter setting used to manufacture the scaffolds 57

Table 3.4 Potential clinical applications for the scaffolds as per their elastic modulus found in literature 71

Table 4.1 Potential clinical applications for the amine-modified scaffolds as per their elastic modulus found in literature 91

Table 4.2 Potential clinical applications for the amine-modified scaffolds as per their elastic modulus found in literature 101

Table 4.3 Band assignments for the spectra of Figure 4.20 and componential categorization. 108

Table 4.4 Table elaborating on various bonds found in Figure 4.14 and componential categorization 110

Table 5.1 Visual depiction of the macroscopic tissue response to the implantation of various scaffold types, as well as the sham surgery control, upon termination at two different time points (two days and seven days) 122

Table 5.2 The varying immune responses at two-days post-implantation according to the scaffold type 124

Table 5.3 The immune response at seven days elicited by the various scaffold types 127

CHAPTER 1

INTRODUCTION AND BACKGROUND

1.1 Background to the Study

With the rise of 3D printing as a revolutionary method of tissue engineering (Chua and Yeong, 2014), researchers are racing to find novel and innovative approaches to maximize the efficiency of the process so that the concept may be utilized successfully in clinical practice. While 3D bioprinting technology has proven innovative, it has unfortunately been plagued with problems which limit its ultimate clinical use. These problems range from the lack of biocompatible materials to problems with printability as well as mechanical strength that does not match that of native tissues (Murphy and Atala, 2014).

The 3D bioprinting process relies on the optimization of a number of variables in order to be considered successful. Reviews have been undertaken on printing processes in order to ascertain their success and potential, as well as problems (Dababneh and Ozbolat, 2014, Billiet *et al*., 2012). Overall limitations included suboptimal chemical and mechanical properties, compromised resolution, decreased cell viability, impracticality, a dearth in printable materials and lack of biocompatibility of bioprinting processes (Dababneh and Ozbolat, 2014).

As 3D bioprinting was built on aspects of traditional tissue engineering, scaffolding is one of the most important aspects to consider (El-Sherbiny and Yacoub, 2013). Scaffolding provides a framework and support for subsequent tissue development. Thus, the scaffolds printed must comply with a number of criteria including non-toxic biodegradability (Velasco *et al*., 2015) and scaffold architecture with a highly interconnected porous structure that allows effective cell penetration and nutrient transportation (Chan and Leong, 2008). Further, scaffolds must display suitable mechanical properties such as the retention of structure when implanted into the body,

so as to comply with the mechanical functions of the native tissue that it is meant to substitute or repair (Velasco *et al*., 2015). Scaffolds should also be biocompatible and bioactive, wherein cells must be able to adhere, function normally, and migrate onto and eventually through the scaffold and begin to proliferate (O'Brien, 2011). Scaffolds should also avoid eliciting immune responses, which may reduce healing or result in rejection by the body (Do *et al*., 2015). One of the most important properties of a scaffold is appropriate surface modification and topography to support cell adhesion, without which new tissue would not grow (Le *et al*., 2013). Reviews of materials used in scaffoldings have been done and reflect the sentiment that, as yet, there is no one ideal material that encompasses all of the properties necessary for an optimal scaffold (Sundaramurthi *et al*., 2016).

1.2 Rationale and Motivation for this Study

In order to overcome the afore-described limitations, a novel concept is to utilize 3D printers as an initial, instead of final, process. Therefore, post-processing would be the most important step in the bioprinting process. Current methods of post-processing, including cell encapsulators, perfusion bioreactors and bio-monitoring systems (Munaz *et al*., 2016), are used less to induce functionalization and are used more to encourage scaffold assembly, remodeling and cellular maturation into functional tissue (Mironov *et al*., 2011). While useful in its current capacity, the concept of post-processing could and should be revitalized and revolutionized in order to play more of an active role in the development of engineered tissue with desired properties. Post-processing allows for an effective solution to problems arising from the printing process, and also allows for simpler, more convenient modifications as well as increased control over the properties of the scaffold thus permitting customizable functionalization.

As scaffolds provide a framework that supports cell adhesion, proliferation and tissue formation (Xu *et al*., 2012), their fabrication is of utmost importance. By using 3D printers to create scaffolds,

and then utilizing manipulations in order to modify the scaffolds, many of the limitations listed above in relation to scaffolding characteristics could be overcome. The concepts of such modifications have been utilized in other methods of scaffold production for tissue engineering with varying success rates (Chen *et al*., 2006, Nisbet *et al*., 2008).

Previous studies have used chemical modifications in order to isolate functional groups for molecular attachment, however, the effect of chemical modifications on the physical properties of scaffolds could prove to be beneficial once determined. Properties introduced or optimized following modification may include enhanced hydrophilicity, mechanical strength, controlled porosity, increased bio-adhesiveness and controlled degradation (Asa'ad *et al*., 2016). Using printing as an initial step and thereafter using chemical modifications will solve problems relating to the printing process, as well as assisting in the incorporation of molecular attachments that cannot handle the temperature-controlled parameters of the 3D printer.

Functionalization of scaffolds though chemical modifications post-fabrication can result in scaffolds with enhanced properties. This will be undertaken by altering the chemical makeup of non-seeded 3D printed scaffolds in order to isolate and activate certain functional groups, and using these activated functional groups to attach bioactive molecules to the scaffold. The effects of these chemical modifications on scaffolds, post-printing, will be determined and evaluated.

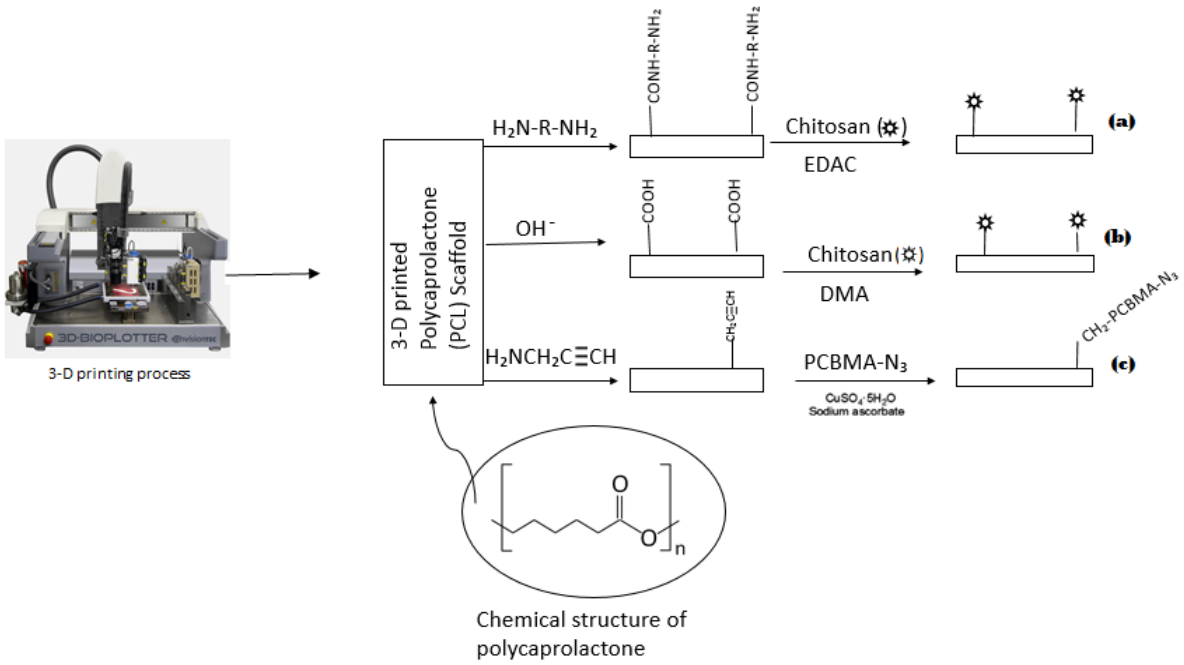


Figure 1.1 Schematic concept of three types of scaffold modification with various molecular attachments, employing a polycaprolactone (PCL) scaffold as an example; (a) Type 1 modification: Aminolysis of the PCL scaffold and subsequent chitosan attachment. (b) Type 2 modification: Hydrolysis of the PCL scaffold and subsequent chitosan attachment. (c) Type 3 modification: The PCL scaffold was alkynylated by aminolysis and subsequently grafted with zwitterionic PCBMA-N_3 (Adapted from (Li *et al.*, 2013, De Luca *et al.*, 2014))

1.3 Factors to Consider in 3D Bioprinting for Tissue Engineering

1.3.1 Biological Considerations in Tissue Engineering

Tissue engineering relies on bioactivity in order to produce the desired outcome. As a result, biological considerations are extremely important as they can impact the activity of the engineered tissue during its formation.

The most important consideration is that of bioactivity. Engineered tissue is ultimately required to replace or repair tissue, and as such, must be able to function as the native tissue. Even though it is obviously necessary to utilize materials that are biocompatible (Wu and Hsu, 2015), one of the most important aspects to consider is the inflammatory response of the body, which almost always accompanies the introduction of a biomaterial – as it is considered a foreign body. This inflammation involves cells such as macrophages and mast cells, which can compromise the

growth and proliferation of cells (Shastri, 2009). Thus, efforts must be made to limit adverse and damaging responses.

The next consideration is with regards to biological requirements apart from specified cellular growth. This includes angiogenesis, innervation, molecular signaling and recruitment of pluripotent cells (Shastri, 2009), all of which need to be accounted for depending on the specific intended environment. Because this relies on heterogeneity of cells in a singular tissue which must be appropriately spatially distributed, and appropriately stimulated for differentiation and proliferation (Shastri, 2009), the process can get significantly more complicated than initially envisioned.

Finally, the local biological environment must also be considered and exploited, as often, strategies utilized prior to implantation to modulate cell function are compromised within the intended environment (Shastri, 2009). It would be remiss to assume that the behaviour of materials, conditions and responses planned in formulation stages would be replicated *in vivo*. As such, limiting unnecessary molecular attachments and dependency on exogenous factors would improve the *in vivo* activity.

The final consideration is that of degradation. The construct that is used must be made of a material which can degrade via normal bodily processes, and the degradation products must be non-toxic and able to be cleared by the body (Rahaman *et al*., 2011).

1.3.2 Mechanical Specifications for 3D Bioprinting

A pertinent and interesting conclusion regarding scaffold behaviour has been that the scaffold's physical properties relate to tissue morphogenesis. Studies have shown that various mechanical properties including elastic modulus, pore size and pore orientation, affect the differentiation of

cells (Shastri, 2009). As such, it is essential to design a geometrically appropriate structure which will promote cellular activity.

Another important specification is that the scaffolds must present with a porous three-dimensional architecture, as that mechanical specification contributes to the equally important biological consideration of bioactivity, by permitting diffusion of nutrients, vascularization etc. (Rahaman *et al*., 2011).

One of the most important mechanical considerations is that of load-bearing. The body withstands mechanical stresses daily, whether inflicted upon the body by the body, or external forces. This means that any engineered tissue will be required to withstand the same forces. For this to happen, the scaffold must present with suitable mechanical properties that can withstand loads in the same directions and orientations as the body (Hutmacher, 2000), while still promoting cellular growth. Lastly, degradation behaviour is similarly critical, and has to be proportion to the rate of tissue infiltration and production (Liebschner *et al*., 2005).

Other mechanical considerations in the 3D bioprinting for tissue engineering realm include (Liebschner *et al*., 2005):

- Biomaterial boundaries and scale compared to defect
- Scaffold geometry with regards to the complexity of internal micro structure and its effect on cellular loading
- Patient specific/site specific design parameters
- Defined required mechanical properties in intended anatomical region
- Large pore geometry that can limit cell growth

1.3.3 Printing Compatibility of Materials for Use in Bioprinting

Bioprinting utilizes 3D designs in conjunction with bioadditive manufacturing technologies (Ozbolat and Yu, 2013) in order to produce architecturally sound constructs that are intended to be biomimetic (Skardal and Atala, 2015). As such, materials must be 'printable'. Materials must possess ideal viscosity, solidifying properties, the ability to withstand shear stresses, should not clog the needle tip, and should ideally extrude as a continuous filament (Chung *et al*., 2013), in order to produce a construct with precisely designed geometry with good resolution.

1.4 Novelty of this study

- Utilizing 3D printing as an initial step of scaffold design, instead of the final outcome in order to have enhanced control over the properties of scaffolds for individualized clinical applications.
- Overcoming of limitations of the bioprinting process and materials employed therein by utilizing methods which will address the problems presented by printing and cannot be used prior to or during the printing process.
- Overcoming limitations of macromolecule incorporation into 3D printed scaffolds by using post-fabrication attachment methods to demonstrate the functionalization ability of CM-SCAFFs.

1.5 Aim and Objectives

This investigation aims to assess the effects of chemical modifications and subsequent functionalization on 3D printed scaffolds for potentially enhanced application in tissue engineering. This will be achieved by fulfilling the following objectives:

1) Selection of appropriate polymers, chemical functionalization methods and functional groups.
2) Printing of scaffolds using a 3D bioprinter and subsequent activation via chemical modification and functionalization with biomolecules.
3) Elucidation of physicochemical and physicomechanical properties.

4) *In vitro* testing of the scaffolds by immersing scaffolds in simulated body fluid and subsequent analysis for transitions in mechanical properties, microstructure and bioerosional properties.
5) Implantation of scaffold into rats for *in vivo* testing of tissue response and subsequent histological analysis for determination of biocompatibility.

Synopsis of Dissertation

Chapter One outlines the problem and highlights the rationale for the study. It is an introduction to the study that covers the background and introduction. A summary of the aims and objectives is included in this chapter.

Chapter Two focuses on bioink development and printing strategies. It elaborates on materials utilized, as well as the latest trends in modifying properties of bioinks and surrounding physical parameters which influence its overall structure and function.

Chapter Three describes the preliminary formulation design process, as well as the formulation and development of a novel bioink combination, and the effect of plasticizers on this formulation. Various testing analysed both the bioink itself, as well as the printed construct.

Chapter Four describes the post-printing chemical modifications including aminolysis and hydrolysis, and the attachment of hyaluronic acid to the scaffold. Testing done in this chapter was mainly to confirm the chemical modifications, as well as to evaluate the effects of the chemical modifications on the mechanical properties of the printed scaffold.

Chapter Five is a comprehensive description of the *in vivo* testing done in order to assess the biocompatibility, tissue response and degradation of the initially printed scaffold when compared to the post-printing chemically modified scaffolds.

Chapter Six summarizes the study done in the form of results concluded and also makes recommendations for future works and developments.

References

Asa'ad, F., Pagni, G., Pilipchuk, S. P., Giannì, A. B., Giannobile, W. V. & Rasperini, G. 2016. 3D-Printed Scaffolds and Biomaterials: Review of Alveolar Bone Augmentation and Periodontal Regeneration Applications. *International Journal of Dentistry,* 2016.

Billiet, T., Vandenhaute, M., Schelfhout, J., Van Vlierberghe, S. & Dubruel, P. 2012. A review of trends and limitations in hydrogel-rapid prototyping for tissue engineering. *Biomaterials,* 33**,** 6020-6041.

Chan, B. & Leong, K. 2008. Scaffolding in tissue engineering: general approaches and tissue-specific considerations. *European spine journal,* 17**,** 467-479.

Chen, J., Chu, B. & Hsiao, B. S. 2006. Mineralization of hydroxyapatite in electrospun nanofibrous poly (L-lactic acid) scaffolds. *Journal of Biomedical Materials Research Part A: An Official Journal of The Society for Biomaterials, The Japanese Society for Biomaterials, and The Australian Society for Biomaterials and the Korean Society for Biomaterials,* 79**,** 307-317.

Chua, C. K. & Yeong, W. Y. 2014. *Bioprinting: principles and applications*, World Scientific Publishing Co Inc.

Chung, J. H., Naficy, S., Yue, Z., Kapsa, R., Quigley, A., Moulton, S. E. & Wallace, G. G. 2013. Bioink properties and printability for extrusion printing living cells. *Biomaterials Science,* 1**,** 763-773.

Dababneh, A. B. & Ozbolat, I. T. 2014. Bioprinting technology: a current state-of-the-art review. *Journal of Manufacturing Science and Engineering,* 136**,** 061016.

De Luca, A. C., Terenghi, G. & Downes, S. 2014. Chemical surface modification of poly-ε-caprolactone improves Schwann cell proliferation for peripheral nerve repair. *Journal of tissue engineering and regenerative medicine,* 8**,** 153-163.

Do, A.-V., Khorsand, B., Geary, S. M. & Salem, A. K. 2015. 3D Printing of Scaffolds for Tissue Regeneration Applications. *Advanced healthcare materials,* 4**,** 1742-1762.

El-Sherbiny, I. M. & Yacoub, M. H. 2013. Hydrogel scaffolds for tissue engineering: Progress and challenges. *Global Cardiology Science and Practice***,** 38.

Hutmacher, D. W. 2000. Scaffolds in tissue engineering bone and cartilage. *In:* Williams, D. F. (ed.) *The Biomaterials: Silver Jubilee Compendium.* Oxford: Elsevier Science.

Le, X., Poinern, G. E. J., Ali, N., Berry, C. M. & Fawcett, D. 2013. Engineering a biocompatible scaffold with either micrometre or nanometre scale surface topography for promoting protein adsorption and cellular response. *International Journal of Biomaterials,* 2013.

Li, Q., Wang, Z., Zhang, S., Zheng, W., Zhao, Q., Zhang, J., Wang, L., Wang, S. & Kong, D. 2013. Functionalization of the surface of electrospun poly (epsilon-caprolactone) mats using zwitterionic poly (carboxybetaine methacrylate) and cell-specific peptide for endothelial progenitor cells capture. *Materials Science and Engineering: C,* 33**,** 1646-1653.

Liebschner, M., Bucklen, B. & Wettergreen, M. 2005. Mechanical Aspects of Tissue Engineering. *Seminars in Plastic Surgery,* 19**,** 217-228.

Mironov, V., Kasyanov, V. & Markwald, R. R. 2011. Organ printing: from bioprinter to organ biofabrication line. *Current Opinion in Biotechnology,* 22**,** 667-673.

Munaz, A., Vadivelu, R., St. John, J., Barton, M., Kamble, H. & Nguyen, N.-T. 2016. Three-dimensional printing of biological matters. *Journal of Science: Advanced Materials and Devices*, 1(1), 1-17

Murphy, S. V. & Atala, A. 2014. 3D bioprinting of tissues and organs. *Nat Biotech,* 32**,** 773-785.

Nisbet, D., Yu, L., Zahir, T., Forsythe, J. S. & Shoichet, M. 2008. Characterization of neural stem cells on electrospun poly (ε-caprolactone) submicron scaffolds: evaluating their potential in neural tissue engineering. *Journal of Biomaterials Science, Polymer Edition,* 19**,** 623-634.

O'Brien, F. J. 2011. Biomaterials & scaffolds for tissue engineering. *Materials Today,* 14**,** 88-95.
Ozbolat, I. T. & Yu, Y. 2013. Bioprinting Toward Organ Fabrication: Challenges and Future Trends. *IEEE Transactions on Biomedical Engineering,* 60**,** 691-699.
Rahaman, M. N., Day, D. E., Bal, B. S., Fu, Q., Jung, S. B., Bonewald, L. F. & Tomsia, A. P. 2011. Bioactive glass in tissue engineering. *Acta biomaterialia,* 7**,** 2355-2373.
Shastri, V. P. 2009. *In vivo* engineering of tissues: Biological considerations, challenges, strategies, and future directions. *Advanced Materials,* 21**,** 3246-3254.
Skardal, A. & Atala, A. 2015. Biomaterials for Integration with 3D Bioprinting. *Annals of Biomedical Engineering,* 43**,** 730-746.
Sundaramurthi, D., Rauf, S. & Hauser, C. 2016. 3D bioprinting technology for regenerative medicine applications. *2016,* 2**,** 19.
Velasco, M. A., Narváez-Tovar, C. A. & Garzón-Alvarado, D. A. 2015. Design, Materials, and Mechanobiology of Biodegradable Scaffolds for Bone Tissue Engineering. *BioMed Research International,* 2015**,** 729076.
Wu, G.-H. & Hsu, S.-H. 2015. polymeric-based 3D printing for tissue engineering. *Journal of medical and biological engineering,* 35**,** 285-292.
Xu, C., Lu, W., Bian, S., Liang, J., Fan, Y. & Zhang, X. 2012. Porous collagen scaffold reinforced with surfaced activated PLLA nanoparticles. *The Scientific World Journal,* 2012.

CHAPTER 2

REVIEW OF BIOPRINTING, METHODS OF FUNCTIONALIZATION AND METHODS OF TUNABILITY

2.1 Introduction

The success of a bioink in the bioprinting process is dependent on the properties of its components and their potential to fulfil criteria of an 'ideal' bioink. Various polymers possess different characteristics, some of which are desirable, and some of which hinder the potential of these constructs. A material design approach is necessary to better assess the valued characteristics of the polymers used, versus their individual weaknesses.

Biocompatibility is considered to be one of the most important properties of a bioink (Murphy and Atala, 2014), and needs to be considered before any structural considerations, due to the applicability of the bioink in a tissue engineering capacity. Thereafter, considerations must be made regarding the actual printing process, which requires the bioink to be viscous enough that it is extrudable or transferable, but not so viscous that it cannot maintain structural fidelity and cell viability once printed. Cell supportive viscosity and printable viscosity differ, which means that either cell damage is at risk or the printability is compromised (Panwar and Tan, 2016). Thus, we expect bioinks to possess some element of shear thinning behaviour (Piras *et al*., 2017). Shear thinning permits the unhindered extrusion of viscous bioinks through limiting the entanglement of chains. In order to ensure that the bioink performs optimally, we must also make considerations for the parameters surrounding the printing process (such as nozzle size, pressure, nozzle shape, temperature) which can affect the amount of stress put on the bioink (Panwar and Tan, 2016).

The next thing to consider is the structural integrity of the bioink once extruded. The architecture of the construct is designed with precise and defined geometry (Murphy and Atala, 2014). It is

thus essential that the material gels/solidifies on the platform instantaneously, in order to prevent spreading and loss of resolution and architectural design (Demirtas *et al*., 2017), and remains intact.

The last considerations involve the action of the bioink once it has produced a printed construct. The construct must permit cellular adherence, proliferation and migration so that new tissue can be formed on the construct, while the construct itself must be susceptible to biodegradation into non-toxic degradation products that the body can safely ride itself of (Murphy and Atala, 2014). The mechanical strength of the printed structure should also be sufficient so as to withstand the loads experienced by the native tissue/organ (Asa'ad *et al*., 2016).

In choosing materials for bioinks, there are natural and synthetic polymers to consider (Holzl *et al*., 2016). A major challenge in the field of 3D bioprinting for tissue engineering is the lack of printable bioinks (Guvendiren *et al*., 2016). This chapter gives an overview of currently available bioink materials, as well as the realm of 3D printing, and focuses on presenting available design strategies, hereunder known as functionalization methods and techniques, used to alter and optimize bioinks in order to exploit them for optimal usage and performance. The methods used for functionalization, as well as their effects and success will be discussed and evaluated in order to promote the applicability and sustainability of bioinks. This chapter will also discuss physical parameters surrounding the printing process, and how these parameters can be altered to change the properties of bioinks and their subsequently printed constructs.

2.2 Materials Used as Bioinks

Currently utilized bioinks are based on both natural and synthetic polymers (Holzl *et al*., 2016). Most natural polymers possess cellular interactivity and biocompatibility (Chen and Liu, 2016) but often lack the mechanical properties needed for them to maintain their structural integrity and

support the physical stress within the *in vivo* microenvironment. On the other hand, synthetic polymers are advantageous due to their potential for modification, which could be explored to induce bioactivity along with providing more control over their structure and architecture (Chen and Liu, 2016). However, synthetic polymers prove to be challenging due to their poor biocompatibility, poor cellular adhesion, toxic degradation products, as well as a loss of mechanical properties during the degradation process (Kirchmajer *et al*., 2015). A comparison of the bioinks commonly employed are elaborated on in Table 2.1

Table 2.1 Materials commonly used in bioinks

Material	**Advantages**	**Ref**	**Disadvantages**	**Ref**
Alginate	• Gels rapidly when ionically crosslinked • Biocompatible • Cheap	(Zhang *et al*., 2017b) (Hospodiuk *et al*., 2017) (Hospodiuk *et al*., 2017)	• Minimal cell recognition and adhesion • Slow degradation when not crosslinked • Low mechanical strength	(Hospodiuk *et al*., 2017) (Jia *et al*., 2014) (Holzl *et al*., 2016)
Gelatin	• Encourages cellular growth • Thermoresponsive sol-gel transition	(Zhou *et al*., 2017, Holzl *et al*., 2016) (Holzl *et al*., 2016, Pan *et al*., 2016, Schuurman *et al*., 2013)	• Liquifies at physiological temperatures • Poor mechanical properties	(Holzl *et al*., 2016) (Hospodiuk *et al*., 2017, Thakur *et al*., 2017b)

Hyaluronic Acid	• Biodegradable • Biocompatible	(Holzl *et al*., 2016, England *et al*., 2017) (Holzl *et al*., 2016, Hospodiuk *et al*., 2017)	• Highly hydrophilic • Not mechanically stable • Slow gelation rate	(Pescosolido *et al*., 2011) (Pescosolido *et al*., 2011) (Hospodiuk *et al*., 2017)
Polyethylene glycol (PEG)	• Biocompatible • Hydrophilic • Exhibits shear thinning behaviour	(Serra *et al*., 2014) (Serra *et al*., 2014, Jeong and Gutowska, 2002) (Zhang *et al*., 2017b)	• Poor mechanical strength • Poor cell adhesion	(Hospodiuk *et al*., 2017) (Morris *et al*., 2017)
Poly (lactic acid) (PLA)	• Excellent mechanical strength • Biodegradable • Biocompatible	(Zeng *et al*., 2017) (Zeng *et al*., 2017, Serra *et al*., 2014) (Zeng *et al*., 2017)	• Poor cell interaction and adhesion • Low hydrophilicity	(Zeng *et al*., 2017) (Zeng *et al*., 2017)
Poly (ε-caprolactone) (PCL)	• Biocompatible • Biodegradable • Thermoplastic • Excellent mechanical properties	(Park *et al*., 2016) (Park *et al*., 2016) (Hoque *et al*., 2009) (Park *et al*., 2016), (Zhang *et al*., 2017a)	• Absence of biological properties	(Luk *et al*., 2013)

2.2.1 Natural Polymers

Gelatin is a naturally occurring water soluble polymer (Schuurman *et al*., 2013, Pan *et al*., 2016) commonly used as a bioink due to the presence of cell responsive cues on its surface (Holzl *et al*., 2016), as well as its thermoresponsive gelling when cooled (Pan *et al*., 2016, Holzl *et al*., 2016). However, it is this thermoresponsiveness which allows it to liquify at physiological

temperatures (Holzl *et al*., 2016), along with its poor mechanical properties (Hospodiuk *et al*., 2017) which limit its usage.

Alginate, an inexpensive, biocompatible anionic polysaccharide polymer extracted from brown seaweed (Ozbolat and Hospodiuk, 2016), is used in 3D bioprinting due to its rapid gelation when ionically crosslinked (Hospodiuk *et al*., 2017). However, it is difficult to use in tissue engineering because of its minimal cell activity in terms of recognition and adhesion (Hospodiuk *et al*., 2017). Hydroxyapatite is a natural polymer with its value as an additive with bioactive properties (Wang *et al*., 2016). It is effective in that it does not affect material properties, is less fragile than other polymers, and contributes by encouraging cellular differentiation and proliferation (Wang *et al*., 2016).

Hyaluronic acid is a linear glycosaminoglycan found abundantly in the extracellular matrix (ECM) (Panwar and Tan, 2016). Its purpose in tissue relates to hydration of the ECM, and also plays a role in cellular growth, migration and differentiation (Panwar and Tan, 2016). It is biocompatible as well as biodegradable, but use may be limited by its extremely hydrophilic nature which results in fast hydrolysis (Panwar and Tan, 2016), and its slow gelation rate which can impact structural fidelity and contributes to mechanical instability.

Cellulose is a linear polysaccharide obtained from the biosynthesis of plants or bacteria (Piras *et al*., 2017). Methylcellulose is a cellulose derivative obtained by partially substituting hydroxyl groups with methoxy groups and is a suitable additive to support a cell laden matrix and encourages cell proliferation to enhance cellular viability, and also facilitates printing through an increase in viscosity (Schutz *et al*., 2017). Nanocellulose materials (which includes nanofibrillated cellulose, cellulose nanocrystals and bacterial cellulose) display a variety of interesting properties integral to the realm of tissue engineering such as cost-effectiveness, biocompatibility, non-

toxicity, sustainability and biodegradability (Piras *et al*., 2017). Cellulose nanofibrils also display high viscosity and shear-thinning behaviour (Piras *et al*., 2017), and produce constructs exhibiting impressive shape fidelity and good resolution.

Chitosan is a natural polysaccharide polymer widely used in tissue engineering and 3D bioprinting due to its high viscosity for printability, as well as its biodegradability and biocompatibility (Panwar and Tan, 2016). However, chitosan exhibits a slow gelation rate, suboptimal mechanical properties and a limit on cell line applicability (Panwar and Tan, 2016), which makes it a difficult polymer to use individually, but useful in conjunction with other polymers.

2.2.2 Synthetic Polymers

Poly (ε-caprolactone) (PCL) is a low cost, thermoplastic, synthetic polymer with a semicrystalline structure (Hoque *et al*., 2009). For 3D bioprinting related tissue engineering, it is useful because of its low melting point, biocompatibility and biodegradability, as well as its improved mechanical properties (Park *et al*., 2016) when compared to natural polymers. Due to its low melting point, as well as its impressive rheological and viscoelastic properties (Guvendiren *et al*., 2016), PCL can be used in extrusion-based printing. One of the main disadvantages of PCL is its stiffness, as well as its extended degradation (Guvendiren *et al*., 2016) profile which limits its usage. This degradation profile can however be useful in long term tissue regeneration (such as hard tissue engineering).

Poly (lactide-co-glycolide) (PLGA) is a copolymer of Polylactide (PLA) and polyglycolide (PGA) and is known for its biodegradability and biocompatibility (Baolin and Ma, 2014). PLA, more hydrophobic than PGA, degrades at a much slower rate, making it easy to tune the degradation profile of PLGA by altering the lactide/glycolide ratio (Baolin and Ma, 2014). One of the biggest

disadvantages is that processing at high temperatures may induce toxic component formation, as well as structural cross-linking of which the effects are unestablished (Mironov *et al*., 2017).

Pluronic polymers are poloxamer-based triblock copolymers which exhibit excellent printability (Donderwinkel *et al*., 2017) (excluding laser-based bioprinting) and are also thermoresponsive. However, it is plagued by many limitations, including a reliance on high concentrations in order to be utilized in 3D printing (Panwar and Tan, 2016). It presents with weak mechanical properties which results in its erosion within a few hours, but can be crosslinked (Fedorovich *et al*., 2009) or combined with other polymers in order to overcome this. Pluronic is also known to be limited by its poor cellular activity and support, which makes it a difficult polymer to utilize independently (Panwar and Tan, 2016).

Poly (ethylene glycol) (PEG) is a hydrophilic and biocompatible (Panwar and Tan, 2016) polymer, with tailorable mechanical properties. PEG is a useful polymer to consider, due to its ability to be tailored with various functional groups in order to induce desirable properties, as well as its ability to also be used as a backbone for a crosslinked system or as a crosslinker itself (Panwar and Tan, 2016). It does however present with a low viscosity which can make it difficult to use in extrusion printing, but PEG, as well as its derivatives can be used in combinations with other bioinks (Panwar and Tan, 2016). PEG is also limited by its lack of cellular or protein adhesiveness (Morris *et al*., 2017), but can be modified to enhance adhesion.

2.3 3D Bioprinting for Tissue Engineering

3D bioprinting has been a relatively recent and exciting development in the tissue engineering sphere. Bioprinting is a process utilizing computer generated 3D designs to produce architecturally complex models which allows for a closer form of biomimicry than ever before, and the printing process itself allows for controlled production through adjustable parameters, thus providing the opportunity for customized and specialized structures (Zhang *et al*., 2017b).

In order to achieve the desired outcome, many parameters need to be considered, including the printing process, the materials being used, and the variables contributing to tissue growth (Holzl *et al*., 2016). Over the years, information regarding 3D bioprinting and its advancements have reflected that one of the biggest current problems in this field is the lack of a 'perfect' bioink for use in the printing processes (Hospodiuk *et al*., 2017). Because there is a lack of an ideal material available, other aspects of the bioprinting process should be looked and assessed for their tunability to evaluate their effect on the properties of available bioinks.

In this review, we expand on the bioprinting process and discuss the effect of tunable parameters on the properties of bioinks commonly used for tissue engineering. These effects include commonly looked-for traits such as bioactivity, printability and an improvement of mechanical properties to allow the produced construct to ideally withstand the forces of native tissues.

2.3.1 Types of 3D Bioprinting

The success of bioprinting depends on a number of factors, one of which is the printing process itself (Li *et al*., 2016), which has made great strides in recent times. Typically, a bioprinting system consists of a layer-by-layer assembly of bioinks (Sundaramurthi *et al*., 2016) printed using computer aided design (CAD) software which is generated to specifications. This use of CAD files for generating patterns is one of the main advantages of the process as it is easy, user-friendly and convenient to customize (Sundaramurthi *et al*., 2016). Bioprinting, in essence, uses 3D designs to create constructs that mimic the native tissues and are anatomically and functionally appropriate (Sundaramurthi *et al*., 2016).

Bioprinting methods that are commonly used include extrusion-based printing, inkjet based, and laser-assisted printing (Suntornnond *et al*., 2016), which will be briefly elaborated upon and compared below (Figure 2.1).

Inkjet bioprinters (drop-on-demand printers) print a design point-by-point in order to form a structure (Sundaramurthi *et al*., 2016). Inkjet heads (either thermal or piezoelectric) work by ejecting drops of fluid to print a liquid binder onto thin layers of powder, into structures constructed using software (Shirazi *et al*., 2015).

Extrusion printing utilizes pneumatic or mechanical power in order to print onto stationary substrates (Sundaramurthi *et al*., 2016, Ozbolat and Hospodiuk, 2016) in computer generated architectures. The material is deposited via a nozzle orifice (Li *et al*., 2016) as filament, under the control of the computer-generated design, thus producing complex 3D structures (Ozbolat and Hospodiuk, 2016)

Laser-assisted bioprinting typically involves using a pulsed laser beam to irradiate a ribbon coated with liquid biomaterials, causing the biomaterials to undergo evaporation and be deposited onto a substrate as droplets (Li *et al*., 2016). The resolution depends on parameters such as laser energy, wettability and nature of substrate surface, viscosity and bioink surface tension (Murphy and Atala, 2014).

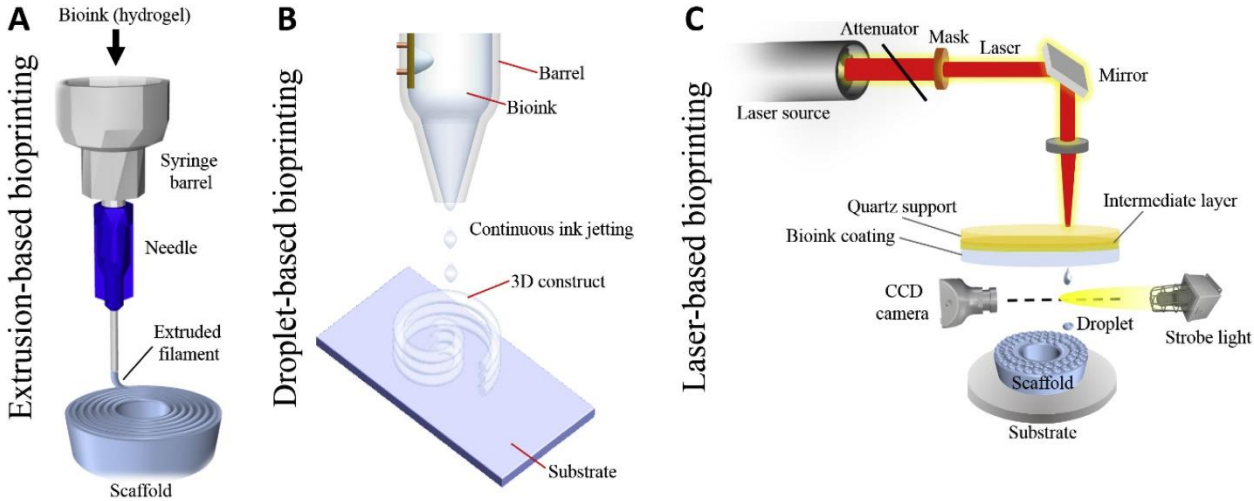


Figure 2.1 Various common bioprinting techniques: a) Extrusion-based bioprinting, b) droplet-based bioprinting, c) laser-based bioprinting. [Ref. (Datta *et al*., 2018); Reproduced with permission from Elsevier B.V. Ltd. © 2018].

Each method of printing comes with its own advantages and disadvantages, as elaborated upon in the table below (Table 2.2). These particular characteristics further complicate the process by limiting the usage of certain materials, or certain applications and outcomes, depending on the method used.

Table 2.2 Comparison of the advantages and disadvantages of commonly used bioprinting methods

Type of printer	**Advantages**	**References**	**Disadvantages**	**References**
Inkjet	• Non-contact printing • Size of droplets and rate and direction of ejection can be controlled with a piezoelectric head • Avoid shear stresses using nozzle-less printing heads • Widely available • Low cost • High throughput	(Xu *et al*., 2013) (Shirazi *et al*., 2015) (Shirazi *et al*., 2015, Murphy and Atala, 2014) (Shirazi *et al*., 2015) (Murphy and Atala, 2014) (Shirazi *et al*., 2015, Murphy and Atala, 2014, Xu *et al*., 2013)	• Droplet size is not uniform in thermal inkjet printers • The nozzle clogs frequently • Cell viability compromised • Hard to use bioinks with high viscosity. • Low cell concentrations preferred	(Shirazi *et al*., 2015) (Murphy and Atala, 2014) (Murphy and Atala, 2014) (Murphy and Atala, 2014) (Murphy and Atala, 2014)
Laser	• Non-contact • Nozzle-free = no clogging • Good cell viability and proliferation • Can deposit cells at high densities with microscale resolution • Wide variety of viscosity and material compatibility	(Li *et al*., 2016) (Li *et al*., 2016) (Li *et al*., 2016) (Murphy and Atala, 2014, Dias *et al*., 2014) (Dias *et al*., 2014)	• Contamination of constructs • Time-consuming process • Shape fidelity requires rapid gelation mechanism	(Murphy and Atala, 2014) (Dias *et al*., 2014) (Murphy and Atala, 2014)
Extrusion	• More control over the material flow • Compatible with many types of viscous materials	(Sundaramurthi *et al*., 2016) (Ozbolat and Hospodiuk, 2016)	• Inks require specific viscoelastic and shear thinning properties	(Ozbolat and Hospodiuk, 2016)

	• Improved control over microarchitecture • High cell viability • Can print high cell densities	(Murphy and Atala, 2014) (Donderwinkel *et al*., 2017) (Ozbolat and Hospodiuk, 2016)	• Must have suitable stabilization and solidification properties • Lower resolution • Nozzle clogging	(Ozbolat and Hospodiuk, 2016) (Ozbolat and Hospodiuk, 2016) (Holzl *et al*., 2016, Ozbolat and Hospodiuk, 2016)

2.4 Scaffolds in Tissue Engineering

Bioprinting utilizes the concept of computer-generated 3D designs, adjustable parameters and bioadditive manufacturing technologies (Ozbolat and Yu, 2013) in order to 'print' precise geometries that will mimic anatomically correct biological structures (Skardal and Atala, 2015). As the purpose of these engineered tissues is to replace and/or repair damaged tissues (Velasco *et al*., 2015), bioinks used to fabricate scaffolds (printed constructs) must meet certain criteria in order to be considered suitable for clinical application. The most obvious specification is biocompatibility and biodegradability (O'Brien, 2011), with both original materials and degradation products being non-toxic (Do *et al*., 2015, Velasco *et al*., 2015). Cells must be able to attach and adhere to the scaffold which should also be capable of encouraging cellular proliferation and differentiation (Chan and Leong, 2008) in order to promote bioactivity. Scaffold architecture is also vital (O'Brien, 2011) in terms of porosity, morphology, connectivity and orientation which can be controlled through bioink and printing method choice. These parameters play a paramount role in determining the transfer and movement of nutrient, oxygen and waste through the engineered complex (Velasco *et al*., 2015, Chan and Leong, 2008). Good mechanical properties are vital to scaffolds, as the engineered tissue must prove stable over time, as well as strong enough to withstand applied forces during implantation and *in vivo* (Do *et al*., 2015, O'Brien, 2011).

2.5 Functionalization of Scaffolds for Optimal Properties

As there is currently no 'perfect' bioink, functionalization is a practical way forward in order to incorporate desirable properties and overcome limitations (Figure 2.2). However, it is important to note that the characteristics of the material, as well as the produced construct all depend on the desired outcome – i.e. the target tissue or organ. Because of the complexity of the human body, there is immense variability amongst different tissues and organs with regards to their structural and physiological requirements (Zhang *et al*., 2017), and as such, functionalizations are dependent on these requirements and must be tailored as necessary. The outcomes of various methods of functionalizations are critically discussed below, with a focus on optimizing mechanical properties, printability, biocompatibility and bioactivity.

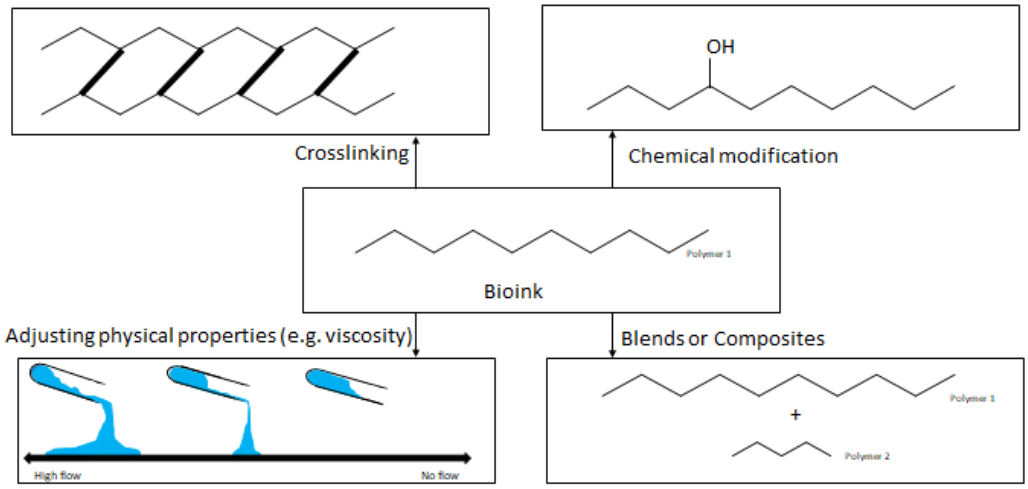


Figure 2.2 Schematic summary of various methods of functionalization

2.5.1 Functionalization for Improving Mechanical Integrity

In the quest for attaining the desirable properties in the polymer for 3D printing, chemical functionalization has been explored in numerous ways and one such method is the introduction of methacrylate groups. Functionalization of polymers (such as gelatin, hyaluronic acid, poly (hydroxymethylglycolide-co-ε-caprolactone)) with unsaturated methacrylate groups (Schuurman *et al*., 2013) results in polymers which are photopolymerizable (Zhou *et al*., 2017) and form a

more mechanically-stable construct (Shin *et al*., 2012). An increase in the degree of methacrylation (Shin *et al*., 2012), has been proven to increase the stiffness of constructs (Nichol *et al*., 2010) when measured against various strain levels, however, the compressive modulus is mainly affected by the methacrylated polymer concentration (Shin *et al*., 2012, Duan *et al*., 2014). Combining methacrylated polymers with each other – such as covalently binding methacrylated gelatin (gelMA) to methacrylated poly (hydroxymethylglycolide-co-ε-caprolactone) blended with poly-ε-caprolactone – produced constructs with a higher mechanical resistance ((7.7 ± 2.4 N) and integrity (Boere *et al*., 2014), when compared to a compound of gelMA bound to a non-methacrylated blend which showed low compressive strength (71 ± 4% for the unmethacrylated blend compared to 43 ± 5% for the methacrylated blend), decreased recovery and a lack of integration of materials. This inferred that the presence of methacrylated polymers positively influences the mechanical properties.

Mechanical properties are also shown to be influenced by covalent grafting of a reinforcing thermoplastic network to a hydrogel (Boere *et al*., 2015), or blending of a thermoplastic polymer with another polymer (Hoque *et al*., 2009), also results in constructs with improved mechanical strength and integrity. The thermosensitive nature of constructs enables immediate solidification of constructs when deposited onto thermoregulated platforms (Boere *et al*., 2015).

A study compared various hydrogels (agarose, alginate, gelatin methacrylamide and BioINK – a PEGMA based hydrogel) and their respective equilibrium modulus in order to evaluate their potential to be used as articular and fibro-cartilage. Results showed that the equilibrium modulus of the studied polymers were not of an equal or superior standard to that of native human cartilage, but that with reinforcement with PCL (a thermoplastic material) microfibers, the equilibrium modulus improved to within the acceptable range (Daly *et al*., 2016).The mechanical properties can be varied according to the potential tissue by altering the fiber spacing (Melchels *et al*., 2016),

fiber diameter and the molecular weight of the polymer. Another method of employing thermoplastic fibers is to produce constructs via the alternate deposition of thermoplastic fibers and hydrogels, and this process can be tailored by altering characteristics such as fiber spacing, thickness and orientation (Schuurman *et al*., 2011, Melchels *et al*., 2016)

Hydrogel reinforcing gels have also been studied with favorable results (Melchels *et al*., 2016). The use of a hydrogel maintains the improved mechanical properties due to the support structure, as well as improves control over degradation kinetics (Thakur *et al*., 2017a). The use of a hydrogel also contributes to the usage of these inks for bioprinting soft tissues - for which not many reinforcing options exist (Melchels *et al*., 2016). Blends of a polymer with different molecular weights may also affect the mechanical strength of constructs. This would be a noteworthy method of functionalization because of the absence any additives, and therefore the chance of adverse interactions is minimized. A combination of a higher ratio of high molecular weight alginate blended with a lower ratio of low molecular weight alginate (2:1) produced a mechanically stable construct, similar to that of native tissue (Park *et al*., 2016).

Conditions surrounding crosslinking are important as well. UV exposure, used in photopolymerization, can be used to control the stiffness and swelling of the hydrogels (Schuurman *et al*., 2013), with longer exposure leading to stiffer constructs and slower degradation (Jia *et al*., 2016). Temperature has also proven to play a significant role in the mechanical properties of the gels, with solutions stored and allowed to form thermal gels before exposure to UV appearing to produce significantly stiffer constructs than solutions maintained at higher temperatures (Schuurman *et al*., 2013). Lower temperatures can also slow the crosslinking process down and lead to a greater ordered crosslinked structure with improved mechanical properties (Augst *et al*., 2006). An increase in crosslinker concentration and crosslinking density

(Kesti *et al*., 2015) has shown to lead to higher degrees of crosslinking, thus enhancing structural integrity (Pan *et al*., 2016) and mechanical properties (Daly *et al*., 2016).

Crosslinking agents themselves also play a role in the mechanical properties of scaffolds. Glutaraldehyde was shown to improve the stability and mechanical strength when used as a crosslinker for collagen-based scaffolds and has shown an impressive decrease in degradation behaviour with an increase in concentration. However, glutaraldehyde was also proven to decrease the flexibility of scaffolds and result in a drastic increase in the stiffness of scaffolds with increasing concentrations (Pan *et al*., 2016). Functional crosslinkers also provide an interesting avenue for enhancing mechanical properties. Bioactive glass possesses impressive bioactive properties, and when used in combination with alginate, acts as a crosslinker. The alginate self-crosslinks through the Ca^{2+} provided by the bioactive glass (Zhao *et al*., 2016) and produces constructs with impressive compressive strength as well as bioactivity.

Interpenetrating networks have been utilized in order to enhance mechanical strength by combining the properties of each material (Kesti *et al*., 2015) and improvements have been made upon the concept through utilizing ‘double networks’ (Gong *et al*., 2003) – which are specialized interpenetrating networks, composed of materials with opposing mechanical properties, that have been proven to possess high fracture stress and toughness - and including a two-step photocrosslinking wherein the first polymer is crosslinked to form a rigid and brittle network, followed by the diffusion of the second polymer into the first network and photocrosslinking it to form a second soft and ductile network. As such, the initial rigid network is responsible for handling stress throughout the material, while the second network prevents fracture (Shin *et al*., 2012). Double networks lacking interconnection have been reported to be stronger than if there is interconnection (Nakajima *et al*., 2009).

The utilization of multiple cross-linking mechanisms also contributes greatly to an increase in mechanical strength. Thermoresponsive polymers undergo rapid physical crosslinking (Thakur *et al*., 2017a) once deposited, allowing for initial shape fidelity (Skardal *et al*., 2010). Thereafter, the polymers undergo covalent crosslinking via photopolymerization which encourages added network stability (Boere *et al*., 2015). An interesting example of this is with regards to a decellularized extracellular matrix (dECM) bioink, which mimics the native environment (Crapo *et al*., 2011). Improving mechanical properties was achieved through covalent crosslinking through adding vitamin B2 (riboflavin) - a biocompatible photocrosslinker (Tirella *et al*., 2012). The study also employed a dual mechanism by implementing further physical crosslinking, through thermally triggered collagen fibrillogenesis (Helseth and Veis, 1981) and this dual crosslinking exhibited a stable storage modulus superior to that of singularly crosslinked constructs. It was also observed that an increase in vitamin B2 decreased the stiffness of constructs, demonstrating that each crosslinking step contributes to the overall mechanical profile and constructs can be tailored as required (Jang *et al*., 2016).

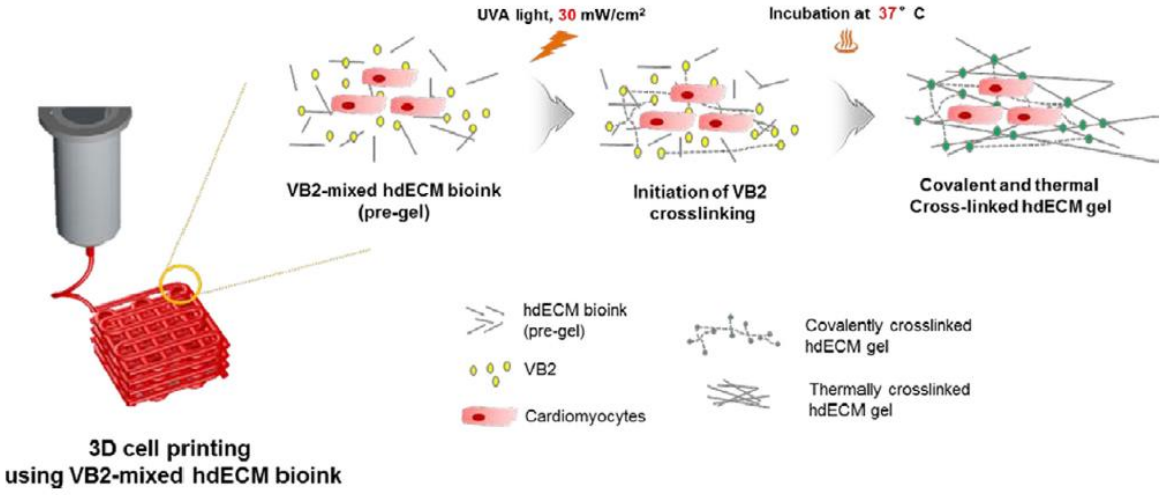


Figure 2.3 Schematic illustration of a two-step crosslinking mechanism that applies concurrent crosslinking of vitamin B2-induced covalent crosslinking and thermal crosslinking [Ref. *(*Jang *et al.*, 2016); Reproduced with permission from Elsevier B.V. Ltd. © 2016]

Some crosslinkers only partially crosslink polymers, and as such, the degradation rates of such materials may still be too fast to be clinically applicable. Thus, by utilizing the concept of secondary crosslinking, constructs produced can be further stabilized resulting in stronger more durable constructs with longer degradation times (Rutz *et al*., 2015). Utilizing secondary materials as binders has also proven to be an effective manner of enhancing mechanical integrity. Zhang *et al*. (Zhang *et al*., 2014) used PVA (polyvinyl alcohol) as a binder and effectively decreased the brittleness of the scaffolds, thus enhancing their compressive strength. The degree of polymerization of PVA binder also resulted in a low solubility at physiological temperatures, which enables the scaffolds to retain their mechanical integrity for longer (Zhang *et al*., 2014).

Other materials have been studied to determine their effect on mechanical properties. Addition of hyaluronic acid has resulted in an enhanced compressive modulus (Rajaram *et al*., 2014). The addition of silk fibroin to carboxylated agarose/hydroxyapatite composites improved the mechanical strength to supersede that of cancellous bone in the human body (Hu *et al*., 2016). Carboxymethyl chitosan, through ionic bonding of functional groups, proved to improve mechanical properties of the resulting construct (Huang *et al*., 2016). PEGTA was shown to enhance mechanical stability due to its enhanced crosslinking density through a branched tetravalent structure, and numerous active crosslinking sites (Jia *et al*., 2016).

2.5.2 Functionalization for Improving Printability

Printability dictates the ultimate structure and functionality of the printed construct, and is based on the printing process as well as alterable bioink properties - including flow properties, elastic modulus, shear thinning behaviour and viscoelasticity (Sultan *et al*., 2017). Generally, printability can be improved through an increase in the ink's viscosity, decreasing the gelation time, or both (Jang *et al*., 2016). Shear thinning behaviour can be identified by a decrease in viscosity with increased shear stress (Boere *et al*., 2015) and is desirable because it limits chain entanglement,

thus allowing smooth extrusion (Panwar and Tan, 2016) with quick recovery. Spreading, deformation, reduced porosity and collapse of subsequent layers are risked when printing materials with too low viscosity, however, a formulation that is too viscous can result in a blocked nozzle (Wüst *et al*., 2014), disjointed extrusion and constructs with limited integration (He *et al*., 2016). Materials must be printable and be sufficiently viscoelastic that they are extrudable, followed by rapid recovery so that the printed layers remain self-sustaining (Miculescu *et al*., 2018), distinct and possess high shape fidelity (Duan *et al*., 2014). The viscosity of materials can be adjusted through polymer density (Rhee *et al*., 2016) and polymer concentration. High concentrations are generally the key to producing good printing fidelity (Jia *et al*., 2016), with low concentrations presenting with poor printing quality.

There are many materials which can be added to improve viscosity and induce shear thinning behaviour as well as improve shape fidelity. For example, nanocellulose provides shear thinning with impressive shape fidelity and good resolution, when added to a solution (Markstedt *et al*., 2015). Methylcellulose (Schutz *et al*., 2017), hyaluronic acid (Wüst *et al*., 2014, Schuurman *et al*., 2013) and hydroxyapatite (Wüst *et al*., 2014) facilitate printing through an increase in viscosity. PCL is characterized by its non-water solubility, which, when used in conjunction with other materials, could prevent setting reactions in a syringe environment. PCL also contributes towards printability because of its high viscosity, which allows the extrusion of materials (Pei *et al*., 2016). Polyvinyl alcohol is added to crosslinking solutions and increases the viscosity of the solution, thereby preventing printed strands from floating and thus allowing stable structures to form (England *et al*., 2017).

Gelation can be controlled through adjusting the concentration of both the polymer and its crosslinking solution (Pan *et al*., 2016), and also through the addition of a retardation agent which would dictate the extent of crosslinking and its subsequent rheological properties. This must be

undertaken carefully, as it can yield formulations which are too viscous for printing and will lead to poor quality scaffolds. A solution to bioinks which do not rapidly solidify upon extrusion could be the addition of a thermoresponsive polymer which gels under temperature-related conditions. Thus, such a polymer, once co-extruded with another polymer, rapidly gels upon deposition under certain temperature conditions, allowing the other polymer to solidify while still maintaining the desired structure (Kesti *et al*., 2015). Combination bioinks have proven be advantageous in optimizing properties, as shown by Wüst *et al*. (Wüst *et al*., 2014) by employing a blend of three different materials (alginate-gelatin-hyaluronic acid) to establish mechanical stability during and after the printing process. The viscosity of the compound was found to be directly dependent on the concentration of one of the polymers (hyaluronic acid) (Rajaram *et al*., 2014), thus altering the printability of the bioink. Another component (gelatin) contributed through the instantaneous, albeit weak, solidification of the construct once it was printed – due to its thermal gelation process. The last component (alginate) allowed the construct to be chemically crosslinking, post-printing, in order to maintain long term stability (Wüst *et al*., 2014).

Enzymatic crosslinking of gelatin methacryloyl was studied using a highly specific, non-toxic crosslinker - Ca^{2+}-independent microbial transglutaminase (MTGase). Results showed that MTGase concentration affects the viscosity of the solution (Zhou *et al*., 2017) and that the addition of the MTGase enzyme also catalyzed the crosslinking in gelatin thus resulting in an increased crosslinking degree (Bae *et al*., 2009), which has been shown to correlate to viscosity as well. Highly viscous bioinks which do not possess shear thinning behaviours can make extrusion impossible. Chemical modifications, such as sulfation of the polymer can partially degrade the structure which decreases the molecular weight and thus the viscosity of the solution (Müller *et al*., 2017). Utilizing proportions of low molecular weight polymers also results in a lower viscosity. Such properties can be tuned by blending a higher ratio of high molecular weight polymers (Park

et al., 2016), increasing the concentration, or weakly chemically crosslinking solutions (Rutz *et al*., 2015), should a higher viscosity be desired.

2.5.3 Functionalization for Enhancing Biocompatibility and Bioactivity

Bioactivity is an important functionality of any printed scaffold as they form the platform for new tissue growth and should be able to simulate an environment similar to the native tissue. Thus, scaffolds must not only be biocompatible, but should also encourage cellular function and tissue integration (Guvendiren *et al*., 2016), as well as possess adequate porosity to enable nutrient and cell diffusion (Zhang *et al*., 2017a). Processes such as UV light exposure must be appropriately timed and modified as longer periods decrease cell viability, but increase stiffness and decrease the degradation rate (Colosi *et al*., 2016), but shorter periods decrease the mechanical integrity of the construct and thus the constructs exhibit less structure for cells attachment and spreading (Jia *et al*., 2016).

The chemical crosslinking process has proven to have an effect on water uptake with an increase in crosslinker concentration causing a reduction in swelling (Bigi *et al*., 2002) and water uptake (Pan *et al*., 2016), which could compromise cellular viability and proliferation. The presence of excessive crosslinker may lead to loss of cell adhesion, thus lower concentrations should be used to encourage better cell adhesion and growth (Pan *et al*., 2016). Highly crosslinked densities inhibit the secretion and formation of new tissue, whereas lower crosslinking densities encourage matrix formation (Schuurman *et al*., 2013). Additionally, ionic crosslinking has proven to be less damaging to cell viability than chemical crosslinking (Duan *et al*., 2014), and should be considered as an alternative where possible.

It is important to note the effect that crosslinkers may have on cell viability. Crosslinkers such as ethylene glycol diglycidyl ether (EDGE) and glutaraldehyde, while effective, are known to be

highly toxic and the produced scaffolds require intensive detoxifying strategies, whilst crosslinkers such as genipin and citric acid have emerged as significantly more cytocompatible, as well as citric acid being cost-effective, and should be considered (Oryan *et al*., 2018). With regards to photocrosslinking, some chemical photogenerators are cytotoxic and their dissolvement may require toxic solvents (Rouillard *et al*., 2011). A way forward may be to combine chemical and physical crosslinking methods, which could make the crosslinking process more effective, as well as less cytotoxic (Oryan *et al*., 2018).

Materials can undergo modifications which encourages bioactivity and one such method involved alginate, which is considered bioinert (Jia *et al*., 2014), but upon modification by introduction of sulfur groups permitted the binding of growth factors (Arlov *et al*., 2014) and also encouraged cellular proliferation (Mhanna *et al*., 2014). Alginate sulfate has also been proven to possess mitogenic activity which exhibits superior cellular proliferation (Müller *et al*., 2017). Another method of encouraging bioactivity is through the removal of materials post-printing. Although alginate is important in the printing process, it is bioinert and its removal post-printing can drastically improve the spreading and proliferation of cells, without compromising the density of the cells (Jia *et al*., 2016). Thermoplastics used in blends, like alginate, often provide valuable support to a material during printing and facilitate the solidification of constructs. However, their removal can also increase cell viability, due to the creation of a more open and porous network which increases diffusion of nutrients and cells (Kesti *et al*., 2015).

Various materials can be added to bioinks in order to induce or promote bioactivity. Fibrin gel is known as the golden standard for enhancement of bioactivity, due to its peptide sequences (Mastbergen *et al*., 2013). The incorporation of an inorganic phase, such as calcium phosphate, into constructs has been proven to improve bioactivity (Egorov *et al*., 2016). Silicon-substituted hydroxyapatite, which is able to work even at low concentrations, exhibits enhanced bioactivity

with improved tissue growth. Nguyen *et al*. (Nguyen *et al*., 2017) observed that cells bioprinted in non-cytotoxic nanocellulose based environments exhibit high cell viabilities. Carboxymethyl chitosan to be highly porous with large pore definition, which is considered a factor in providing a cell conducive environment (Huang *et al*., 2016). Polyethylene oxide and polycation polyethyleneimine have proven to encourage cellular attachment, differentiation and proliferation (Rajaram *et al*., 2014).

The addition of 4-arm PEGTA also produces constructs with a useful porous structure which has proven to induce increased cell growth and spreading (Jia *et al*., 2016). Hyaluronic acid contributes towards a supportive cellular environment through its anabolic effect on extracellular matrix synthesis (Boere *et al*., 2015) and ability to improve chondrogenesis, but this effect only works at low concentrations (Schuurman *et al*., 2013). The addition of mesoporous bioactive glass (MBG) stimulates cellular differentiation, as well as cell proliferation which is directly dependent on the concentration of MBG (Pei *et al*., 2016). Positively charged polylysine (PLL) is widely used to promote cell adhesion via enhancing electrostatic interaction with negatively charged ions of the cell membrane (Cui *et al*., 2016).

An interesting modification involves nanostructuring (inducing nanopores) (Frisman *et al*., 2011) gels. Pluronic lacks the ability to maintain long term cell viability (Fedorovich *et al*., 2009). Unmodified Pluronic was mixed with diacrylated Pluronic and printed. The subsequent elution of the unmodified Pluronic lead to a nanostructured construct with a low polymer concentration, thus encouraging bioactivity and long-term cell viability (Müller *et al*., 2015). The molecular weight of bioinks also affects bioactivity. Low molecular weight inks enable better mass transfer, cell migration and proliferation, however, low molecular weight scaffolds lack well defined features (Park *et al*., 2016). Therefore, bioinks prepared with a combination of high molecular weight: low

molecular weight (2:1) presented with enhanced cell viability and proliferation, without compromising the printability and structure (Park *et al*., 2016)

2.6 Methods of Tunability of 3D Printing Process

During the 3D bioprinting process, there are various parameters to consider which have an effect on the behaviour of bioinks during the printing process, and the subsequent structure formed. These parameters include temperature and concentration, which in turn affect various important properties of the bioink such as viscosity, mechanical stability and printability.

2.6.1 Altering Temperature

Temperature modulation is an important parameter to consider when bioprinting for the purpose of tissue engineering. Many aspects must be taken into consideration such as the temperature needed to maintain cellular viability during the 3D printing process, when compared to the temperatures required for the printing process itself – which includes the melting of polymers, and the subsequent structural fidelity.

Temperature adjustments are useful in polymers which utilize crosslinking as a manner of gelation. Lower temperatures during gelation can slow the crosslinking process down, as seen in the case of ionically crosslinked alginate, resulting in a structure with improved mechanical properties due to its greater ordered crosslinked structure (Augst *et al*., 2006).

Tissue engineering also requires materials to maintain structural fidelity when placed under physiological conditions, including the temperature of the body, which makes temperature-responsiveness an interesting parameter to consider when creating a bioink. Polymers which gel under these physiological temperatures are useful in maintaining structural fidelity when placed in the body, while maintaining a solution form at room temperature in order to permit printing. An

example of this would be the synthetic polymer - poly (N-isopropylacrylamide) (PNIPAAM), which exhibits a physiologically friendly gelation temperature (30-37°C) (Suntornnond *et al*., 2016). Within this range, the PNIPAAM chains are subjected to a coil-globule transition and hydrophobic interactions between these chains are created to form a gel, and this contributes to structural fidelity under physiological conditions (Donderwinkel *et al*., 2017). Another example is methylcellulose which produces a thermo-responsive hydrogel when mixed in an aqueous solution. An increase in temperature induces a sol-gel transition, and this transition is also accompanied by a change from hydrophilic in the solution state to hydrophobic in gel state (Cochis *et al*., 2018). Additionally, this gel state and the surface hydrophobicity at physiological temperatures permit the adherence and proliferation of cells (Cochis *et al*., 2018), making it a useful polymer for maintenance of structural fidelity, as well as useful in terms of bioactivity. Agarose exhibits pronounced hysteresis and gels at below 18-42°C, thus remaining a liquid to enable easy printing, but solidifies once printed onto a cooled surface (Tan *et al*., 2016) when double stranded helices aggregate (Arnott *et al*., 1974). This behaviour can make it a good polymer to ensure instantaneous solidification to ensure structural fidelity. Collagen is another polymer that is useful as an additive in soft tissue engineering, but takes a longer time to gel (at 37°C) compared to other thermoresponsive hydrogels (Suntornnond *et al*., 2016). Pluronic gelation relies on temperature, as well as concentration, and occurs through an interaction of micelles. In terms of temperature, Pluronic F127 gels at 10-40°C which makes it suitable for printing at room temperature and usable at physiological temperatures. Due to its lack of long-term cell viability, it is commonly used for its ideal printing properties as a sacrificial material (Suntornnond *et al*., 2016).

However, materials which only gel at physiological temperatures can prove to be a problem through the compromise of initial structural fidelity when printed at room temperature. For this reason, it is also useful to consider polymers which can contribute instantaneous gelling once

printed. A polymer such as gelatin forms a helix below 35°C (Donderwinkel *et al*., 2017), where helix-chain aggregation causes gelation, and as such can be used to gel at room temperature. In a bioprinting environment, gelatin should be printed at an increased temperature which will decrease the viscosity of the solution (Billiet *et al*., 2014) thus encouraging printability. However, this decrease in viscosity will obviously inhibit gelation for instantaneous structural fidelity upon printing, and this issue must be rectified by deposition onto a cooled surface in order to solidify (Duan *et al*., 2013).

Thermoplastic polymers are another option in terms of temperature-dependent bioinks. Their melt-responsiveness to high temperatures and subsequent plastic behaviours upon cooling, results in structures with impressive mechanical strength and resolution. As such, they are often used for mechanical support in hybrid bioprinting through the co-deposition of hydrogels and thermoplastic polymers (Schuurman *et al*., 2011). Thermoplastic polymers also have the advantage of mechanical tunability through parameters such as the molecular weight of the polymer, strand spacing, strand size and strand orientation (Olubamiji *et al*., 2016). However, it is important to note that the usually high temperatures required for melting thermoplastic polymers may impair the viability of cells, and as such, constructs would rely on cell-seeding post-printing (You *et al*., 2017).

The temperature dependency of polymers is thus useful to note as the above polymers can be used as additives in bioinks to induce long-term gelling at physiological temperatures, or instantaneous gelling at room temperature, depending on what property the bioink lacks.

2.6.2 Altering Concentration

Concentration dependency is a vital and easy-to-manipulate property of bioinks. Often, as proven below, viscosity of a solution is concentration dependent and this is useful in assessing the

printability of a solution. Varying concentrations can also be used to improve bioactivity, as well as mechanical properties, which ultimately makes it an incredibly important parameter to consider during preformulation.

As mentioned previously, agarose is a commonly used polymer in soft tissue engineering. Not only does it display thermogelling which is useful in its structural fidelity post-printing, but its viscosity is directly concentration dependent (Forget *et al*., 2017), which is a useful property during printing when higher viscosities are required. Hydroxyapatite has also been used as an additive in order to increase the viscosity of a formulation, thus enhancing the printability, and at the same time, increases the biocompatibility (Wust *et al*., 2014). Utilizing low concentrations of silicon-substituted hydroxyapatite, results in even better bioactivity (Meseguer-Olmo *et al*., 2013). 4-arm poly (ethylene glycol)- tetra-acrylate (PEGTA) is also often used in bioinks. It works by increasing viscosity through its mechanism of increasing mass concentration, resulting in constructs with good printing fidelity (Jia *et al*., 2016).

Hyaluronic acid has proven its use as an additive as well, the consequence of which is concentration dependent. Due to its naturally occurring abundance in native tissues, hyaluronic acid may prove valuable in a cellular environment. It exhibits an anabolic effect on ECM synthesis (Boere *et al*., 2015), and has proven to enhance chondrogenesis, thus confirming its value in a cellular environment, and works at low concentrations. Hyaluronic acid also presents as a more viscous material which would be useful as an additive to alter the viscosity of a bioink to improve extrusion-based printability (Schuurman *et al*., 2013). In this case, a higher concentration is required when compared to the concentration used to enhance bioactivity (Boere *et al*., 2015).

Additionally, in terms of bioactivity, the concentration of mesoporous bioactive glass (MBG) directly impacts cellular differentiation, as well as cell proliferation (Pei *et al*., 2016).

It was also previously mentioned that gelatin becomes liquid at physiological temperatures. This can be overcome and a physiologically stable hydrogel (Nichol *et al*., 2010) can be formed through the modification of gelatin with unsaturated methacrylate groups (Schuurman *et al*., 2013) to GelMA, which is also photopolymerizable (Zhou *et al*., 2017) thus expanding its potential for use. This GelMA can be used in blends with other polymers, with an increase in GelMA concentration, at a constant degree of methacrylation, exhibiting significantly improved mechanical properties in the produced construct (Schuurman *et al*., 2013). In terms of alginate which requires ionic crosslinking in order to be efficiently utilized in bioprinting, an increase in crosslinker concentration leads to higher degrees of crosslinking, which results in enhanced recovery and structural integrity (Pan *et al*., 2016).

2.7 Concluding Remarks

Bioinks exhibit a promising role in tissue engineering and regenerative medicine with the potential to dominate the industry, but is still in its infancy and requires a lot more research and development in order to be fully understood and exploited to its full potential. Despite great strides in technological advances, the development of bioinks still remains insufficient, and as yet, there has been no report of a singular bioink which fulfils all of the properties required to be bioprinted for tissue engineering. There is also a dearth of existing materials, and research should be dedicated towards discovering and developing novel bioinks. The utopian scenario would be the discovery of new materials that are specifically applicable for the purpose of 3D bioprinting, along with the development of more cost-effective bioprinting technology. Realistically, research should focus on what is currently available by dedicating research towards understanding, improving and optimizing the properties of existing materials, so as to enhance their applicability. The ‘ideal’ bioink, as mentioned above, exhibits a range of properties such as good printability, structural fidelity and mechanical strength, as well as biocompatibility and bioactivity. It is essential to quantify the properties of biomaterials and compare them to those of the ‘ideal’ bioink, so that

their strengths may be exploited and weaknesses combatted through functionalizations and modifications. An alternative way forward is to further research physical properties relating to the materials used and the actual printing process, and exploit them as necessary. Overall, it is essential that research be focused on bioink development and subsequent manipulation of their properties, if the realm of tissue engineering is expected to advance.

References

Arlov, Ø., Aachmann, F. L., Sundan, A., Espevik, T. & Skjåk-Bræk, G. 2014. Heparin-Like Properties of Sulfated Alginates with Defined Sequences and Sulfation Degrees. *Biomacromolecules,* 15**,** 2744-2750.

Arnott, S., Fulmer, A., Scott, W., Dea, I., Moorhouse, R. & Rees, D. 1974. The agarose double helix and its function in agarose gel structure. *Journal of molecular biology,* 90**,** 269-284.

Asa'ad, F., Pagni, G., Pilipchuk, S. P., Giannì, A. B., Giannobile, W. V. & Rasperini, G. 2016. 3D-Printed Scaffolds and Biomaterials: Review of Alveolar Bone Augmentation and Periodontal Regeneration Applications. *International Journal of Dentistry,* 2016.

Augst, A. D., Kong, H. J. & Mooney, D. J. 2006. Alginate hydrogels as biomaterials. *Macromol Biosci,* 6**,** 623-33.

Bae, H. J., Darby, D. O., Kimmel, R. M., Park, H. J. & Whiteside, W. S. 2009. Effects of transglutaminase-induced cross-linking on properties of fish gelatin–nanoclay composite film. *Food chemistry,* 114**,** 180-189.

Baolin, G. & Ma, P. X. 2014. Synthetic biodegradable functional polymers for tissue engineering: a brief review. *Science China. Chemistry,* 57**,** 490-500.

Bigi, A., Cojazzi, G., Panzavolta, S., Roveri, N. & Rubini, K. 2002. Stabilization of gelatin films by crosslinking with genipin. *Biomaterials,* 23**,** 4827-32.

Billiet, T., Gevaert, E., De Schryver, T., Cornelissen, M. & Dubruel, P. 2014. The 3D printing of gelatin methacrylamide cell-laden tissue-engineered constructs with high cell viability. *Biomaterials,* 35**,** 49-62.

Boere, K. W., Blokzijl, M. M., Visser, J., Linssen, J. E. A., Malda, J., Hennink, W. E. & Vermonden, T. 2015. Biofabrication of reinforced 3D-scaffolds using two-component hydrogels. *Journal of Materials Chemistry B,* 3**,** 9067-9078.

Boere, K. W., Visser, J., Seyednejad, H., Rahimian, S., Gawlitta, D., Van Steenbergen, M. J., Dhert, W. J., Hennink, W. E., Vermonden, T. & Malda, J. 2014. Covalent attachment of a three-dimensionally printed thermoplast to a gelatin hydrogel for mechanically enhanced cartilage constructs. *Acta biomaterialia,* 10**,** 2602-2611.

Chan, B. P. & Leong, K. W. 2008. Scaffolding in tissue engineering: general approaches and tissue-specific considerations. *European Spine Journal,* 17**,** 467-479.

Chen, F.-M. & Liu, X. 2016. Advancing biomaterials of human origin for tissue engineering. *Progress in polymer science,* 53**,** 86-168.

Cochis, A., Bonetti, L., Sorrentino, R., Contessi Negrini, N., Grassi, F., Leigheb, M., Rimondini, L. & Farè, S. 2018. 3D Printing of Thermo-Responsive Methylcellulose Hydrogels for Cell-Sheet Engineering. *Materials (Basel, Switzerland),* 11**,** 579.

Colosi, C., Shin, S. R., Manoharan, V., Massa, S., Costantini, M., Barbetta, A., Dokmeci, M. R., Dentini, M. & Khademhosseini, A. 2016. Microfluidic Bioprinting of Heterogeneous 3D Tissue Constructs Using Low-Viscosity Bioink. *Advanced Materials,* 28**,** 677-684.

Crapo, P. M., Gilbert, T. W. & Badylak, S. F. 2011. An overview of tissue and whole organ decellularization processes. *Biomaterials,* 32**,** 3233-3243.

Cui, H., Zhu, W., Holmes, B. & Zhang, L. G. 2016. Biologically Inspired Smart Release System Based on 3D Bioprinted Perfused Scaffold for Vascularized Tissue Regeneration. *Adv Sci (Weinh),* 3**,** 1600058.

Daly, A. C., Critchley, S. E., Rencsok, E. M. & Kelly, D. J. 2016. A comparison of different bioinks for 3D bioprinting of fibrocartilage and hyaline cartilage. *Biofabrication,* 8**,** 045002.

Datta, P., Barui, A., Wu, Y., Ozbolat, V., Moncal, K. K. & Ozbolat, I. T. 2018. Essential Steps In Bioprinting: From Pre- To Post-Bioprinting. *Biotechnology Advances,* 36**,** 1481-1504.

Demirtas, T. T., Irmak, G. & Gumusderelioglu, M. 2017. A bioprintable form of chitosan hydrogel for bone tissue engineering. *Biofabrication,* 9**,** 035003.

Dias, A. D., Kingsley, D. M. & Corr, D. T. 2014. Recent advances in bioprinting and applications for biosensing. *Biosensors,* 4**,** 111-136.
Do, A.-V., Khorsand, B., Geary, S. M. & Salem, A. K. 2015. 3D Printing of Scaffolds for Tissue Regeneration Applications. *Advanced healthcare materials,* 4**,** 1742-1762.
Donderwinkel, I., Van Hest, J. C. & Cameron, N. R. 2017. Bioinks for 3D bioprinting: recent advances and future prospects. *Polymer Chemistry,* 8**,** 4451-4471.
Duan, B., Hockaday, L. A., Kang, K. H. & Butcher, J. T. 2013. 3D bioprinting of heterogeneous aortic valve conduits with alginate/gelatin hydrogels. *J Biomed Mater Res A,* 101.
Duan, B., Kapetanovic, E., Hockaday, L. A. & Butcher, J. T. 2014. Three-dimensional printed trileaflet valve conduits using biological hydrogels and human valve interstitial cells. *Acta biomaterialia,* 10**,** 1836-1846.
Egorov, A. A., Fedotov, A. Y., Mironov, A. V., Komlev, V. S., Popov, V. K. & Zobkov, Y. V. 2016. 3D printing of mineral–polymer bone substitutes based on sodium alginate and calcium phosphate. *Beilstein Journal of Nanotechnology,* 7**,** 1794-1799.
England, S., Rajaram, A., Schreyer, D. J. & Chen, X. 2017. Bioprinted fibrin-factor XIII-hyaluronate hydrogel scaffolds with encapsulated Schwann cells and their *in vitro* characterization for use in nerve regeneration. *Bioprinting,* 5**,** 1-9.
Fedorovich, N. E., Swennen, I., Girones, J., Moroni, L., Van Blitterswijk, C. A., Schacht, E., Alblas, J. & Dhert, W. J. 2009. Evaluation of photocrosslinked Lutrol hydrogel for tissue printing applications. *Biomacromolecules,* 10**,** 1689-96.
Forget, A., Blaeser, A., Miessmer, F., Kopf, M., Campos, D. F. D., Voelcker, N. H., Blencowe, A., Fischer, H. & Shastri, V. P. 2017. Mechanically Tunable Bioink for 3D Bioprinting of Human Cells. *Adv Healthc Mater,* 6.
Frisman, I., Seliktar, D. & Bianco-Peled, H. 2011. Nanostructuring PEG-fibrinogen hydrogels to control cellular morphogenesis. *Biomaterials,* 32**,** 7839-46.
Gong, J. P., Katsuyama, Y., Kurokawa, T. & Osada, Y. 2003. Double-Network Hydrogels with Extremely High Mechanical Strength. *Advanced Materials,* 15**,** 1155-1158.
Guvendiren, M., Molde, J., Soares, R. M. D. & Kohn, J. 2016. Designing Biomaterials for 3D Printing. *ACS Biomaterials Science & Engineering,* 2**,** 1679-1693.
He, Y., Yang, F., Zhao, H., Gao, Q., Xia, B. & Fu, J. 2016. Research on the printability of hydrogels in 3D bioprinting. *Scientific Reports,* 6**,** 29977.
Helseth, D. & Veis, A. 1981. Collagen self-assembly *in vitro*. Differentiating specific telopeptide-dependent interactions using selective enzyme modification and the addition of free amino telopeptide. *Journal of Biological Chemistry,* 256**,** 7118-7128.
Holzl, K., Lin, S., Tytgat, L., Van Vlierberghe, S., Gu, L. & Ovsianikov, A. 2016. Bioink properties before, during and after 3D bioprinting. *Biofabrication***,** 10.1088/1758-5090/8/3/032002.
Hoque, M. E., San, W. Y., Wei, F., Li, S., Huang, M.-H., Vert, M. & Hutmacher, D. W. 2009. Processing of polycaprolactone and polycaprolactone-based copolymers into 3D scaffolds, and their cellular responses. *Tissue Engineering Part A,* 15**,** 3013-3024.
Hospodiuk, M., Dey, M., Sosnoski, D. & Ozbolat, I. T. 2017. The bioink: A comprehensive review on bioprintable materials. *Biotechnology Advances*.
Hu, J.-X., Ran, J.-B., Chen, S., Jiang, P., Shen, X.-Y. & Tong, H. 2016. Carboxylated Agarose (CA)-Silk Fibroin (SF) Dual Confluent Matrices Containing Oriented Hydroxyapatite (HA) Crystals: Biomimetic Organic/Inorganic Composites for Tibia Repair. *Biomacromolecules,* 17**,** 2437-2447.
Huang, J., Fu, H., Wang, Z., Meng, Q., Liu, S., Wang, H., Zheng, X., Dai, J. & Zhang, Z. 2016. BMSCs-laden gelatin/sodium alginate/carboxymethyl chitosan hydrogel for 3D bioprinting. *RSC Advances,* 6**,** 108423-108430.
Jang, J., Kim, T. G., Kim, B. S., Kim, S. W., Kwon, S. M. & Cho, D. W. 2016. Tailoring mechanical properties of decellularized extracellular matrix bioink by vitamin B2-induced photo-crosslinking. *Acta Biomaterialia,* 33**,** 88-95.

Jeong, B. & Gutowska, A. 2002. Lessons from nature: stimuli-responsive polymers and their biomedical applications. *Trends in biotechnology,* 20**,** 305-311.
Jia, J., Richards, D. J., Pollard, S., Tan, Y., Rodriguez, J., Visconti, R. P., Trusk, T. C., Yost, M. J., Yao, H. & Markwald, R. R. 2014. Engineering alginate as bioink for bioprinting. *Acta Biomaterialia,* 10**,** 4323-4331.
Jia, W., Gungor-Ozkerim, P. S., Zhang, Y. S., Yue, K., Zhu, K., Liu, W., Pi, Q., Byambaa, B., Dokmeci, M. R. & Shin, S. R. 2016. Direct 3D bioprinting of perfusable vascular constructs using a blend bioink. *Biomaterials,* 106**,** 58-68.
Kesti, M., Müller, M., Becher, J., Schnabelrauch, M., D'este, M., Eglin, D. & Zenobi-Wong, M. 2015. A versatile bioink for three-dimensional printing of cellular scaffolds based on thermally and photo-triggered tandem gelation. *Acta biomaterialia,* 11**,** 162-172.
Kirchmajer, D. M., Gorkin Iii, R. & In Het Panhuis, M. 2015. An overview of the suitability of hydrogel-forming polymers for extrusion-based 3D-printing. *Journal of Materials Chemistry B,* 3**,** 4105-4117.
Li, J., Chen, M., Fan, X. & Zhou, H. 2016. Recent advances in bioprinting techniques: approaches, applications and future prospects. *Journal of Translational Medicine,* 14**,** 271.
Luk, J. Z., Cooper-White, J., Rintoul, L., Taran, E. & Grøndahl, L. 2013. Functionalised polycaprolactone films and 3D scaffolds via gamma irradiation-induced grafting. *Journal of Materials Chemistry B,* 1**,** 4171-4181.
Markstedt, K., Mantas, A., Tournier, I., Martinez Avila, H., Hagg, D. & Gatenholm, P. 2015. 3D bioprinting human chondrocytes with nanocellulose-alginate bioink for cartilage tissue engineering applications. *Biomacromolecules,* 16.
Mastbergen, S. C., Saris, D. B. & Lafeber, F. P. 2013. Functional articular cartilage repair: here, near, or is the best approach not yet clear? *Nat Rev Rheumatol,* 9**,** 277-90.
Melchels, F. P., Blokzijl, M. M., Levato, R., Peiffer, Q. C., De Ruijter, M., Hennink, W. E., Vermonden, T. & Malda, J. 2016. Hydrogel-based reinforcement of 3D bioprinted constructs. *Biofabrication,* 8**,** 035004.
Meseguer-Olmo, L., Vicente-Ortega, V., Alcaraz-Baños, M., Calvo-Guirado, J. L., Vallet-Regí, M., Arcos, D. & Baeza, A. 2013. In-vivo behaviour of Si-hydroxyapatite/polycaprolactone/DMB scaffolds fabricated by 3D printing. *Journal of Biomedical Materials Research Part A,* 101**,** 2038-2048.
Mhanna, R., Kashyap, A., Palazzolo, G., Vallmajo-Martin, Q., Becher, J., Moller, S., Schnabelrauch, M. & Zenobi-Wong, M. 2014. Chondrocyte culture in three dimensional alginate sulfate hydrogels promotes proliferation while maintaining expression of chondrogenic markers. *Tissue Eng Part A,* 20**,** 1454-64.
Miculescu, F., Maidaniuc, A., Miculescu, M., Dan Batalu, N., Cătălin Ciocoiu, R., Voicu, Ş. I., Stan, G. E. & Thakur, V. K. 2018. Synthesis and Characterization of Jellified Composites from Bovine Bone-Derived Hydroxyapatite and Starch as Precursors for Robocasting. *ACS Omega,* 3**,** 1338-1349.
Mironov, A. V., Grigoryev, A. M., Krotova, L. I., Skaletsky, N. N., Popov, V. K. & Sevastianov, V. I. 2017. 3D printing of PLGA scaffolds for tissue engineering. *J Biomed Mater Res A,* 105**,** 104-109.
Morris, V. B., Nimbalkar, S., Younesi, M., Mcclellan, P. & Akkus, O. 2017. Mechanical properties, cytocompatibility and manufacturability of chitosan: PEGDA hybrid-gel scaffolds by stereolithography. *Annals of biomedical engineering,* 45**,** 286-296.
Müller, M., Becher, J., Schnabelrauch, M. & Zenobi-Wong, M. 2015. Nanostructured Pluronic hydrogels as bioinks for 3D bioprinting. *Biofabrication,* 7**,** 035006.
Müller, M., Öztürk, E., Arlov, Ø., Gatenholm, P. & Zenobi-Wong, M. 2017. Alginate sulfate–nanocellulose bioinks for cartilage bioprinting applications. *Annals of Biomedical Engineering,* 45**,** 210-223.

Murphy, S. V. & Atala, A. 2014. 3D bioprinting of tissues and organs. *Nat Biotech,* 32**,** 773-785.
Nakajima, T., Furukawa, H., Tanaka, Y., Kurokawa, T., Osada, Y. & Gong, J. P. 2009. True chemical structure of double network hydrogels. *Macromolecules,* 42**,** 2184-2189.
Nguyen, D., Hägg, D. A., Forsman, A., Ekholm, J., Nimkingratana, P., Brantsing, C., Kalogeropoulos, T., Zaunz, S., Concaro, S. & Brittberg, M. 2017. Cartilage Tissue Engineering by the 3D Bioprinting of iPS Cells in a Nanocellulose/Alginate Bioink. *Scientific Reports,* 7**,** 658.
Nichol, J. W., Koshy, S., Bae, H., Hwang, C. M., Yamanlar, S. & Khademhosseini, A. 2010. Cell-laden microengineered gelatin methacrylate hydrogels. *Biomaterials,* 31**,** 5536-5544.
O'Brien, F. J. 2011. Biomaterials & scaffolds for tissue engineering. *Materials Today,* 14**,** 88-95.
Olubamiji, A. D., Izadifar, Z., Si, J. L., Cooper, D. M., Eames, B. F. & Chen, D. X. 2016. Modulating mechanical behaviour of 3D-printed cartilage-mimetic PCL scaffolds: influence of molecular weight and pore geometry. *Biofabrication,* 8**,** 025020.
Oryan, A., Kamali, A., Moshiri, A., Baharvand, H. & Daemi, H. 2018. Chemical crosslinking of biopolymeric scaffolds: Current knowledge and future directions of crosslinked engineered bone scaffolds. *Int J Biol Macromol,* 107**,** 678-688.
Ozbolat, I. T. & Hospodiuk, M. 2016. Current advances and future perspectives in extrusion-based bioprinting. *Biomaterials,* 76**,** 321-43.
Ozbolat, I. T. & Yu, Y. 2013. Bioprinting Toward Organ Fabrication: Challenges and Future Trends. *IEEE Transactions on Biomedical Engineering,* 60**,** 691-699.
Pan, T., Song, W., Cao, X. & Wang, Y. 2016. 3D Bioplotting of Gelatin/Alginate Scaffolds for Tissue Engineering: Influence of Crosslinking Degree and Pore Architecture on Physicochemical Properties. *Journal of Materials Science & Technology,* 32**,** 889-900.
Panwar, A. & Tan, L. P. 2016. Current status of bioinks for micro-extrusion-based 3D bioprinting. *Molecules,* 21**,** 685.
Park, Y.-O., Myung, S.-W., Kook, M.-S., Jung, S.-C. & Kim, B.-H. 2016. Cell Proliferation on Macro/Nano Surface Structure and Collagen Immobilization of 3D Polycaprolactone Scaffolds. *Journal of Nanoscience and Nanotechnology,* 16**,** 1415-1419.
Pei, P., Qi, X., Du, X., Zhu, M., Zhao, S. & Zhu, Y. 2016. Three-dimensional printing of tricalcium silicate/mesoporous bioactive glass cement scaffolds for bone regeneration. *Journal of Materials Chemistry B,* 4**,** 7452-7463.
Pescosolido, L., Schuurman, W., Malda, J., Matricardi, P., Alhaique, F., Coviello, T., Van Weeren, P. R., Dhert, W. J., Hennink, W. E. & Vermonden, T. 2011. Hyaluronic acid and dextran-based semi-IPN hydrogels as biomaterials for bioprinting. *Biomacromolecules,* 12**,** 1831-1838.
Piras, C. C., Fernández-Prieto, S. & De Borggraeve, W. M. 2017. Nanocellulosic materials as bioinks for 3D bioprinting. *Biomaterials Science,* 5**,** 1988-1992.
Rajaram, A., Schreyer, D. & Chen, D. 2014. Bioplotting alginate/hyaluronic acid hydrogel scaffolds with structural integrity and preserved Schwann cell viability. *3D Printing and Additive Manufacturing,* 1**,** 194-203.
Rhee, S., Puetzer, J. L., Mason, B. N., Reinhart-King, C. A. & Bonassar, L. J. 2016. 3D bioprinting of spatially heterogeneous collagen constructs for cartilage tissue engineering. *ACS Biomaterials Science & Engineering,* 2**,** 1800-1805.
Rouillard, A. D., Berglund, C. M., Lee, J. Y., Polacheck, W. J., Tsui, Y., Bonassar, L. J. & Kirby, B. J. 2011. Methods for photocrosslinking alginate hydrogel scaffolds with high cell viability. *Tissue Eng Part C Methods,* 17**,** 173-9.
Rutz, A. L., Hyland, K. E., Jakus, A. E., Burghardt, W. R. & Shah, R. N. 2015. A multimaterial bioink method for 3D printing tunable, cell-compatible hydrogels. *Advanced Materials,* 27**,** 1607-1614.
Schutz, K., Placht, A. M., Paul, B., Bruggemeier, S., Gelinsky, M. & Lode, A. 2017. Three-dimensional plotting of a cell-laden alginate/methylcellulose blend: towards biofabrication

of tissue engineering constructs with clinically relevant dimensions. *J Tissue Eng Regen Med,* 11**,** 1574-1587.
Schuurman, W., Khristov, V., Pot, M. W., Van Weeren, P. R., Dhert, W. J. & Malda, J. 2011. Bioprinting of hybrid tissue constructs with tailorable mechanical properties. *Biofabrication,* 3**,** 021001.
Schuurman, W., Levett, P. A., Pot, M. W., Van Weeren, P. R., Dhert, W. J., Hutmacher, D. W., Melchels, F. P., Klein, T. J. & Malda, J. 2013. Gelatin-methacrylamide hydrogels as potential biomaterials for fabrication of tissue-engineered cartilage constructs. *Macromol Biosci,* 13**,** 551-61.
Serra, T., Ortiz-Hernandez, M., Engel, E., Planell, J. A. & Navarro, M. 2014. Relevance of PEG in PLA-based blends for tissue engineering 3D-printed scaffolds. *Materials Science and Engineering: C,* 38**,** 55-62.
Shin, H., Olsen, B. D. & Khademhosseini, A. 2012. The mechanical properties and cytotoxicity of cell-laden double-network hydrogels based on photocrosslinkable gelatin and gellan gum biomacromolecules. *Biomaterials,* 33**,** 3143-3152.
Shirazi, S. F. S., Gharehkhani, S., Mehrali, M., Yarmand, H., Metselaar, H. S. C., Kadri, N. A. & Osman, N. A. A. 2015. A review on powder-based additive manufacturing for tissue engineering: selective laser sintering and inkjet 3D printing. *Science and Technology of Advanced Materials,* 16**,** 033502.
Skardal, A. & Atala, A. 2015. Biomaterials for Integration with 3D Bioprinting. *Annals of Biomedical Engineering,* 43**,** 730-746.
Skardal, A., Zhang, J., Mccoard, L., Xu, X., Oottamasathien, S. & Prestwich, G. D. 2010. Photocrosslinkable hyaluronan-gelatin hydrogels for two-step bioprinting. *Tissue Engineering Part A,* 16**,** 2675-2685.
Sultan, S., Siqueira, G., Zimmermann, T. & Mathew, A. P. 2017. 3D printing of nano-cellulosic biomaterials for medical applications. *Current Opinion in Biomedical Engineering*.
Sundaramurthi, D., Rauf, S. & Hauser, C. 2016. 3D bioprinting technology for regenerative medicine applications. *2016,* 2**,** 19.
Suntornnond, R., An, J. & Chua, C. K. 2016. Bioprinting of Thermoresponsive Hydrogels for Next Generation Tissue Engineering: A Review. *Macromolecular Materials and Engineering*.
Tan, Y. J., Tan, X., Yeong, W. Y. & Tor, S. B. 2016. Hybrid microscaffold-based 3D bioprinting of multi-cellular constructs with high compressive strength: A new biofabrication strategy. *Scientific Reports,* 6.
Thakur, S., Govender, P., Mamo, M., Tamulevičius, S., Mishra, Y. & Thakur, V. K. 2017. Progress in lignin hydrogels and nanocomposites for water purification: Future perspectives. *Vacuum*, 146, 342-355
Thakur, S., Govender, P., Mamo, M., Tamulevičius, S. & Thakur, V. K. 2017. Recent progress in gelatin hydrogel nanocomposites for water purification and beyond. *Vacuum,* 146, 396-408
Tirella, A., Liberto, T. & Ahluwalia, A. 2012. Riboflavin and collagen: New crosslinking methods to tailor the stiffness of hydrogels. *Materials Letters,* 74**,** 58-61.
Velasco, M. A., Narváez-Tovar, C. A. & Garzón-Alvarado, D. A. 2015. Design, Materials, and Mechanobiology of Biodegradable Scaffolds for Bone Tissue Engineering. *BioMed Research International,* 2015**,** 729076.
Wang, X.-F., Lu, P.-J., Song, Y., Sun, Y.-C., Wang, Y.-G. & Wang, Y. 2016. Nano hydroxyapatite particles promote osteogenesis in a three-dimensional bio-printing construct consisting of alginate/gelatin/hASCs. *RSC Advances,* 6**,** 6832-6842.
Wust, S., Godla, M. E., Muller, R. & Hofmann, S. 2014. Tunable hydrogel composite with two-step processing in combination with innovative hardware upgrade for cell-based three-dimensional bioprinting. *Acta Biomater,* 10.

Wüst, S., Godla, M. E., Müller, R. & Hofmann, S. 2014. Tunable hydrogel composite with two-step processing in combination with innovative hardware upgrade for cell-based three-dimensional bioprinting. *Acta biomaterialia,* 10**,** 630-640.
Xu, T., Zhao, W., Zhu, J.-M., Albanna, M. Z., Yoo, J. J. & Atala, A. 2013. Complex heterogeneous tissue constructs containing multiple cell types prepared by inkjet printing technology. *Biomaterials,* 34**,** 130-139.
You, F., Eames, B. F. & Chen, X. 2017. Application of Extrusion-Based Hydrogel Bioprinting for Cartilage Tissue Engineering. *International Journal of Molecular Sciences,* 18**,** 1597.
Zeng, S., Ye, J., Cui, Z., Si, J., Wang, Q., Wang, X., Peng, K. & Chen, W. 2017. Surface biofunctionalization of three-dimensional porous poly (lactic acid) scaffold using chitosan/OGP coating for bone tissue engineering. *Materials Science and Engineering: C,* 77**,** 92-101.
Zhang, J., Zhao, S., Zhu, Y., Huang, Y., Zhu, M., Tao, C. & Zhang, C. 2014. Three-dimensional printing of strontium-containing mesoporous bioactive glass scaffolds for bone regeneration. *Acta biomaterialia,* 10**,** 2269-2281.
Zhang, K., Fu, Q., Yoo, J., Chen, X., Chandra, P., Mo, X., Song, L., Atala, A. & Zhao, W. 2017. 3D bioprinting of urethra with PCL/PLCL blend and dual autologous cells in fibrin hydrogel: an *in vitro* evaluation of biomimetic mechanical property and cell growth environment. *Acta biomaterialia,* 50**,** 154-164.
Zhang, Y. S., Yue, K., Aleman, J., Mollazadeh-Moghaddam, K., Bakht, S. M., Yang, J., Jia, W., Dell'erba, V., Assawes, P. & Shin, S. R. 2017. 3D bioprinting for tissue and organ fabrication. *Annals of biomedical engineering,* 45**,** 148-163.
Zhao, F., Zhang, W., Fu, X., Xie, W. & Chen, X. 2016. Fabrication and characterization of bioactive glass/alginate composite scaffolds by a self-crosslinking processing for bone regeneration. *RSC Advances,* 6**,** 91201-91208.
Zhou, M., Lee, B. H. & Tan, L. P. 2017. A dual crosslinking strategy to tailor rheological properties of gelatin methacryloyl.

CHAPTER 3
IDENTIFYING APPROPRIATE MATERIALS AND OPTIMISING THE BIOINK FORMULATION

3.1 Introduction

Bioinks must present with biological compatibility (O'Brien, 2011), as well as printing compatibility (Chung *et al*., 2013), and should possess post-printing behaviour which enables it to retain its architecturally biomimetic printed structure (Murphy and Atala, 2014). As biomaterials had not been originally intended for 3D printing, the required properties are often not found in a singular biomaterial. As such, research should be done in order to identify the most effective biomaterial combinations, as well as research on untraditional biomaterials for their potential in the bioprinting process, in order to contribute towards the currently limited database of available materials.

This chapter assesses various biomaterials for their applicability in the 3D bioprinting process through qualitative testing. The results of these tests were then analysed in order to formulate a bioink that was printed and characterized for its various properties, including mechanical strength, thermal transitions, chemical transitions and *in vitro* degradation behaviour.

3.2 Evaluating Various Polymers for their Potential Use as Bioinks

3.2.1 Materials and Methods

Poly (3-hydroxybutyric acid-co-3-hydroxyvaleric acid) (PHBV) (HV content: 12%), Cellulose Acetate Phthalate (CAP), Propylene Carbonate (PC) and Triethyl Citrate (TEC) were purchased from Sigma-Aldrich (St. Louis, MO, USA). Hydroxypropyl cellulose (HPC) was purchased from Hercules Inc (Wilmington, Delaware, USA). Chloroform was bought from Merck (South Africa). Glycerol and acetone were obtained from Associated Chemical Enterprises (Pty) Ltd (South Africa). Ethanol was purchased from MK Chemical (South Africa). All products were used without modifications unless specified.

3.2.2 Evaluation of Potential Polymers for Bioink Consideration

3.2.2.1 Poly (2-hydroxyethyl methacrylate) (pHEMA)

pHEMA is a hydrophilic polymer which is commonly used to manufacture contact lenses (Dragusin *et al*., 2012). While it does present as soft and flexible, and its physical properties can be easily tailored through formulation chemistry (Flynn *et al*., 2003), it is bioinert, and if unmodified, resists cellular attachment and proliferation (Badea *et al*., 2017). pHEMA has also been shown to resist biodegradation (Atzet *et al*., 2008), which may induce undesirable immune responses, as well as negatively affect de novo-tissue growth and functionality. As such, it does present with limited usage in biomedical applications, unless modified.

3.2.2.2 Poly (3-hydroxybutyric acid-co-3-hydroxyvaleric acid) (PHBV)

PHBV is an aliphatic polyester (Chiulan *et al*., 2018) produced by microorganisms (Ferreira *et al*., 2002). It is a relatively more expensive polymer (Javadi *et al*., 2010), when compared to other readily available materials, but is less crystalline than its homopolymer (polyhydroxybutyrate) (Pascu *et al*., 2013), is highly biocompatible and biodegradable (Chiulan *et al*., 2018), presents with thermoplastic properties (Kose *et al*., 2003), possesses good oxygen permeability and mechanical strength (Pascu *et al*., 2013). PHBV has not been previously utilized in the 3D bioprinting sphere, and was chosen as the primary polymer to study due to its biological properties which make it a promising avenue for tissue engineering.

PHBV was evaluated for its solubility, gelling and melting properties in order to attempt to create an extrudable formulation (Table 3.1)

Table 3.1 Evaluation of PHBV as a potential bioink for 3D Bioprinting

	PHBV melting	**PHBV gelling**	**PHBV solubility**
Result	The PHBV pellet was melted at 110 °C. The polymer was melted down and possessed impressive mechanical properties. However, it did present as brittle, and would be difficult to print due to its lack of flow properties, even when melted.	PHBV was dissolved in toluene under heating. Upon cooling, it became a gel, thus displaying thermoreversible gelling properties. While this would be a useful property during the printing process, the gelled structure does not present with optimal resolution or structural fidelity. A second method of stabilizing would be required. Extraction of the solvent would also be necessary as it would not simply evaporate, and this would also compromise the structural fidelity.	PHBV was dissolved in chloroform under heat. The solution was homogenous and the polymer was observed to have completely dissolved. However, it was too viscous to be used as a bioink, as when it was extruded it did not solidify at all.

These results from various methods of attempting to formulate a PHBV bioink lead to the decision to consider utilizing a second polymer which could contribute its own properties, thus potentially improving printability, structural fidelity, as well as cost-effectiveness

3.2.3 Effect of combination of polymers

Following the identification of the primary polymer, various other polymers were assessed for their effect upon blending with PHBV

3.2.3.1 Hydroxypropyl Cellulose (HPC)

HPC is methylcellulose which has been modified through the attachment of propylene glycol ether groups to its anhydroglucose groups (Fatimi *et al*., 2008). HPC is available in different grades,

with varying degrees of substitution, cross-linking density, pH and temperature sensitivity, and rheological behaviour (Majee, 2016) exhibiting its potentially extensive usage. HPC has also proven to positively affect the viscosity of a formulation to assist in efficient extrusion for bioprinting processes (Stewart, 2017), making it a viable candidate as an additive polymer.

3.2.3.2 Cellulose Acetate Phthalate (CAP)

CAP, an uncommon 3D bioprinting material, is a mixed ester of cellulose (Dobos *et al*., 2015) commonly used as enteric tablet coating material due to its pH dependent solubility (Roxin *et al*., 1998). Little research has been done on it as a possible bioink, with most research being dedicated to its contributions as a pharmaceutical excipient (Dobos *et al*., 2015), perhaps due to its solubility in physiological pH. However, it is inexpensive, non-toxic (Neurath *et al*., 2001), biocompatible, and has shown potential in promoting cellular growth (Shrestha *et al*., 2016), making it a promising polymer to consider for tissue engineering.

3.2.3.3 Effects of Concentration

The polymers identified above were blended and subjected to the printing process in order to evaluate their printability and subsequent structural properties. Table 3.2 shows the various polymers blended at different concentrations and their effects.

Table 3.2 Printability of various polymers in various concentrations

Conc. of PHBV	**Concentration of HPC**			**Concentration of CAP**			
	2%	**5%**	**10%**	**2%**	**5%**	**10%**	**35%**
5%	Formulation not viscous enough to extrude continuous filaments	Extrudes filaments, but layers collapse in on each other as the construct takes too long to solidify.	Construct solidifies slowly, as such the structure cannot sustain structural fidelity.	Formulation not viscous enough to extrude continuous filaments	Formulation is extrudable as a low viscosity solution, but doesn't solidify effectively	Formulation is extrudable, but does not solidify, which results in compromised resolution and structural fidelity.	Formulation exhibits improved printability, adherent layers, rapid solidification, good resolution and clearly defined pores.
10%	Formulation not viscous enough to extrude continuous filaments	Formulation not viscous enough to extrude continuous filaments	Extrudes continuous filament, but layers collapse before solidification occurs	Formulation not viscous enough to extrude continuous filaments	Extrudable, but cannot print subsequent layers due to slow solidification	Extrudable, but doesn't solidify rapidly, thus subsequent layers are compromised	Formulation can be extruded, but no adhesion present between layers.
15%	Formulation not viscous enough to extrude continuous filaments	Formulation not viscous enough to extrude continuous filaments	Extrudes continuous filaments which initially display adherence, but subsequent layers separate and lose their structure	Formulation not viscous enough to extrude continuous filaments	Extrudes filaments, however, filaments present as short, thin and easily breakable. Layers also do not adhere to each other.	Formulation is printable and results in adherent layers. However, solidification is slow resulting in compromised fidelity and resolution.	Formulation is extrudable but produces non-adherent filaments, resulting in a brittle, separated structure.

The results of Table 3.2 show that an increase in concentration of CAP, when combined with a lower concentration of PHBV results in a homogenous and printable novel bioink (a

combination of two previously unprintable polymers) – of which the most successful combination has been highlighted. The increase in CAP concentration improved the pore architecture control, as well as the resolution of the printed structure.

3.2.4 Effect of Plasticizers

Plasticizers are necessary to overcome brittleness and enhance flexibility, as well as to improve flow properties (Mohsin *et al*., 2011). They work by interfering with molecular interactions and decreasing the intermolecular forces, thus increasing the mobility of the chains and resulting in improved flexibility and extensibility (Wongsasulak *et al*., 2010). Plasticizers are selected for specific systems, depending on required criteria including compatibility, amount needed and desired physical properties (Mohsin *et al*., 2011).

3.2.4.1 Triethyl Citrate (TEC)

Triethyl Citrate is a citrate ester, derived from naturally occurring citric acid, and characterized by its non-toxicity (Labrecque *et al*., 1997). It is commonly used as a plasticizer and possesses favorable physiological properties, making it a compatible option for tissue engineering applications (Ke and Sun, 2003).

3.2.4.2 Propylene Carbonate (PC)

Propylene Carbonate is a commonly utilized plasticizer used to improve ionic conductivity (Ahmad and Isa, 2016). It has also found other uses as a low-toxicity (Schäffner *et al*., 2008) solvent (Buchholz, 1997) to dissolve polymers (Sabir *et al*., 2009), a viscosity altering agent (Gibson and Tipton, 2006), a hydrophilic enhancer (Parker *et al*., 2001) or a plasticizer (Berggren *et al*., 1997, Shukla, 2004) as part of a drug delivery system. However, its use as a plasticizer in tissue engineering applications is not well documented, even though it is presented in literature as biocompatible (Berggren *et al*., 1997, Sharma *et al*., 2018) and biodegradable (Schäffner *et al*., 2008, Lucas and Halar, 1997), which are essential properties in the tissue engineering sphere. The ability of PC to improve conductivity could also potentially increase the printed constructs

potential for use in tissue engineering, as electrical conductivity improves bioactivity of the construct (Guo and Ma, 2018).

3.2.4.3 Glycerol

Glycerol is characterized by its water solubility, high-boiling point, and syrupy appearance with a sweet taste (Mohsin *et al*., 2011). It is often recognized as one of the most suitable plasticizers (Liu *et al*., 2013), and presents as non-toxic, hydroscopic, and possesses a high boiling point (Zhang and Grinstaff, 2014). As it is a naturally occurring metabolite (Zhang and Grinstaff, 2014), it is biocompatible and biodegradable, making it an ideal component of a tissue engineering system.

3.3 Preparation of the PHBV-CAP Bioink

Poly (3-hydroxybutyric acid-co-3-hydroxyvaleric acid) (PHBV) was blended with Cellulose Acetate Phthalate (CAP) in order to create the novel bioink combination.

While this blend is a novel bioink, PHBV is well documented for its brittleness (Magalhães and Andrade, 2013). In order to develop a clinically applicable bioink, parameters such as flexibility and resilience must be considered. The concept of plasticization was considered and further cemented by the concept that plasticizers improve the water resistance of CAP (Malm *et al*., 1951), and could retard its solubility in water. Preliminary studies to assess printability observed that glycerol and propylene carbonate were more effective as additives which did not inhibit the printing process, while formulations blended with triethyl citrate did not print well, with the produced structures being architecturally compromised, due to the viscosity upon extrusion. Thus, from the results of these preliminary studies, propylene carbonate and glycerol were utilized as plasticizers and evaluated for their effect on the bioink and its printed construct.

3.3.1 Materials and Methods

3.3.1.1 Materials

Poly (3-hydroxybutyric acid-co-3-hydroxyvaleric acid) (PHBV) (HV content: 12%), Cellulose Acetate Phthalate (CAP), Propylene Carbonate (PC) and Phosphate Buffered Saline (PBS) tablets were purchased from Sigma-Aldrich (St. Louis, MO, USA). Chloroform was bought from Merck (South Africa). Glycerol and acetone were obtained from Associated Chemical Enterprises (Pty) Ltd (South Africa). Ethanol was purchased from MK Chemical (South Africa). All products were used without modifications unless specified.

3.3.1.2 Synthesis of the Novel PHBV-CAP Bioink

PHBV (5% w/v) was dissolved in chloroform under heating (60°) and agitation to produce Solution A. The plasticizers (Propylene Carbonate and Glycerol) were added to Solution A as 10% w/w of the initial PHBV weight, as the solution was liquid and would allow integration of the plasticizer in the entire polymer. CAP (50% w/v) was prepared in acetone to produce Solution B. Thereafter, Solution A was added to Solution B and stirred at room temperature for approximately 10 minutes - until homogenous. A total of 3 final solutions were produced 1) PHBV-CAP (plasticizer-free) (PC), 2) PHBV-CAP-Glycerol (PC-G) and 3) PHBV-CAP-Propylene Carbonate (PC-PC).

3.3.1.3 Viscoelastic Assessment of the Bioinks

Prior to 3D-bioprinting, the bioink was evaluated using an Elasto-Sens^{TM}Bio instrument (Rheolution, Montreal, Canada), a non-destructive and contactless technique which quantifies the dynamic displacement response of materials when subjected to a low amplitude vibration, for its change in physical properties (gelling and stiffness) over a variety of temperatures. This technique utilizes a laser to measure the displacement of the material during the vibrations. It is a useful measurement with regards to the properties of bioinks, as it helps to identify the temperature at which printing will be easiest, as well as elaborates on the behaviour of the bioink over a range in

temperature. Prior to printing, 5ml of each solution (PC, PC-PC, PC-G) was placed in detachable sample holders on top of the elastic membrane and placed in the thermal chamber of the instrument and thereafter run from 25°C to 37°C at 1 °C intervals. The test was conducted in triplicate. The data obtained measured the storage modulus (G′), and tan δ of each sample when subjected to temperature changes.

3.3.1.4 Blueprinting and Manufacture of the 3D Bioprinted Scaffolds Using the PHBV-CAP Bioink

A 3D-Bioplotter® (EnvisionTEC®, GmBH, Germany) was used to manufacture the scaffolds via a 2-step process. Firstly, the scaffold parameters were blueprinted on Magics® V18 and thereafter Bioplotter® RP software was used for stereolithographic (STL) file importation and structure fabrication (10x10x5mm with an internal linear structure). Secondly, VisualMachine software was used to regulate the 3D-Bioplotter arm and the internal structure of the scaffold.

3.3.1.5 Determination of the Chemical Transitions within the 3D-Bioprinted Scaffolds

The manufactured 3D-Bioprinted scaffolds and the native biomaterials (PHBV and CAP) were characterized for their chemical transitions by Fourier Transform Infrared (FT-IR) spectroscopy (PerkinElmer Spectrum 100, FT-IR Spectrometer, Beaconfield, UK) fitted with a universal ATR Polarization Accessory. Analysis was undertaken at high resolution with the wavelength ranging from 4000-650 cm^{-1}. Results were then analyzed for the presence of functional groups through spectral comparison with the native PHBV and CAP.

3.3.1.6 Thermal Characterization of the 3D-Bioprinted Scaffolds

The 3D-Bioprinted scaffolds were thermally analyzed via Differential Scanning Calorimetry (DSC) (Mettler Toledo, DSC-1 STARe System, Schwerzernback, Switzerland) in order to characterize the thermal properties (melting point, glass transition temperature, degradation) of the PHBV-CAP blend, as well as the effect of the plasticizers on the thermal properties of the blend. Samples of 6-8mg were weighed into aluminium crucible pans (40DL) and sealed with a 0.2 mm opening

pierced in the lid to create an open system. Samples were heated under a N_2 atmosphere with a 200ml/min flow-rate. Samples were exposed to a temperature range between 25-300°C at a rate of 10°C/min and the thermal profiles were subsequently analyzed.

3.3.1.7 Mapping of the Surface Morphology of the 3D-Bioprinted Scaffolds

Surface morphology is an essential aspect of tissue engineering, as the structure, roughness and presence of pores all dictate and affect the potential of tissue growth (Chang and Wang, 2011). The surface morphology of the 3D-Bioprinted scaffolds and the chemically functionalized scaffolds were examined by Scanning Electron Microscopy (SEM) (FEI Nova NanoLab SEM, FEI Co., Hillsboro, OR, USA). Samples were sputter-coated with Au/Pt using an EPI coater (SPI Model sputter-coater and control unit, Hester, PA, USA) before mounting and viewing.

3.3.1.8 Determination of the Mechanical Properties of the 3D-Bioprinted Scaffolds

The biomimetic mechanical properties of the 3D-Bioprinted scaffolds, as well as the chemically functionalized scaffolds, were evaluated using a BioTester 5000 Biomaterials Tester (CellScale, Waterloo, ON, Canada) equipped with a 5N load cell and a TA.XTplus Texture Analyzer (Stable MicroSystems, Surrey, UK). Biaxial tensile testing (using a BioTester 5000) was critical to evaluate the biomechanical properties of the scaffolds due to the directionality-oriented structure that was printed. For this test, scaffolds were equilibrated for 3 hours by incubation in PBS (37°C) before analysis. Samples were then mounted using BioRakes tines to position them beneath a crown press setup used to exert pressure onto the tines for adequate sample piercing. ASTM (American Society for Testing and Materials) standards provide guidelines for various materials and their available standardized tests, testing methods and parameters. As per ASTM D638 standards, the test was run at a rate of 1 mm/min, and the ramp displacement was set at 10% of the size of the original scaffold. The scaffolds were tested in triplicate and tensile Young's modulus (representative of biomaterial stiffness) was calculated from the linear elastic portion of the stress-

strain curves generated from the mean Force and Displacement curves in both x- and y- direction (n=3).

It is essential to compare the tensile properties to the constructs' compressive properties, as different tissues have different requirements for each type of force, depending on their applications. A TA. XTplus Texture Analyzer was used for compression testing of the scaffolds. A ¾'' spherical ball-probe was used to exert a force of 50N onto the mounted samples. The test ran in triplicate at a strain rate of 20%/sec and the Distance set at 1mm. Results were captured as a Force-Distance profile that was then converged to a stress-strain curve to compute the compression Young's modulus.

3.3.1.9 Comparative Biodegradation Rate Analysis of the 3D-Bioprinted Scaffolds

The biodegradation behaviour of the 3D-bioprinted scaffolds were compared. Scaffolds were washed thrice with deionized water and immersed into 20ml of PBS (pH 7.4; 37°C) (n=3). Thereafter the scaffolds were placed in an orbital shaker maintained at 37°C and 25rpm. Scaffolds were then removed at various time intervals (0, 2, 4, 6, 9, 11, 14 and 17 days) and weighed after being dried. Acidic degradation may result in byproducts which can cause autocatalysis and speed up degradation (Gong *et al*., 2003); the medium was replaced every second day in order to avoid this by simulating the physiological environment, wherein degradation products are eliminated from the body through different processes, as well as to prevent contamination.

The degradation behaviour was calculated as follows (Equation 1):

$$\%\, Degraded = \frac{W_0 - W'}{W_0}\, x\, 100 \qquad \ldots Equation\, 1$$

Where:

W' = final weight of the scaffold

W_0 = initial weight of the scaffold

The degradation rate was also calculated through determining the dry mass ratio as follows (Equation 2)

$$Dry\ Mass\ Ratio\ = \frac{M}{M_0} \qquad \ldots Equation\ 2$$

Where

M = The weight of the removed scaffold at a specific time

M_0 = The initial weight of the scaffold

The values were then used to construct a graph from which the degradation rate was calculated using the slope of the graph (Shih, 2015).

3.4 Results and Discussion

3.4.1 Manufacturing of the 3D-Bioprinted Scaffolds using the 3D Bioplotter

The bioink was transferred into a 30cc cartridge and extruded using a 25G plastic needle tip as per the parameters in Table 3.3. The bioink was printed into a petri dish containing 10ml deionized water. The layers were deposited successfully at a 90° angle to the underlying plotting platform, along an alternating x- and y- axis and solidified upon extrusion. The printed scaffolds were then stored at room temperature until further physicochemical and physicomechanical characterization.

Table 3.3 Summary of 3D-Bioprinting parameter setting used to manufacture the scaffolds

	Pressure (bar)	Temperature (°C)	Speed (m/s)
PC-PC	~1.1	26	20
PC-G	~1.7	31	20
PC	~1.6	27	20

In preparing the bioink, multiple concentrations of each polymer had to be tested in terms of printability. While the PHBV was effective at low concentrations, the concentration of CAP had to be far higher in order to permit printability. Lower concentrations of CAP resulted in difficult

printing, and could only print scaffolds with larger strand widths, with the produced constructs demonstrating lower resolution, whereas when the concentration was increased, the bioink could be printed into smaller, more defined dimensions. The printing process was undertaken as mentioned above. Once printed, the bioink's initial solidification was a result of acetone removal, which was facilitated by the presence of deionized water, due to the lower density of acetone when compared to that of water. Solidification was further improved upon the removal of water and subsequent evaporation of chloroform. The bioink was printed into a petri dish of deionized water secured upon the metal platform, as well as only onto the metal platform. Whilst both conditions did not inhibit the solidification of the bioink, the presence of water maintained the definition of the structure through slight swelling, whilst the scaffold printed onto the platform itself collapsed in on itself and did not possess clear or defined pores (Figure 3.1).

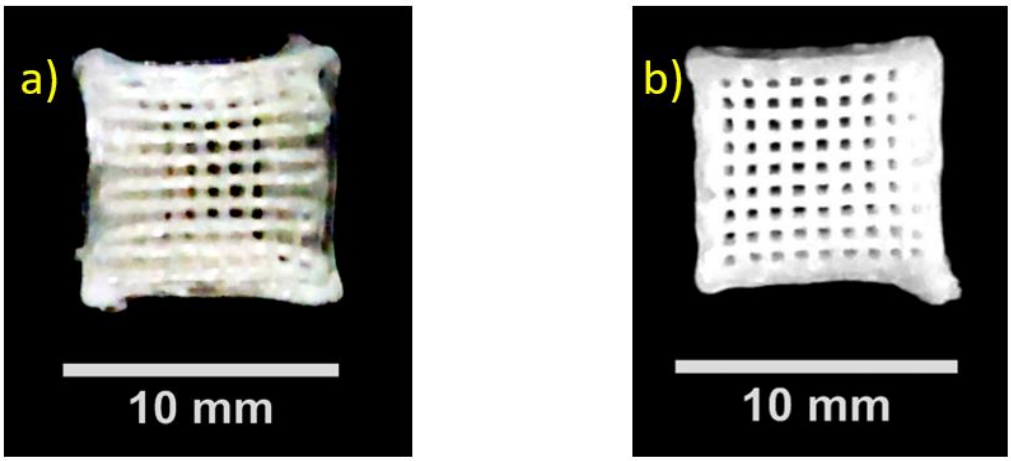


Figure 3.1 Visual depiction of the difference in fabricated scaffolds which were printed a) onto a metal platform versus b) into a petri dish filled with deionized water placed on the metal platform

Once the scaffolds were printed, they were dried and weighed, as well as measured with the average dimensions recorded (~ 8.64 x 8.55 x 4.2mm). Upon drying, the scaffolds were shown to

shrink in comparison to the theoretical dimensions (10 x 10 x 5mm) which can be attributed to the swelling behaviour of the constructs when printed.

3.4.2 Physicomechanical Analysis of the Bioink

Bioinks require materials which are easily flowable, but which also present with good solidification properties when extruded and under physiological conditions. It is useful for bioinks to act favourably at ambient temperatures, as it makes them easier to print at room temperature, without requiring other interventions which can prove tedious and increase the variables which require close control, and also does not utilize harsh conditions which can prove detrimental to cells that may be part of the bioink.

Tests measuring the viscoelastic behaviour of materials under various temperature conditions permit the identification of temperature parameters to be used in the printing process. Tan d, shown in Figure 3.2a, is the ratio of shear storage modulus to that of the loss modulus, and elaborates on the gelling behaviour of the material. Figure 3.2b, which depicts the shear storage modulus, represents the elastic solid response of the material. In Figure 3.2a, none of the samples display tan $\delta > 1$, confirming that none of them transition to a liquid state over the temperature range.

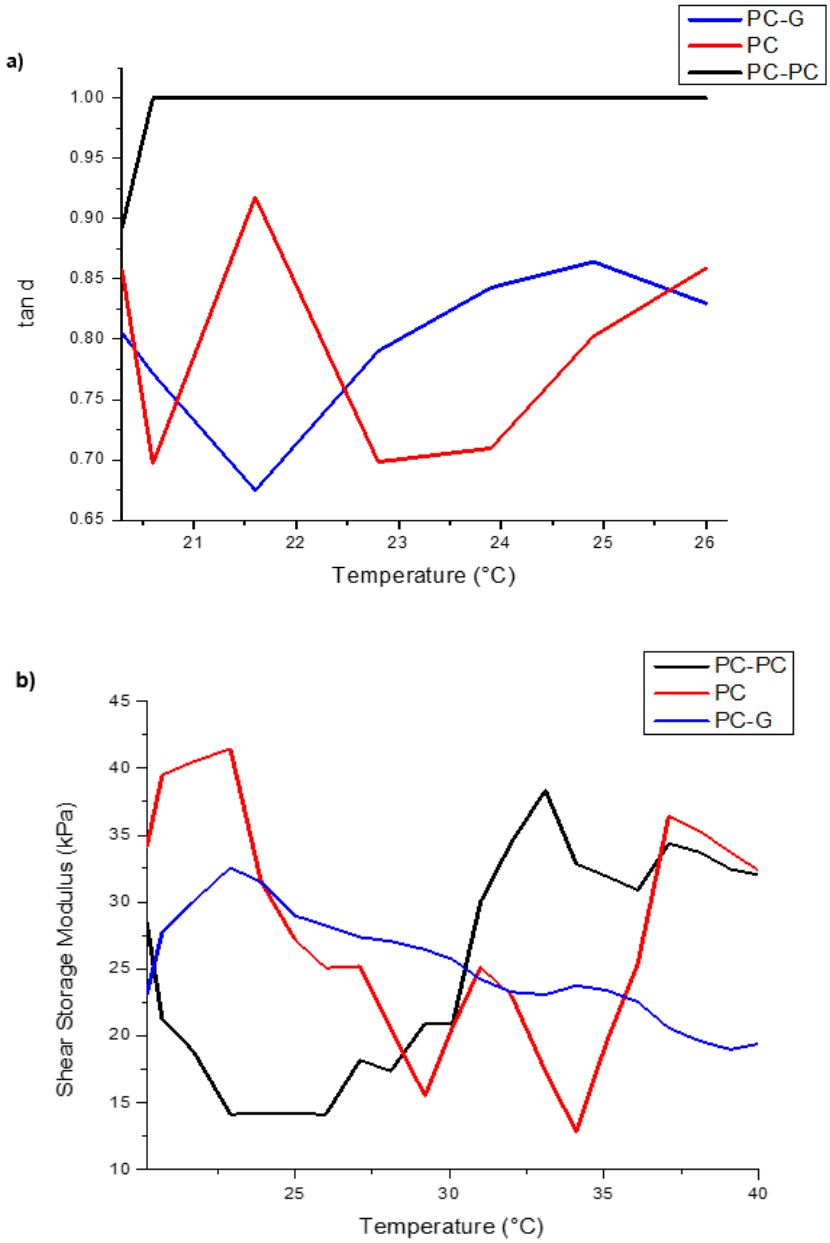


Figure 3.2 a) Graphical depiction of the change in tan d in plasticized compared to non-plasticized scaffolds as a function of temperature (SD: <0.6) b) Graphical depiction of the change in shear storage modulus in plasticized scaffolds compared to non-plasticized scaffolds as a function of temperature

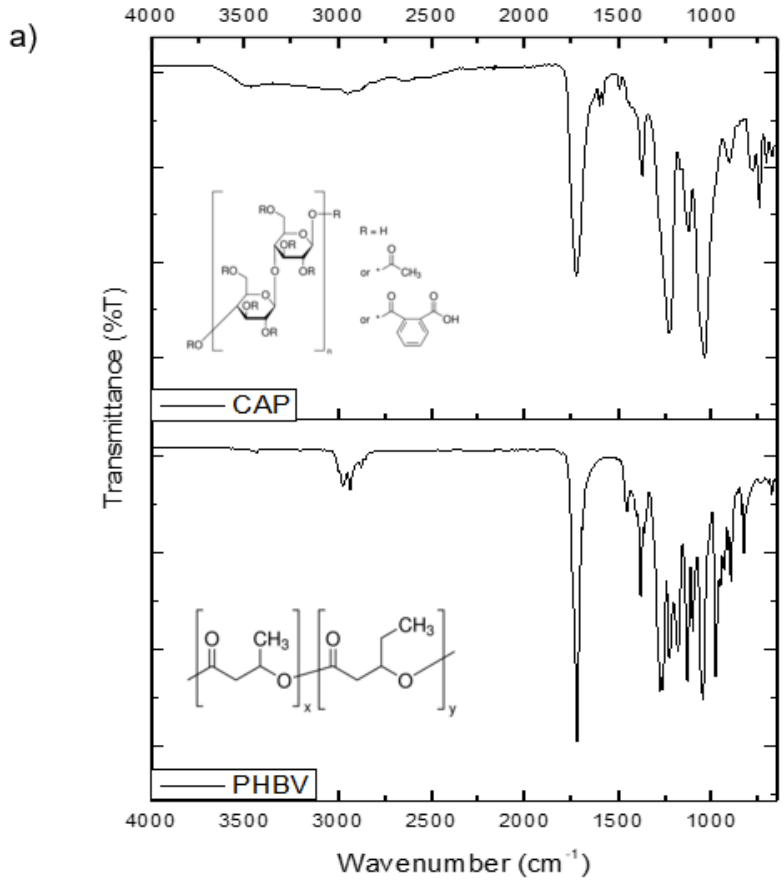
As can be observed from Figure 3.2a, PC exhibits considerably more solid-like behaviour under ambient temperatures. The addition of glycerol as a plasticizer causes the plasticized bioink to exhibit similar behaviour to that of the non-plasticized bioink, but exhibits less solid-like behaviour

than PC at ambient temperatures. The solid-like behaviour exhibited by these bioinks may potentially be useful in terms of immediate structural fidelity once printed, but because the test is contactless, it cannot predict the effect of shear stress on the behaviour of the bioink and its subsequent response when printed. The behaviour exhibited thus implies that the material should be printed at a higher temperature which would encourage flowability. PC-PC, on the other hand, presents with more gel-like behaviour under ambient temperatures, thus predicting an ambient printing temperature.

Figure 3.2b is useful in predicting the potential stiffness of the construct over a variation in temperature by displaying the changes in shear storage modulus. A decrease in shear storage modulus is attributed to a weakening in mechanical rigidity and solid behaviour. In terms of the printing process, it is useful to understand these values as they can be predictive of mechanical properties of printed constructs. PC presents as most mechanically strong at 22.9°C, which correlates with the decreased tan d presented in Figure 3.2a. While the material exhibits an increase in mechanical strength at 37°C, it is not as rigid as it was at 22.9°C which does indicate a compromise in mechanical properties over the temperature change, even though it will remain solid at physiological temperatures. PC-G, as a material, presents as inefficient for the printing process. While it is possible to print it at higher temperatures as necessitated by the information in Figure 3.2a, the material itself does not reach close to a gelling point, thus potentially compromising the printing process. The bioink also presents with a steady decrease in shear storage modulus over the assessed temperature range (Figure 3.2b). This decrease predicts inferior mechanical properties at physiological temperatures, when compared to the other two formulations. PC-PC exhibits its most solid-like behaviour at physiological temperatures, after a steady increase in shear storage modulus across the temperature range. This increase implies that the material's mechanical properties improve when placed under physiological temperatures, when compared to the other formulations.

3.4.3 Chemical Transitions of Bioprinted Scaffolds

The 3D bioprinted scaffolds composed of PHBV and CAP, as well as different plasticizers (PC and glycerol) were successfully fabricated using 3D Bioplotter® (EnvisionTEC). PC-PC scaffolds were then chemically functionalized. The scaffolds were all subjected to analysis of their chemical structure in order to assess the chemical transitions due to the blending of polymers – when compared to individual native polymers (Figure 3.3a) - as well as the effects of the plasticizers (Figure 3.3b) on the chemical structure of the polymer blend.



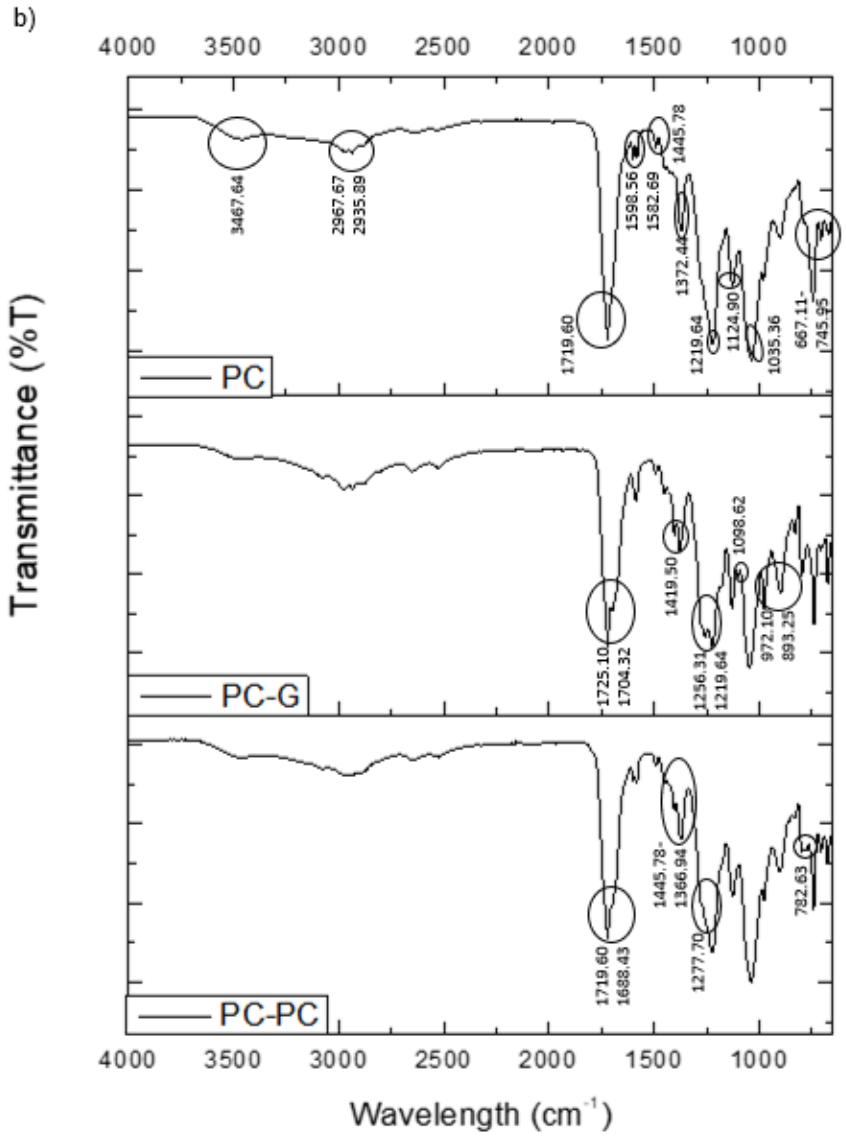


Figure 3.3 a) FTIR spectra and chemical structures of the native materials (PHBV and CAP), b) FTIR spectra of the two plasticized PHBV-CAP (PC-PC, PC-G) as well as the non-plasticized PHBV-CAP (PC)

PHBV and CAP were the native materials utilized as a blend in this study. The PC spectrum displays evidence of a blended formulation with a primarily CAP structure, which is a reasonable conclusion due to the high concentration used, as seen in the presence of the band at ~3467 cm^{-1} and 1372 cm^{-1} which is due to the -OH in CAP, However, the C=O stretching peak at ~1719 cm^{-1} is a result of the additive effect of the PHBV to the CAP, thus increasing the intensity of the

peak as per PHBV, but retaining a similar broadness to that of native CAP. A slight change in shape indicates overlapping bonds. The band at ~1219 cm^{-1} is also characteristic of the ester bond. There is also increased intensity in the peaks at ~2935.89 cm^{-1} and ~2967.67 cm^{-1} as a result of the CH_2 of PHBV. The bands at ~1582 cm^{-1} and ~1598 cm^{-1} are characteristic of cyclic alkene bonds, which can be attributed to CAP. The multiple overlapping peaks at ~1445 cm^{-1} can be identified as possible overlapping -OH bending. The characteristic peaks of an ortho disubstituted benzene ring (~667-745 cm^{-1}) found in CAP remains constant even after blending, thus showing its stability throughout the blending process. The peak at ~1035 cm^{-1} is representative of the additive effect of C-O-C stretching, as present in both polymers, while the increased intensity and presence of peaks found at ~1372 cm^{-1} and ~1445 cm^{-1} are consistent with the presence of methyl groups in both polymers. This analysis proves the effective blending of the two polymers.

The addition of plasticizers further alters the chemical structure. Although the original PC structure remained as the backbone, there were visible changes to the chemical structure as a result of the glycerol addition. The overlapping bands visible at ~1704 cm^{-1} and ~1725 cm^{-1} are representative of the C-O bond, both from the original formulation and from the glycerol component. The band at ~1419 cm^{-1} is due to the -OH found in glycerol, as is the band at ~1098 cm^{-1} which is due to -OH stretching. At ~1263 cm^{-1}, an additional, partially hidden band is visible, and can be due to the presence of more C-O bonds. There are also additional alkene bonds at ~893 cm^{-1} and ~972 cm^{-1}.

In terms of the effects of propylene carbonate as a plasticizer, there was also an addition to the C-O peak (1688 cm^{-1}) – which presented as overlapping bands - as per the effect of the glycerol. There is also a band at 1277 cm^{-1} due to C-O stretching. Evidence of the methyl groups found in propylene carbonate can be observed at 1366 cm^{-1} and 1445 cm^{-1}. As the structure of propylene carbonate shares many functional groups with the original polymers, it must be noted that many

of these groups do overlap. Thus, the results clearly show that the plasticizers were both well-integrated into the formulation, as per the changes in chemical structure.

The production of the blends can be observed visually in Figure 3.4 below

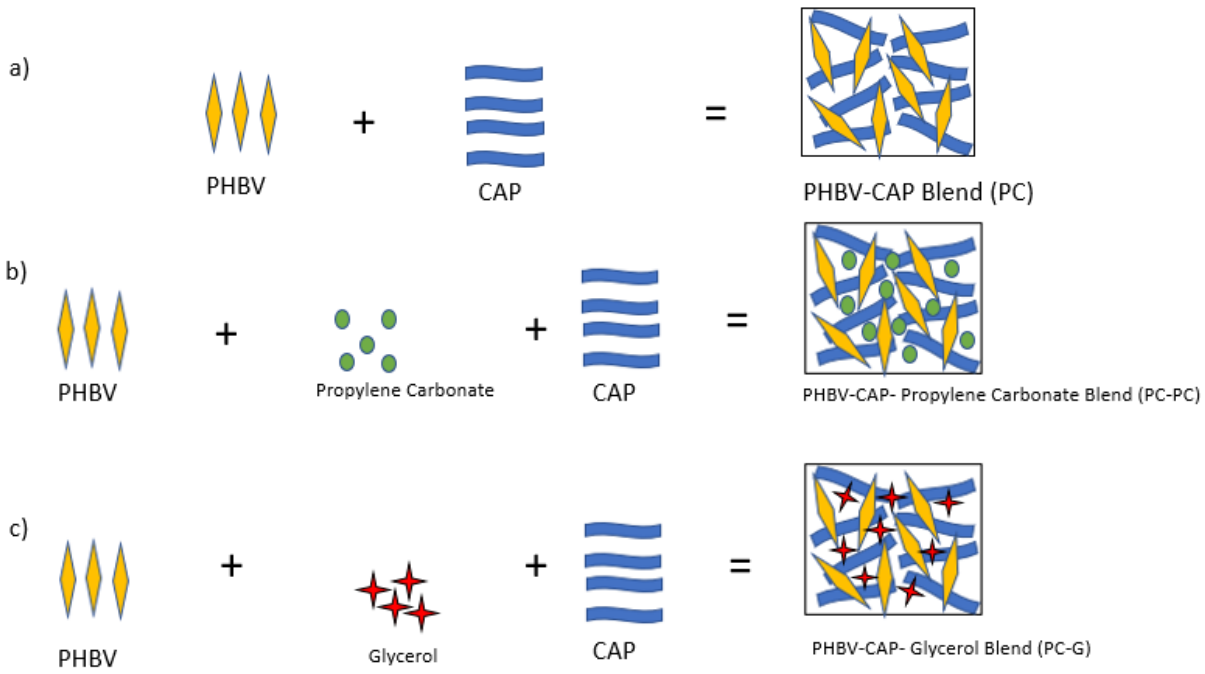
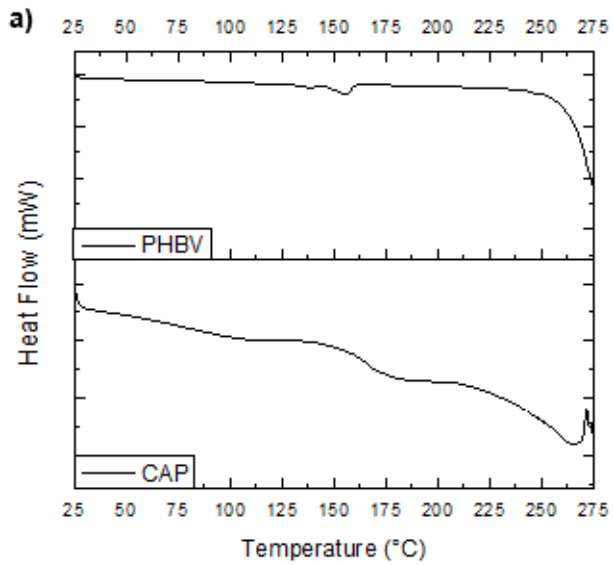
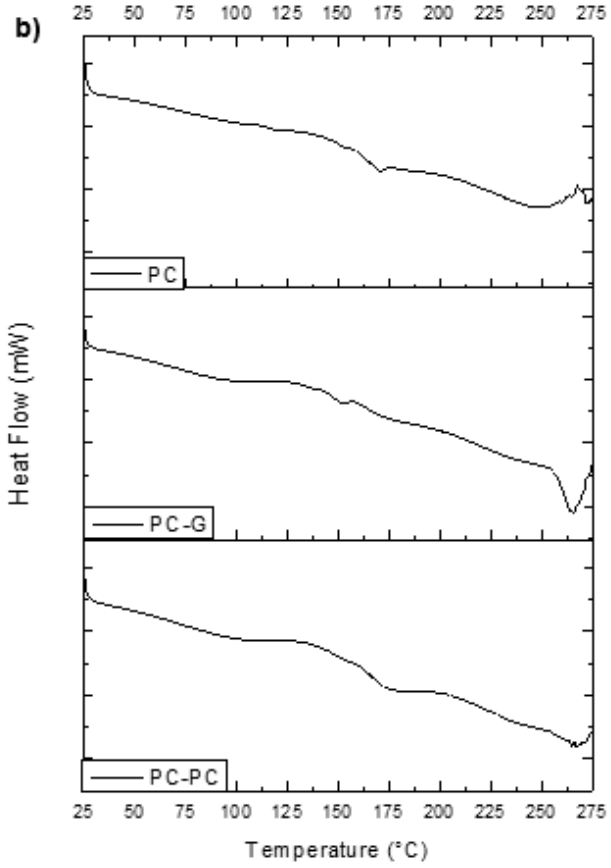


Figure 3.4 Diagrams illustrating production of proposed blends a) PHBV-CAP (PC), b) PHBV-CAP-Propylene Carbonate (PC-PC), c) PHBV-CAP-Glycerol (PC-G)

3.4.4 Thermal Characteristics of Bioprinted Scaffold as well as Native Materials

In the thermograms of the native materials (Figure 3.5a), PHBV exhibits its melting point is at the endothermic peak at 155 °C (Tm_1). The material then undergoes decomposition as signified from the peak at 279 °C (Tm_2), which is within the thermal decomposition range (Shang et al., 2012). In terms of CAP, the glass transition temperature (Tg) is reported to be between 171°C and 175°C (Béchard et al., 1995) and was found to be 172°C and the material then proceeds to undergo decomposition at 266°C.





↑exo

Figure 3.5 DSC Thermograms showing the behaviour of a) native materials b) non-plasticized scaffolds compared to the plasticized scaffold

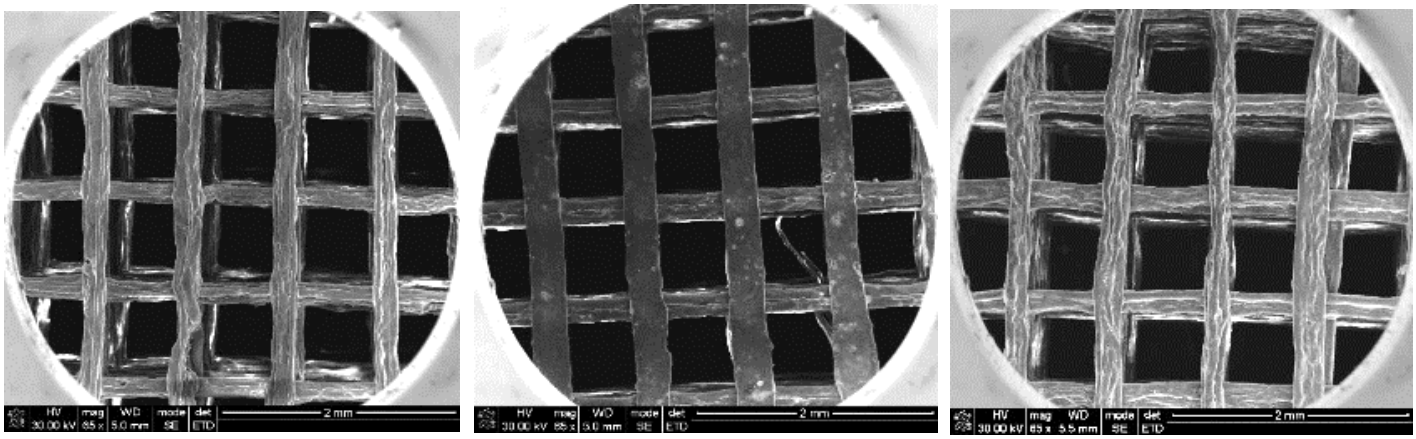
The blend (PC) (Figure 3.5b) presents with a melting temperature of 171°C, the shift of which is due to the blending process. There is evidence of another peak at ~251°C, signifying its decomposition, which is lower than that of both PHBV and CAP. These two peaks are suggestive of the influence of the blended polymers on the crystallinity of the final structure. It is useful to note that because of the difference between the melting temperature and the decomposition temperature of the blend, there is a large processing window.

The effect of plasticization is also evident in Figure 3.5b. While glycerol (PC-G) decreases the melting temperature to ~153°C, propylene carbonate (PC-PC) improves the melting temperature to 173°C, with both plasticizers reflecting decomposition around 265°C.

3.4.5 Surface Morphology Mapping of 3D Bioprinted Scaffolds

Surface morphology is an important characteristic because of the manner by which it can impact various functions, such as mechanical stability and nutrient diffusion. Figure 3.6 (a-c) shows the surface morphology of the fabricated scaffolds.

The images highlight scaffolds with clearly defined architecture, and material layer adhesion, thus proving that the material in question is appropriate for the 3D printing process. It must be noted, however, that the material does undergo some visible contraction upon dehydration, as displayed by the rough and uneven surface morphology. This may prove advantageous, however, in terms of cellular attachment due to the potential for cells to adhere between the grooves as an anchor, as well as in terms of swelling behaviour, wherein the scaffolds have more potential to swell to their hydrated form without compromising structural integrity.



(a) (b) (c)

Figure 3.6 SEM images of (a): PC, (b): PC-G, (c): PC-PC (magnification for all: x65)

Figure 3.6 also provides a more detailed visualization regarding the porous nature of the scaffold. There are visible, interconnected pores with well-defined margins – as per the design. The interconnectivity between the pores improves the available surface area which would encourage cellular attachment and proliferation, and the pores also allow nutrients to flow through the structure, in turn encouraging cellular growth. The visibility of the pores is also indicative of the usefulness of the 3D printing process, which allows the design of intricate internal structures and specific pore architecture.

3.4.6 Mechanical Properties of 3D Bioprinted Scaffolds

Scaffolds utilized in tissue engineering will naturally be subjected to loads bared by the body. As such, mechanical testing is one of the most important characterizations, in order to ensure that materials meet the standards posed by the native tissues (Vazquez *et al*., 2016).

Figure 3.7 shows the difference in tensile strength between PC and the plasticized scaffolds PC-G and PC-PC, while Figure 3.8 compares the compression strength of PC-PC and PC-G to that

of PC. It must be noted that under the maximum force (load cell), none of the constructs reached fracture point in either testing scenario.

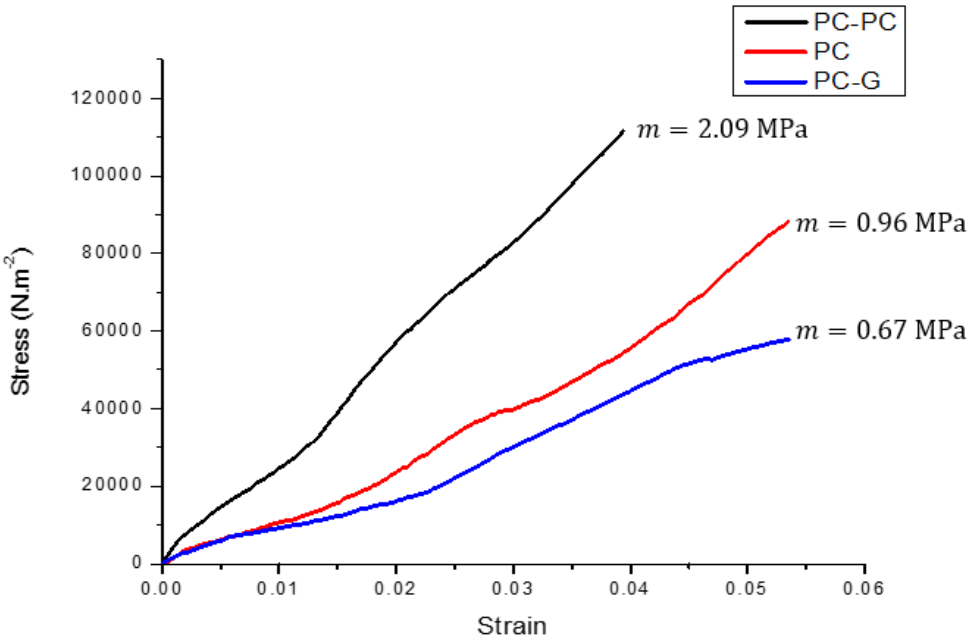


Figure 3.7 A stress-strain curve comparing the tensile properties of plasticized scaffolds to the non-plasticized scaffold (Strain SD: <0.02)

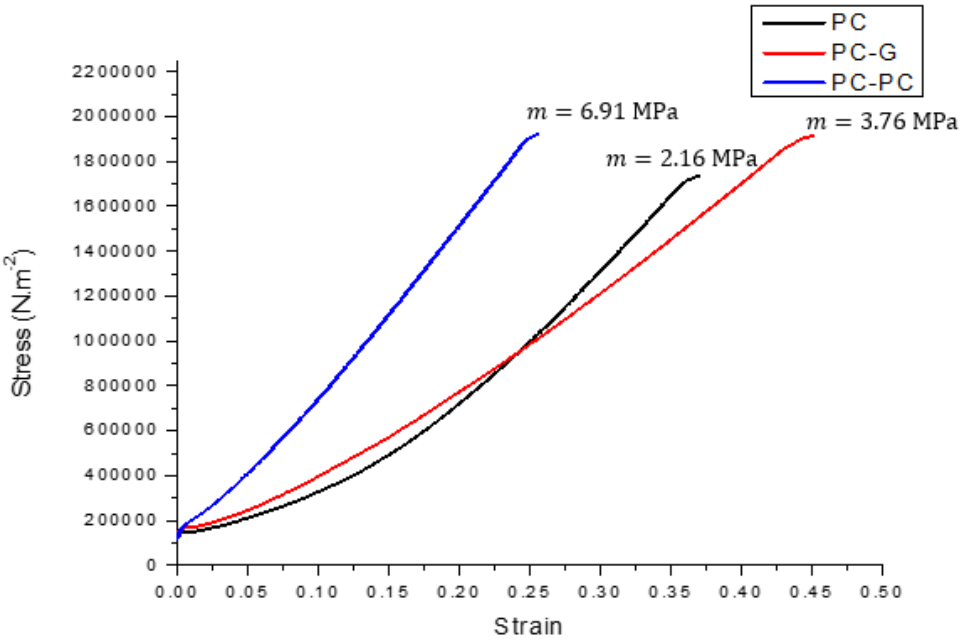


Figure 3.8 A stress-strain curve comparing the compression properties of plasticized scaffolds to the non-plasticized scaffold (Strain SD <0.04)

As can be observed in Figure 3.7, PC has a relatively low Young's modulus (~0.9MPa), which makes it susceptible to deformation, as is also evidenced by the scaffold itself deforming (experiencing more strain) under lower stresses. Figure 3.8 exhibits similar results in terms of compression strength, with PC displaying a Youngs modulus of ~2.16 MPa, and requires lower stress to deform.

Glycerol, as a plasticizer, improves the flexibility of the scaffold – which could be attributed to glycerol's many hydroxyl groups. This improvement in flexibility is shown in Figure 3.7, where the Young's modulus is lowered to ~0.67MPa. However, this decrease also reduces the forces required for the scaffold to deform. In contrast, the Young's modulus in compression testing (Figure 3.8) improved to ~3.76MPa. This showed that in compression testing, PC-G presents as more resistance to deformation. However, this behaviour is not a constant, and only occurs after the scaffold has already been subjected to stresses and experienced deformation. When compared to PC-PC, PC-G also exhibits a much higher strain under the maximum stress in both cases.

Utilizing propylene carbonate as a plasticizer (PC-PC) resulted in considerably superior results, when compared to the other two formulations, potentially implying that the addition of an ester contributes positively towards enhancing mechanical properties. In terms of tensile strength (Figure 3.7), PC-PC exhibits a much higher resistance to deformation and requires much higher stresses to experience considerable strain, with an impressive Young's modulus of ~2.09MPa which is significantly higher than that of the others. PC-PC also exhibits a higher Young's modulus for compression testing (~6.91 MPa) rendering it the stiffest out of the three, and thus the scaffold most likely to be durable under load-bearing applications. PC-PC also experienced the least deformation under maximum stresses, and this resistance could prove useful in clinical applicability.

The produced scaffolds can potentially be utilized for a variety of clinical purposes, depending on mechanical requirements. This proves that not only does the novel combination produce a construct which can be used across a range of tissues, but that plasticizers contribute positively towards the versatility of the 3D bioprinted construct as elaborated upon further in Table 3.4.

Table 3.4 Potential clinical applications for the scaffolds as per their elastic modulus found in literature

Scaffold	**Potential Clinical Application**	**Ref**

PC	• Skin
	• Auricular cartilage
	  ➢ Tragus
	  ➢ Concha
	  ➢ Antitragus
	  ➢ Antihelix)
	• Nasal Cartilage
	  ➢ Septal
	  ➢ Alar
	• Reproductive system
	  ➢ Cardinal ligament
	  ➢ Uterosacral ligament
	  ➢ Uterus
	• Articular cartilage
		(Serup *et al*., 2006, Griffin *et al*., 2016b, Griffin *et al*., 2016a, Baah-Dwomoh *et al*., 2016, Vidal-Lesso *et al*., 2014)

PC-G	• Skin
	• Reproductive system
	  ➢ Vagina
	  ➢ Cardinal ligament
	  ➢ Uterosacral ligament
	  ➢ uterus
	• Articular cartilage
		(Serup *et al*., 2006, Vidal-Lesso *et al*., 2014, Baah-Dwomoh *et al*., 2016)

PC-PC	• Skin
	• Bone
	  ➢ Radius
	  ➢ Tibia
	  ➢ mandible – without cortical layer)
	• Reproductive system
	  ➢ Vagina
	  ➢ Uterosacral ligament
	  ➢ Uterus
	• Articular cartilage
		(Serup *et al*., 2006, Lakatos *et al*., 2014, Baah-Dwomoh *et al*., 2016, Vidal-Lesso *et al*., 2014)

3.4.7 In Vitro Degradation Behaviour of the Produced Scaffolds

It is important to assess the degradation behaviour of scaffolds used in tissue engineering due to the body's physiological conditions which differ so greatly from the ambient environment. Scaffolds must not only be load-bearing, but should also be biodegradable and have a known degradation rate so that they may be tailored as per application requirements.

Figure 3.9 shows the *in vitro* degradation behaviour of the produced scaffolds.

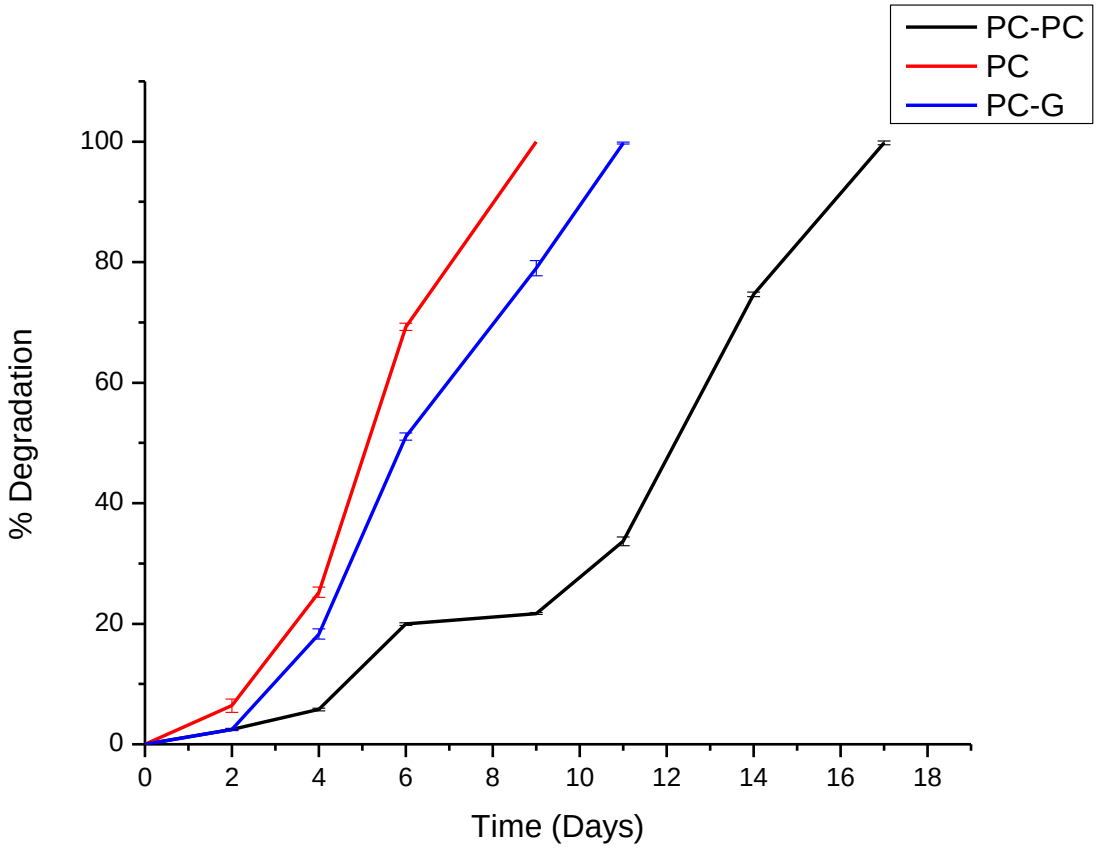


Figure 3.9 *In vitro* degradation behaviour of plasticized scaffolds (PC-PC, PC-G) vs. the non-plasticized scaffold (PC) (SD<2)

As per Figure 3.9, the PC scaffolds displayed complete degradation within 9 days, confirming that both polymers are biodegradable and do degrade under physiological pH. A critical observation is that due to the pH-dependent (neutral/basic) solubility of CAP, a decrease in the concentration

of CAP could potentially slow the degradation of the scaffold, however, this may complicate and hinder the printing process.

The effect of the plasticizers was shown to prolong the degradation of the scaffold. The PC-G scaffold fully degraded at approximately 11 days, while the PC-PC scaffold proved to be the best of the three and degraded within 17 days, thus showing that the addition of plasticizers is beneficial in increasing the amount of time in which the scaffolds degrade.

The degradation rate was also calculated for the plasticized scaffolds compared to the non-plasticized scaffold, taking into account the mass loss over time (Figure 3.10).

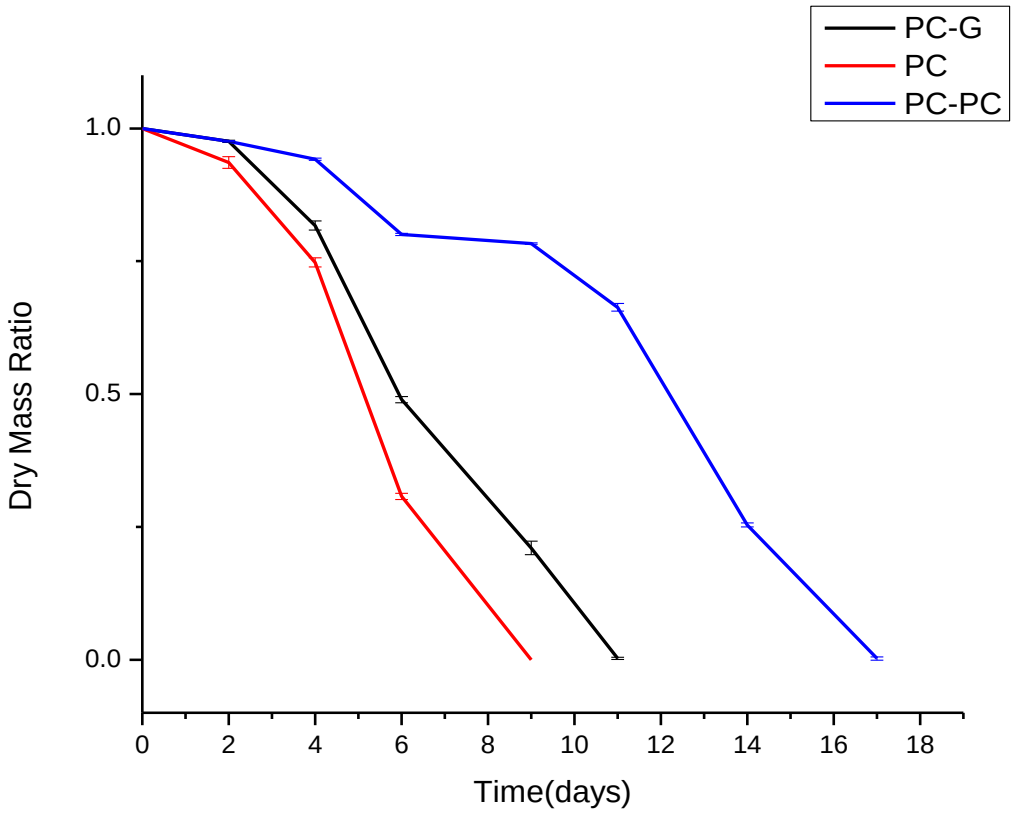


Figure 3.10 *In vitro* degradation rate of plasticized scaffolds (PC-PC, PC-G) vs. the non-plasticized scaffold (PC) (SD<0.1)

The degradation behaviour of the scaffold can be attributed to the neutral solubility of CAP as well as the autocatalytic behaviour of PHBV which relies on hydrolytic degradation. The degradation behaviour is not constant and is dependent on polymer mass, as shown by its change in behaviour as the mass decreases.

The rate of degradation of PC and PC-G followed first-rate degradation behaviour with rate constants of 0.1 day^{-1} and 0.09 day^{-1} respectively, while PC-PC presented with two-stage first order degradation behaviour with a rate constant of 0.02 day^{-1} during the first stage, and then experiencing an increase with a rate constant of 0.1 $day^{-1,}$ showing that the degradation rate increases as a result of mass loss. The degradation rate of PC-G and PC-PC was similar for the first two days, and then PC-G began to degrade at a faster rate. This could be attributed to the additional -OH groups found in glycerol which sped up the hydrolytic degradation. The half-life of the specific scaffolds was also observed, with PC displaying a half-life of was 5 days, compared to PC-G at 6 days and PC-PC which presented with the longest half-life of 12 days. PC-PC was thus proven to be the most durable in a simulated physiological environment.

3.5 Concluding Remarks

3D bioprinting is a promising approach to scaffold fabrication, but the lack of availability of printable biomaterials (bioinks) has limited its application. The novel bioink combination presented in this dissertation contributes to the available materials, and has been assessed successfully for its printability. 3D bioprinting of this novel bioink enabled the production of a scaffold under ambient temperature conditions, with controlled architecture, pore orientation, size and interconnection, and this scaffold was further assessed and found to have a wide clinical applicability.

The effects of plasticization on the bioink combination were also elaborated upon, with both plasticizers improving the biomechanical properties of the printed constructs. Glycerol, however, exhibited a more rapid degradation rate, but was still an improvement on the non-plasticized

construct. Propylene carbonate successfully and significantly enhanced the mechanical properties of the printed constructs by increasing their resistance to deformation showing that the concept of plasticization was shown to play a significant role in determining and expanding potential clinical applications.

In terms of degradation, while the addition of plasticizers does prolong the degradation behaviour, it is still not up to clinical standards. For the sake of comparison, PC plasticization would prove useful in an area such as skin healing where the full epithelium could be regenerated within one to three weeks (Krafts, 2010). In terms of other tissues such as bone, ligaments and cartilage, further research would have to be done to alter the degradation rate as such tissues have complex regeneration processes with various tissue types and additional processes such as nerve regeneration and vascularization, and as such, require extensive time to ensure the entire tissue is regrown. This is a useful characteristic to have quantified, as it ties in with biocompatibility and the body's ability to respond to and process the biomaterials concerned – which is a pertinent consideration in tissue engineering.

References

Ahmad, N. & Isa, M. 2016. Characterization of un-plasticized and propylene carbonate plasticized carboxymethyl cellulose doped ammonium chloride solid biopolymer electrolytes. *Carbohydrate polymers,* 137**,** 426-432.

Atzet, S., Curtin, S., Trinh, P., Bryant, S. & Ratner, B. 2008. Degradable poly(2-hydroxyethyl methacrylate)-co-polycaprolactone hydrogels for tissue engineering scaffolds. *Biomacromolecules,* 9**,** 3370-3377.

Baah-Dwomoh, A., Mcguire, J., Tan, T. & De Vita, R. 2016. Mechanical Properties of Female Reproductive Organs and Supporting Connective Tissues: A Review of the Current State of Knowledge. *Applied Mechanics Reviews,* 68**,** 060801-060801-12.

Badea, A., Mccracken, J. M., Tillmaand, E. G., Kandel, M. E., Oraham, A. W., Mevis, M. B., Rubakhin, S. S., Popescu, G., Sweedler, J. V. & Nuzzo, R. G. 2017. 3D-Printed pHEMA Materials for Topographical and Biochemical Modulation of Dorsal Root Ganglion Cell Response. *ACS Applied Materials & Interfaces,* 9**,** 30318-30328.

Béchard, S. R., Levy, L. & Clas, S.-D. 1995. Thermal, mechanical and functional properties of cellulose acetate phthalate (CAP) coatings obtained from neutralized aqueous solutions. *International Journal of Pharmaceutics,* 114**,** 205-213.

Berggren, R. G., Enscore, D. J., Marks, S. M., Osborne, J. L., Wong, P. S.-L. & Roorda, W. E. 1997. Injectable drug delivery system and method. Google Patents.

Buchholz, B. 1997. Copolymers of trimethylenecarbonate and optionally inactive lactides. Google Patents.

Chang H.I., Wang Y. 2011. Cell responses to surface and architecture of tissue engineering scaffolds. *Regenerative medicine and tissue engineering-cells and biomaterials.* InTechOpen.

Chiulan, I., Frone, A. N., Brandabur, C. & Panaitescu, D. M. 2018. Recent Advances in 3D Printing of Aliphatic Polyesters. *Bioengineering,* 5**,** 2.

Chung, J. H., Naficy, S., Yue, Z., Kapsa, R., Quigley, A., Moulton, S. E. & Wallace, G. G. 2013. Bioink properties and printability for extrusion printing living cells. *Biomaterials Science,* 1**,** 763-773.

Dobos, A. M., Onofrei, M.-D., Tudorachi, N. & Ioan, S. 2015. Structural Orientations of Cellulose Acetate Phthalate/Ethyl Cellulose Blends in Solution. *Journal of Macromolecular Science, Part B,* 54**,** 1092-1104.

Dragusin, D.-M., Van Vlierberghe, S., Dubruel, P., Dierick, M., Van Hoorebeke, L., Declercq, H. A., Cornelissen, M. M. & Stancu, I.-C. 2012. Novel gelatin–PHEMA porous scaffolds for tissue engineering applications. *Soft Matter,* 8**,** 9589-9602.

Fatimi, A., François Tassin, J., Quillard, S., Axelos, M. A. V. & Weiss, P. 2008. The rheological properties of silated hydroxypropylmethylcellulose tissue engineering matrices. *Biomaterials,* 29**,** 533-543.

Ferreira, B. M. P., Zavaglia, C. A. C. & Duek, E. A. R. 2002. Films of PLLA/PHBV: Thermal, morphological, and mechanical characterization. *Journal of Applied Polymer Science,* 86**,** 2898-2906.

Flynn, L., Dalton, P. D. & Shoichet, M. S. 2003. Fiber templating of poly(2-hydroxyethyl methacrylate) for neural tissue engineering. *Biomaterials,* 24**,** 4265-4272.

Gibson, J. W. & Tipton, A. J. 2006. High viscosity liquid controlled delivery system and medical or surgical device. Google Patents.

Gong, J. P., Katsuyama, Y., Kurokawa, T. & Osada, Y. 2003. Double-network hydrogels with extremely high mechanical strength. *Advanced Materials,* 15**,** 1155-1158.

Griffin, M. F., Premakumar, Y., Seifalian, A. M., Szarko, M. & Butler, P. E. M. 2016a. Biomechanical Characterisation of the Human Auricular Cartilages; Implications for Tissue Engineering. *Annals of Biomedical Engineering,* 44**,** 3460-3467.

Griffin, M. F., Premakumar, Y., Seifalian, A. M., Szarko, M. & Butler, P. E. M. 2016b. Biomechanical characterisation of the human nasal cartilages; implications for tissue engineering. *Journal of materials science. Materials in medicine,* 27**,** 11-11.
Guo, B. & Ma, P. X. 2018. Conducting Polymers for Tissue Engineering. *Biomacromolecules,* 19**,** 1764-1782.
Javadi, A., Kramschuster Adam, J., Pilla, S., Lee, J., Gong, S. & Turng, L.-S. 2010. Processing and characterization of microcellular PHBV/PBAT blends. *Polymer Engineering & Science,* 50**,** 1440-1448.
Ke, T. & Sun, X. S. 2003. Thermal and mechanical properties of poly(lactic acid)/starch/methylenediphenyl diisocyanate blending with triethyl citrate. *Journal of Applied Polymer Science,* 88**,** 2947-2955.
Kose, G. T., Korkusuz, F., Korkusuz, P., Purali, N., Ozkul, A. & Hasirci, V. 2003. Bone generation on PHBV matrices: an *in vitro* study. *Biomaterials,* 24**,** 4999-5007.
Krafts, K. P. 2010. Tissue repair: The hidden drama. *Organogenesis,* 6**,** 225-233.
Labrecque, L. V., Kumar, R. A., Davé, V., Gross, R. A. & Mccarthy, S. P. 1997. Citrate esters as plasticizers for poly(lactic acid). *Journal of Applied Polymer Science,* 66**,** 1507-1513.
Lakatos, E., Magyar, L., Bojtar, I. 2014. Material Properties of the Mandibular Trabecular Bone. *Journal of Medical Engineering,* 2014**,** 7.
Liu, H., Adhikari, R., Guo, Q. & Adhikari, B. 2013. Preparation and characterization of glycerol plasticized (high-amylose) starch–chitosan films. *Journal of Food Engineering,* 116**,** 588-597.
Lucas, J. A. & Halar, Z. E. 1997. Low toxicity solvent composition. *Google Patents.*
Magalhães, N. F. & Andrade, C. T. 2013. Properties of melt-processed poly(hydroxybutyrate-co-hydroxyvalerate)/starch 1: 1 blend nanocomposites. *Polímeros,* 23**,** 366-372.
Majee, S. B. 2016. Introductory Chapter: An Overview of Hydrogels. *Emerging Concepts in Analysis and Applications of Hydrogels.* IntechOpen.
Malm, C. J., Emerson, J. & Hiait, G. D. 1951. Cellulose Acetate Phthalate as an Enteric Coating Material. *Journal of the American Pharmaceutical Association (Scientific ed.),* 40**,** 520-525.
Mohsin, M., Hossin, A. & Haik, Y. 2011. Thermal and mechanical properties of poly (vinyl alcohol) plasticized with glycerol. *Journal of Applied Polymer Science,* 122**,** 3102-3109.
Murphy, S. V. & Atala, A. 2014. 3D bioprinting of tissues and organs. *Nat Biotech,* 32**,** 773-785.
Neurath, A. R., Strick, N., Li, Y.-Y. & Debnath, A. K. 2001. Cellulose acetate phthalate, a common pharmaceutical excipient, inactivates HIV-1 and blocks the coreceptor binding site on the virus envelope glycoprotein gp120. *BMC Infectious Diseases,* 1**,** 17-17.
O'Brien, F. J. 2011. Biomaterials & scaffolds for tissue engineering. *Materials Today,* 14**,** 88-95.
Parker, T. L., Joslyn, D. & Nikolic, S. D. 2001. Method of enhancing blood flow in tissue. *Google Patents.*
Pascu, E., Stokes, J. & Mcguinness, G. 2013. *Electrospun composites of PHBV, silk fibroin and nano-hydroxyapatite for bone tissue engineering*.
Roxin, P., Karlsson, A. & Singh, S. K. 1998. Characterization of Cellulose Acetate Phthalate (CAP). *Drug Development and Industrial Pharmacy,* 24**,** 1025-1041.
Sabir, M. I., Xu, X. & Li, L. 2009. A review on biodegradable polymeric materials for bone tissue engineering applications. *Journal of Materials Science,* 44**,** 5713-5724.
Schäffner, B., Andrushko, V., Holz, J., Verevkin, S. P. & Börner, A. 2008. Rh-Catalyzed Asymmetric Hydrogenation of Unsaturated Lactate Precursors in Propylene Carbonate. *ChemSusChem,* 1**,** 934-940.
Serup, J., Grove, G. L. & Jemec, G. B. 2006. *Handbook of non-invasive methods and the skin*, CRC press.

Shang, L., Fei, Q., Zhang, Y. H., Wang, X. Z., Fan, D.-D. & Chang, H. N. 2012. Thermal properties and biodegradability studies of poly (3-hydroxybutyrate-co-3-hydroxyvalerate). *Journal of Polymers and the Environment,* 20**,** 23-28.

Sharma, U., Gitlin, I., Zugates, G. T., Rago, A., Zamiri, P., Busold, R., Freyman, T., Caulkins, R. J., Pham, Q. P. & You, C. 2018. IN SITU FORMING HEMOSTATIC FOAM IMPLANTS. US Patent App. 15/642,968.

Shih, Y. C. 2015. Effects Of Degradation On Mechanical Properties Of Tissue-Engineering Poly (glycolic Acid) Scaffolds.

Shrestha, R., Palat, A., Punnoose, A. & Paul, S. 2016. Electrospun cellulose acetate phthalate nanofibrous scaffolds for 3D culture of primary chondrocytes and neurons. *Tissue Cell*, 48(6), 634

Shukla, A. 2004. Biodegradable vehicles and delivery systems of biolgically active substances. *Google Patents.*

Stewart, B. 2017. 3D Bioprinting Hydrogel for Tissue Engineering an Ascending Aortic Scaffold.

Vazquez, O. R., Avila, I. O., Díaz, J. C. S. & Hernandez, E. 2016. An overview of mechanical tests for polymeric biomaterial scaffolds used in tissue engineering. *Journal of Research Updates in Polymer Science,* 4**,** 168-178.

Vidal-Lesso, A., Ledesma-Orozco, E., Daza-Benítez, L. & Lesso-Arroyo, R. 2014. Mechanical Characterization of Femoral Cartilage Under Unicompartimental Osteoarthritis. *Ingeniería mecánica, tecnología y desarrollo,* 4**,** 239-246.

Wongsasulak, S., Tongsin, P., Intasanta, N. & Yoovidhya, T. 2010. Effect of glycerol on solution properties governing morphology, glass transition temperature, and tensile properties of electrospun zein film. *Journal of Applied Polymer Science,* 118**,** 910-919.

Zhang, H. & Grinstaff, M. W. 2014. Recent Advances in Glycerol Polymers: Chemistry and Biomedical Applications. *Macromolecular Rapid Communications,* 35**,** 1906-1924.

CHAPTER 4

POST-PRINTING CHEMICAL FUNCTIONALIZATION OF SCAFFOLDS AND SUBSEQUENT ANALYSIS

4.1 Introduction

It is widely accepted that the concept of post-processing aims to alter or induce properties into an existing scaffold. Various forms of post-processing have been proposed in the realm of tissue engineering, with varying success.

One method involves chemically 'polishing' which removes unnecessary unreacted or not integrated materials, such as partially melted components (Wysocki *et al*., 2016). Another involves purifying constructs, generally done to remove various unnecessary materials that were used in reactions. This could include traces of organic solvents, and may sometimes consist of neutralizing acid/base residues, or drying to get rid of solvent residues (Suntornnond *et al*., 2015). Post-processing is also used to induce or improve the curing, setting and binding of constructs so that constructs present with good resolution (Bose and Bandyopadhyay, 2013) and structural fidelity. Another form of post-processing involves the addition of a material during the development process, and then its subsequent removal in post-processing. This is done to induce certain properties such as improved porosity and pore structuring (Müller *et al*., 2015, Kesti *et al*., 2015), or remove redundant components (such as bioinert components) (Jia *et al*., 2014) that were only required in a sacrificial capacity. Post-processing has also utilized mechanical processes in order to induce desirable properties, such as anisotropic architecture (Zong *et al*., 2005). Bioactivity is also an often sought after property, and methods of post-processing to induce it include physically entrapping molecules within the structure (Lannutti *et al*., 2007), as well as through bioreactors which can provide biochemical and physical regulatory signals to cells, thus controlling and encouraging their activity in the form of growth and proliferation (Zhao *et al*., 2016).

One of the most important categories of properties, as previously discussed, is mechanical properties. Oftentimes, printed structures not only do not fulfill the mechanical requirements of their proposed engineered tissue, but their defined mechanical properties limit their clinical applicability and variability as well.

An often-ignored parameter in 3D bioprinting for tissue engineering is the tunability of the printed scaffold's chemistry, and whether the exploitation of this parameter could positively affect the properties of printed structures such as the mechanical properties, as well as biological properties such as bioactivity and biocompatibility. In this chapter, we propose post-processing of the previously described scaffolds, through chemically modifying the printed scaffolds with aminolysis and hydrolysis, thus altering their surface chemistry. The altered surface chemistry is then assessed for physicomechanical changes as a result of the post-processing.

To further capitalize on the changes resulting from post-processing, the concept of grafting onto the chemically modified scaffold is assessed. As elaborated upon previously, hyaluronic acid is a linear polysaccharide that is found abundantly throughout the body (Panwar and Tan, 2016). It has multiple functions including cellular signaling, wound repair, matrix organization (Burdick and Prestwich, 2011) and control of tissue hydration (Necas *et al*., 2008). As a biocompatible, biodegradable, naturally occurring polymer, hyaluronic acid is promising in the realm of tissue engineering (Panwar and Tan, 2016). However, it lacks structural fidelity and stability upon printing (Ouyang *et al*., 2016) which can compromise its success in 3D-bioprinting. As such, it is a useful polymer to attempt to graft onto an already 3D bioprinted scaffold, as this would contribute its impressive tissue engineering properties, whilst not being subjected to the printing process.

4.2 Preliminary Formulation Design

4.2.1 Materials and Methods

4.2.1.1 Materials

Hexamethylenediamine was purchased from Sigma-Aldrich (St. Louis, MO, USA), Sodium hydroxide was bought from Merck (South Africa) and propan-2-ol was obtained from Associated Chemical Enterprises (Pty) Ltd (South Africa). N-(3Dimethylaminopropyl)-N′-ethylcarbodiimide hydrochloride (EDC), N-Hydroxysuccinimide (NHS) and Hyaluronic acid were all purchased from Sigma-Aldrich. All products were used without any modifications.

4.2.1.2 Post-Printing Chemical Functionalization and Subsequent Biomacromolecular Attachment

a) Aminolysis

Aminolysis was performed on the PC-PC scaffolds by immersing the washed and dried scaffolds (10x10x5) in a heated (60°C) 1% w/v HMD/propan-2-ol solution (40ml) for 3 minutes under gentle agitation (method adapted from (Wang *et al*., 2009)). The scaffolds were then removed and rinsed with deionized water and allowed to dry for 24hr before characterization.

b) Hydrolysis

Basic hydrolysis was also performed by immersing the dried PC-PC scaffolds into a 1% w/v NaOH-water solution (40ml) for 1 minute under heat (60°C) and gentle agitation (method adapted from (Ke *et al*., 2017)). The scaffolds were then removed and rinsed with deionized water and allowed to dry for 24hr before characterization.

c) Biomacromolecular Attachment

Scaffold samples were washed in deionized water and allowed to air-dry prior to use. The scaffolds were then immersed into a previously prepared EDC/NHS (4:1 (w/w)) activated

hyaluronic acid (0.05g/100ml) aqueous solution for 24 hours at 0-4°C. An acidic pH was used to induce carboxylic acid groups, while a highly basic pH was used to form an amide group (Schante *et al*., 2011). The samples were then rinsed with deionized water to remove non-bound hyaluronic acid, and dried before being used for characterization

4.2.1.3 Chemical Transitions of Chemically Modified 3D Bioprinted Scaffolds and Chemically Modified 3D Bioprinted Scaffolds with Biomacromolecular Attachment

The chemically functionalized 3D printed scaffolds, as well as the chemically modified scaffolds with attached biomacromolecules, were characterized for their chemical transitions by employing a Fourier Transform Infrared (FT-IR) spectrometer (PerkinElmer Spectrum 100, FT-IR Spectrometer) fitted with a universal ATR Polarization Accessory (PerkinElmer Ltd., Beaconfield UK). The samples were analyzed at high resolution with the wavelength ranging from 4000-650cm^{-1}. The results were then analyzed for the presence of the new functional groups according to their expected structure and illustrated by suggested molecular structures.

4.2.1.4 Thermal Characteristics of Chemically Modified 3D Bioprinted Scaffolds

The fibers of chemically functionalized scaffolds were thermally analyzed via differential scanning calorimetry (DSC) (Mettler Toledo, DSC-1 STARe System, Schwerzernback, Switzerland). Samples of 6-8mg were weighed into aluminium crucible pans (40DL) and sealed, with a small (0.2mm) hole pierced in the aluminium lid to create an open system. The samples were heated under a nitrogen atmosphere (Afrox, Germiston, Gauteng, South Africa) with 200ml/min flow rate. The samples were exposed to a temperature range between 25°C and 300°C at the rate of 10°C/min and the thermal profiles were analyzed.

4.2.1.5 Mapping of Surface Morphology of Chemically Modified 3D Bioprinted Scaffolds

Surface morphology of the chemically functionalized scaffold was examined utilizing scanning electron microscopy (SEM) FEI Nova NanoLab SEM (FEI Company, Hillsboro, Oregon, USA). In order to prevent the destruction of the samples, they were initially sputter coated using an EPI coater (SPI Model sputter-coater and control unit, Hester, PA, USA) with carbon and thereafter gold/platinum isotope while mounted. After coating the samples, they were analyzed using a FEI Nova NanoLab SEM (FEI Company, Hillsboro, Oregon, USA).

4.2.1.6 Evaluation of the Mechanical Strength of Chemically Modified 3D Bioprinted Scaffolds

The chemically functionalized scaffold mechanical properties were measured utilizing a BioTester 5000 Biomaterials Tester (CellScale, Waterloo, ON, Canada) equipped with 5 N load cells, as well as TA.XT Plus Texture Analyser (Stable Micro System, Surrey, UK). Biaxial tensile testing (using the BioTester 5000) is critical in evaluating the mechanical properties of 3D printed biomaterials due to the directionality-oriented structure. In order to perform tensile testing, scaffolds were equilibrated for 3 hours through incubation in Phosphate Buffered Saline at 37°C before undergoing testing. The samples were mounted, using the BioRakes tines to pierce the samples in order to position them. Because the material is tough, a crown press was used to exert pressure onto the tines so as to ensure that the tines pierced the sample adequately. ASTM standards (ASTM D638) were followed with regard to the testing parameters. The test was run at a rate of 1mm/min, and the ramp displacement was set at 10% of the size of the original scaffold. The scaffolds were tested in triplicate and Young's modulus, which is representative of material stiffness, was calculated from the linear elastic portion of stress-strain curves produced from the average forces and displacements in both x- and y- directions in triplicate.

The TA.XTPlus Texture Analyzer was used for compression testing. A ¾'' spherical ball probe was used in order to exert a force of 50N onto the samples, which were mounted on the stage.

The test ran in triplicates at a strain rate of 20% per second, and the distance set for 1mm. The results were captured in a force/distance graph, which was then translated to a stress-strain curve in order to calculate the Young's modulus.

4.2.1.7 Comparative Biodegradation Rate Analysis of the Chemically Modified 3D-Bioprinted Scaffolds

The degradation behaviour of the chemically functionalized scaffolds was compared to the already characterized PC-PC scaffold. Scaffolds, in triplicate, were washed thrice with deionized water and immersed into 20ml of PBS (pH 7.4). They were thereafter placed in an orbital shaker maintained at 37 °C and rotating at 20-25rpm. Scaffolds were removed at various time intervals and weighed after being dried. The medium was replaced every second day so as to avoid potential contamination and simulate a physiological environment, wherein degradation products are eliminated from the body through different processes which prevents acidic byproducts from stimulating autocatalysis.

The degradation behaviour was calculated as follows (Equation 1):

$$\% \text{ Degraded} = \frac{W_0 - W'}{W_0} \times 100 \qquad \text{… Equation 1}$$

Where:

W' = final weight of the scaffold

W_0 = initial weight of the scaffold

The degradation rate was also calculated through determining the dry mass ratio as follows (Equation 2)

$$\text{Dry Mass Ratio} = \frac{M}{M_0} \qquad \text{… Equation 2}$$

Where

M = The weight of the removed scaffold at a specific time

M_0 = The initial weight of the scaffold

The values were then used to construct a graph from which the degradation rate was calculated using the slope of the graph (Shih, 2015).

4.3 Results

4.3.1 Aminolysis Chemical Functionalization

4.3.1.1 Chemical Transitions Associated with Aminolysed 3D Bioprinted Scaffolds

FTIR is an ideal method to confirm chemical functionalization, as the scaffolds only underwent surface modification. The scaffolds were composed of PHBV and CAP, with PC as a plasticizer. Post-printing, the scaffolds were washed and allowed to dry before undergoing aminolysis in order to introduce an amine (NH) group into the structure. As per the method which the process was adapted from, the functionalization is proposed to have altered the PHBV compound specifically (Wang *et al*., 2009).

The scaffolds were subjected to analysis of their chemical structure in order to compare the chemical transitions of the amine-functionalized scaffold (Figure 4.1) to the previously characterized PC-PC scaffold.

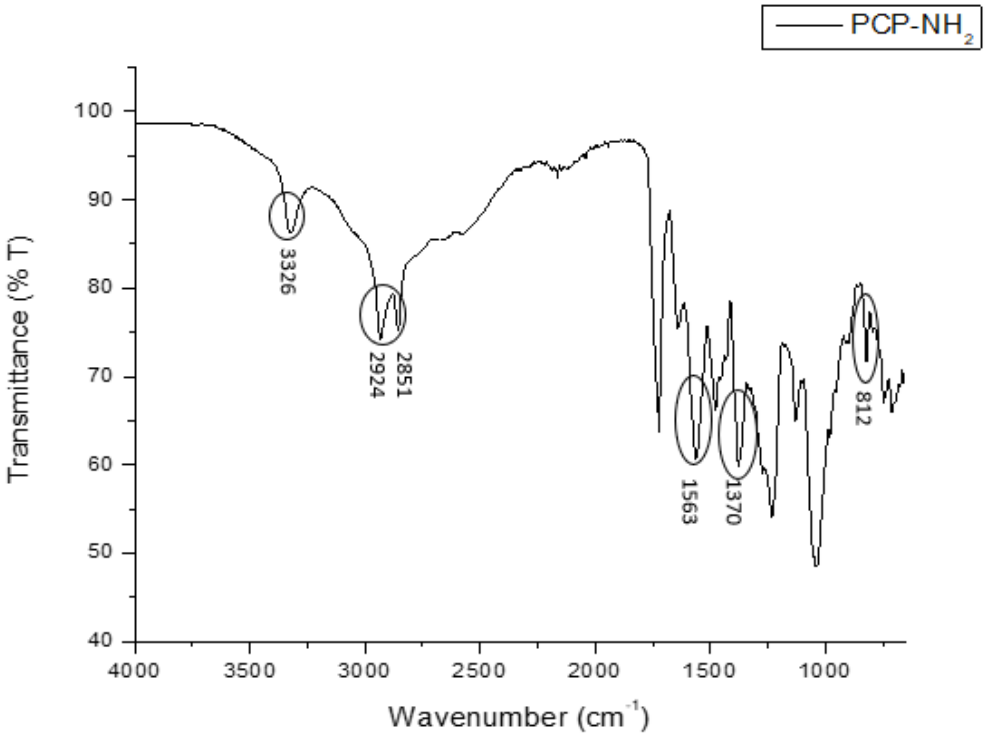


Figure 4.1 FTIR spectra showing the change in chemical structure due to the functionalization of the scaffold through aminolysis

The concept behind post-printing chemical modifications envisioned the permanent alteration of the chemical structure of the already printed scaffolds. This was successfully done in terms of the effects of the aminolysis process, which predicted an amine-functionalized scaffold. The band at ~3326 cm^{-1} is due to the presence of a secondary amine group as reflected by the presence of a characteristic band (smaller, but sharper than an -OH peak) at ~3326 cm^{-1}. This is supported by the presence of a new functional group at ~812 cm^{-1}, which could reflect the presence of N-H. Although not common in secondary amines, the presence of a new and relatively strong band at ~1563 cm^{-1} could also be an N-H band. As a result of the materials used, the double bands at ~2581 cm^{-1} and ~2924 cm^{-1} are proposedly present due to the hexane as part of the hexamethylenediamine.

Figure 4.2 depicts the proposed reaction and chemical structure of the chemically modified scaffold

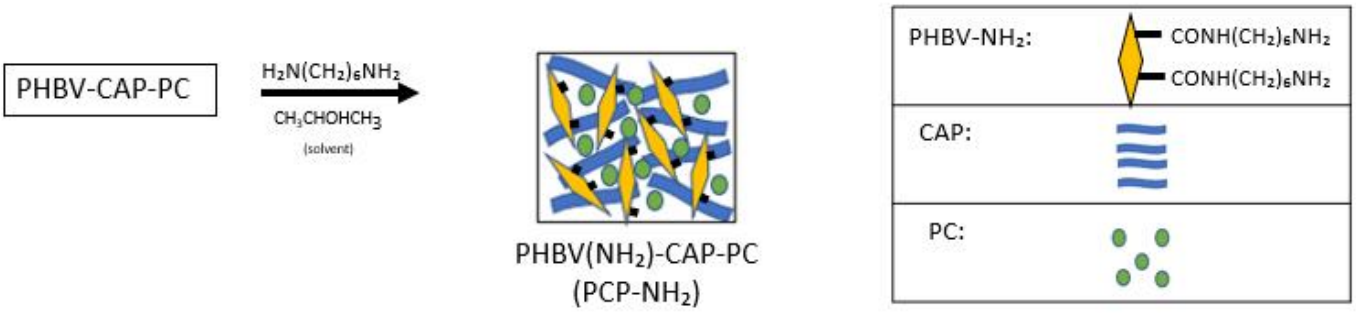


Figure 4.2 Diagram depicting the proposed reaction and chemical structure of the amine-modified scaffold

4.3.1.2 Thermal Transitions Associated with Aminolysed 3D Bioprinted Scaffolds

Thermograms are necessary to observe effects of modifications on the thermal profile of materials, and to observe whether there is any change in the thermal behaviour.

Figure 4.3 reflects thermal changes as a result of aminolysis. The analysis was done on crushed 3D bioprinted and subsequently functionalized fibers.

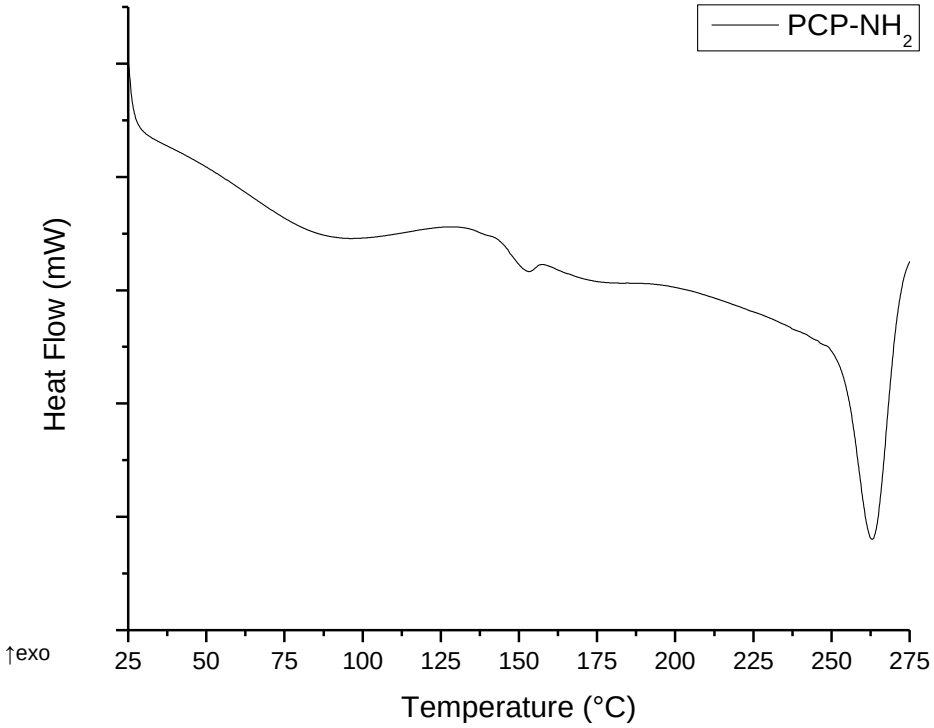


Figure 4.3 DSC thermogram showing the effect of aminolysis based functionalization on the thermal transitions of the scaffold

In comparison to the original polymer compound (PC-PC), aminolysis has not had significantly adverse effects on the thermal profile. The effects of the aminolysis process on the printed PC-PC structure resulted in a decreased melting point (153°C), as well as a decreased degradation point (263°C). While this does compromise the structural integrity of the scaffold in terms of its thermal profile, and could limit further processability; these scaffolds have potential application in tissue engineering, and as a result, will only be subjected to physiological conditions, which are well within the tolerable temperature window.

4.3.1.3 Evaluation of Mechanical Properties of Aminolysed 3D Bioprinted Scaffolds

As mentioned previously, load-bearing is an important aspect to consider when evaluating mechanical properties of scaffolds. Figure 4.4 shows the difference in tensile strength between

PC-PC and the amine-functionalized scaffold - PCP-NH_2, while Figure 4.5 compares the compression strength of PCP-NH_2 to that of PC-PC.

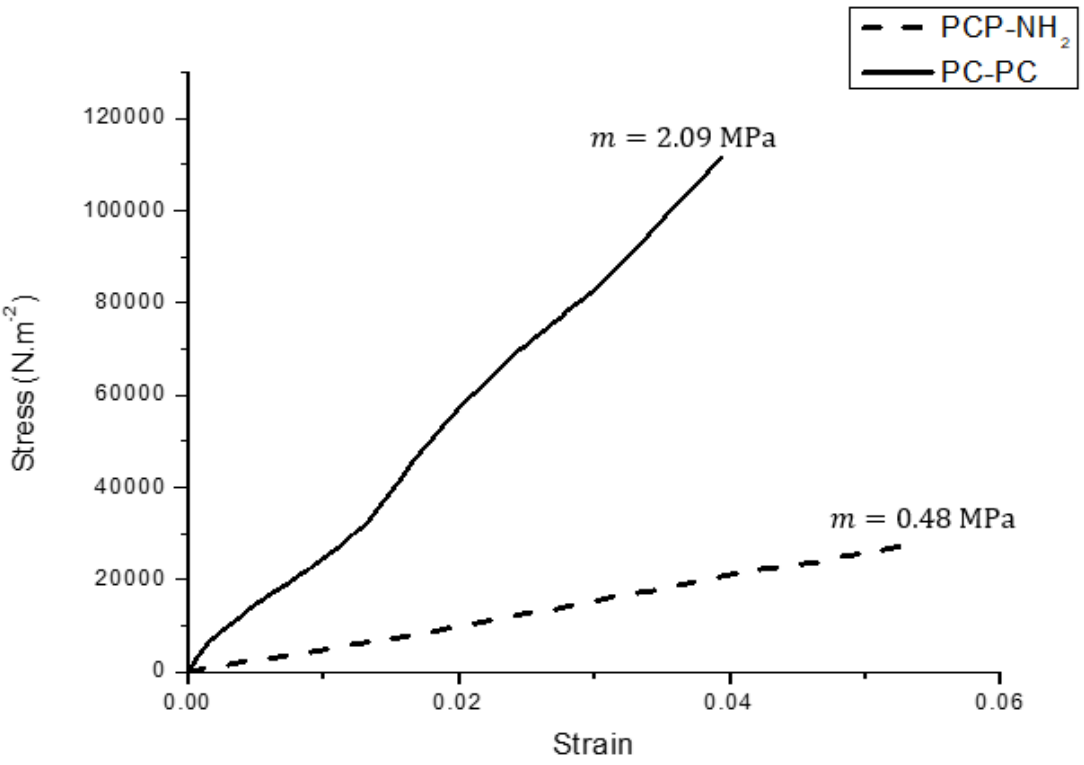


Figure 4.4 A stress-strain curve comparing the tensile properties of an amine-functionalized scaffold (PCP-NH_2) to that of PC-PC (Strain SD: <0.1)

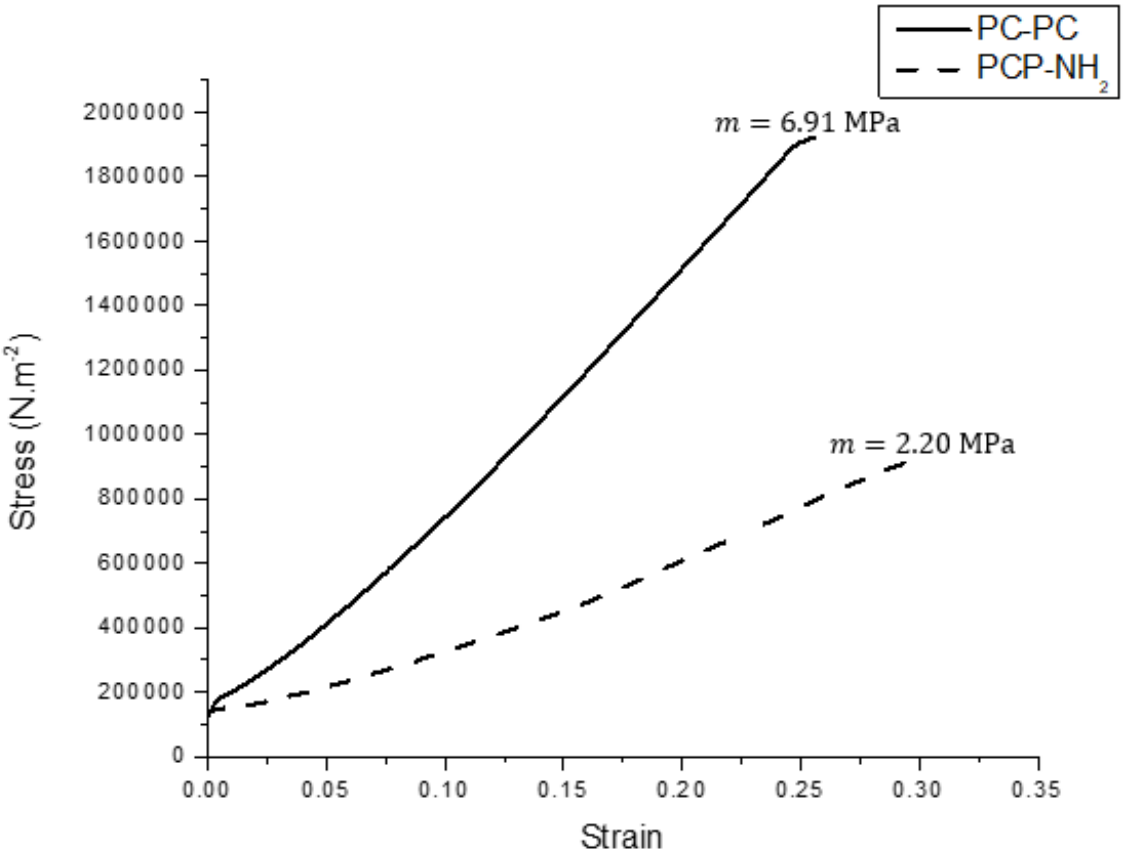


Figure 4.5 A stress-strain curve comparing the compression properties of amine-functionalized scaffolds (PCP-NH_2) when compared to the previously characterized PC-PC (Strain SD <0.2)

The presence of amine groups significantly improved the flexibility of the scaffold with a tensile Youngs modulus of ~0.48MPa. Although this is ultimately a decrease in mechanical strength, it is advantageous in terms of proving that it is possible to alter the mechanical properties of scaffolds in post-printing functionalizations. In terms of compressive strength, the Young's modulus was lowered to ~2.20MPa, which is still higher than that of the initially characterized non-plasticized scaffold (PC), thus exhibiting improved flexibility, but a higher strength than the initial construct. The amine-modified scaffolds can potentially be utilized for a variety of clinical purposes, as shown in Table 4.1, depending on mechanical requirements. This proves that post-printing chemical modifications contribute positively towards the versatility of the 3D bioprinted construct.

Table 4.1 Potential clinical applications for the amine-modified scaffolds as per their elastic modulus found in literature

Modification	Potential Application	Reference

PCP-NH_2	• Skin
	• Auricular cartilage
	  ➢ Tragus
	  ➢ Antitragus
	  ➢ Antihelix
	  ➢ Concha
	• Reproductive system
	  ➢ Ligaments (Cardinal, uterosacral)
	  ➢ Uterus
	• Nasal cartilage
	  ➢ Alar Medial and Alar Lateral cartilages
	• Bone
	  ➢ Tibia
	  ➢ Vertebra
	  ➢ Radius
	• Femoral cartilage
		(Baah-Dwomoh *et al*., 2016, Serup *et al*., 2006, Griffin *et al*., 2016b, Griffin *et al*., 2016a, Lakatos *et al*., 2014, Vidal-Lesso *et al*., 2014)

4.3.1.4 Mapping of Surface Morphology of Aminolysed 3D Bioprinted Scaffolds

Surface morphology is essential in observing the effect of chemical modifications. As such, the following micrograph (Figure 4.6) reflects the change in structural topography and morphology as a result of amine-functionalization.

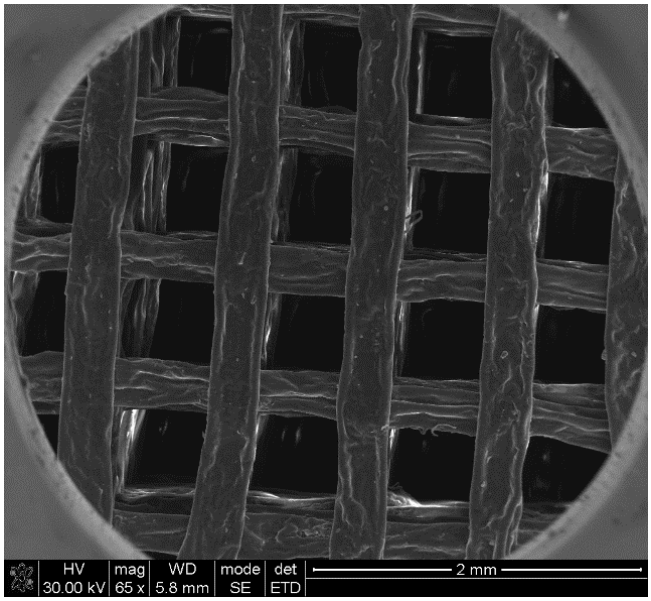


Figure 4.6 SEM image of scaffold post-aminolysis functionalization (mag: 65x)

There is the appearance of a ‘rougher’ surface in some areas, when compared to other micrographs. This is useful to note for further developments regarding cellular growth and proliferation, as roughness could assist with cellular attachment and adherence. Aminolysis has not negatively affected the structural condition, and it looks similar to that of unmodified scaffolds. Thus, aminolysis can be performed without changes in processing conditions, as the structural outcome remains intact.

4.2.1.5 *Evaluation of Biodegradation Behaviour of Aminolysed 3D Bioprinted Scaffolds*

As previously mentioned, it is important to assess the degradation behaviour of scaffolds used in tissue engineering. The biodegradability of scaffolds is necessary due to the nature of tissue engineering where it is essential that the materials are not only compatible with the body, but that the body can effectively break down the scaffold over time and process its degradation products safely and efficiently. It is thus important to assess the degradation of chemically functionalized scaffolds so as to observe the effects of the modifications on the scaffolds. Figure 4.7 shows the *in vitro* degradation behaviour of the amine-functionalized scaffolds.

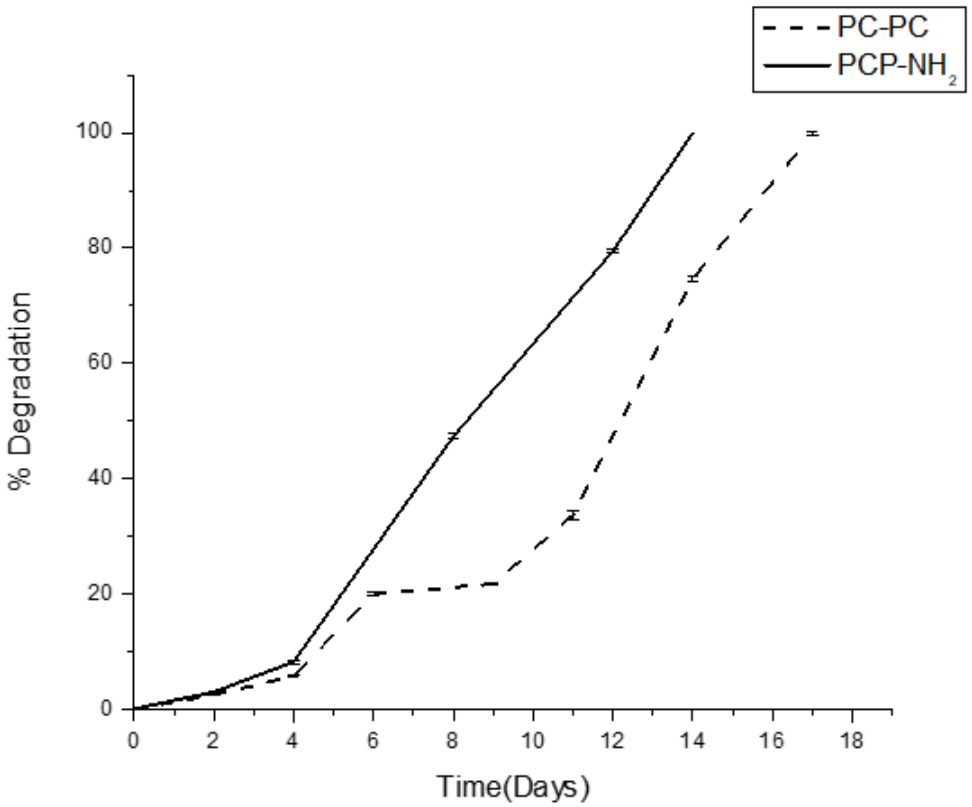


Figure 4.7 Graphical representation of the degradation behaviour of amine-functionalized scaffolds when compared to PC-PC scaffolds (SD <0.8)

In terms of the effects of the post-printing chemical modifications, amine functionalities increased the degradation rate of the scaffolds. The full amine-functionalized scaffold degraded within 14 days, as opposed to the PC-PC degradation of 17 days. This is an expected conclusion, due to the basicity of amines, which speeds up the degradation of the CAP component – a majority component of the scaffold formulation. It is important to note, however, that experimental procedures proved that amine modifications can alter the degradation rate further, depending on the concentration of amines. As such, increased concentrations resulted in even faster degradation, whilst lower concentrations did not have such a severe effect. This could be attributed to the basicity of amines which, and increased basicity results in CAP being degraded more rapidly, thus immersing the scaffold in higher concentrations during the modification process compromises the structural integrity more than during immersion in lower concentrations.

The degradation rate of the aminolysed scaffold compared to PC-PC was also measured, as elaborated upon in the figure below.

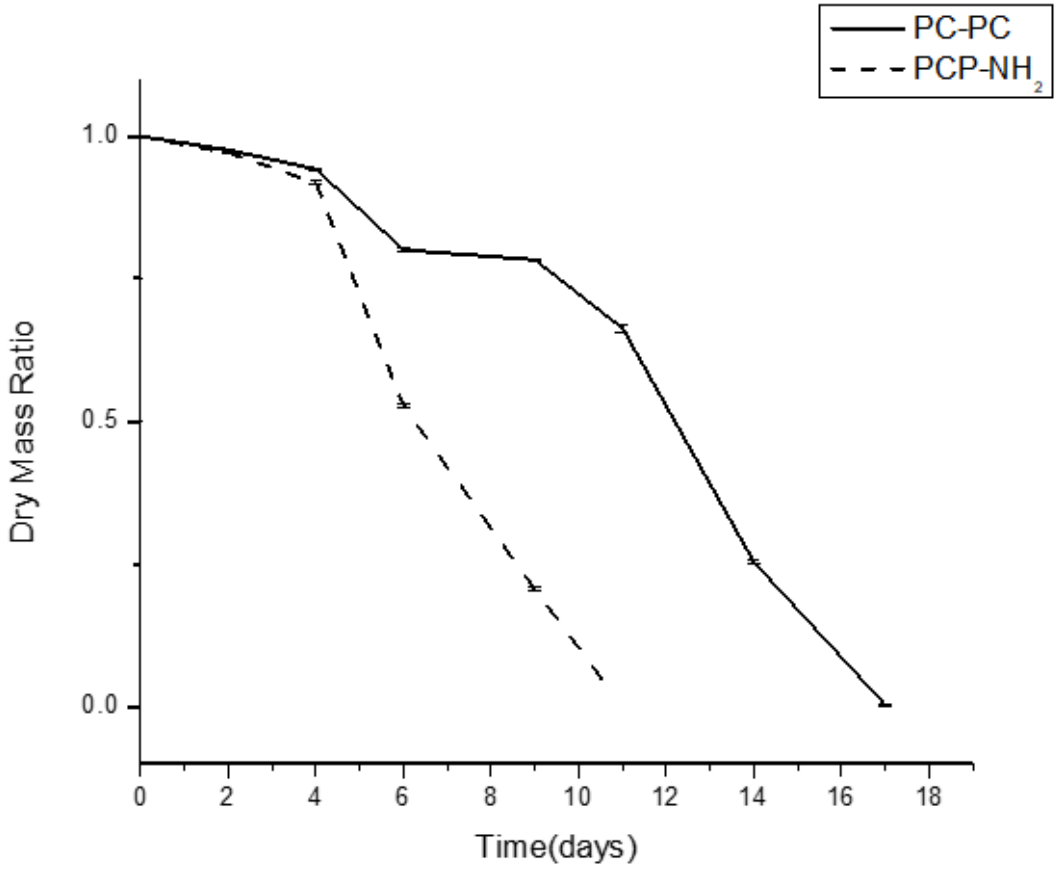


Figure 4.8 Graphical representation of the degradation rate of amine-functionalized scaffolds when compared to PC-PC scaffolds, using dry mass ratio (SD <0.01)

Interestingly enough, the degradation behaviour of both the PCP-NH_2 and the PC-PC scaffold were similar for the first two days, and thereafter, the aminolysed scaffold degraded faster. PCP-NH_2 presented with an initial degradation rate of 0.02 day^{-1} and then increased to a rate of 0.013 day^{-1}. PCP- NH_2 also presents with a half-life of 6 days which is exactly half of that of PC-PC. The comparison shows us that PCP-NH_2 can be used in order to shorten the degradation period whilst still maintaining a proportional half-life and similar degradation rate to that of PC-PC.

4.3.2 Hydrolysis Functionalization

4.3.2.1 Chemical Transitions Associated with Hydrolysed 3D Bioprinted Scaffolds

As mentioned previously, FTIR is an effective measure of determining changes in surface chemistry. The scaffolds were composed of PHBV and CAP, with PC as a plasticizer. Post-printing, the scaffolds were washed and allowed to dry before undergoing basic hydrolysis in order to introduce a hydroxyl (-OH) group into the structure. As per the method from which this process was adapted (Ke *et al*., 2017), the modification is proposed to have altered the PHBV compound specifically.

The scaffolds were subjected to analysis of their chemical structure in order to compare the chemical transitions of the hydroxy-functionalized scaffold (Figure 4.9) to the previously characterized PC-PC scaffold

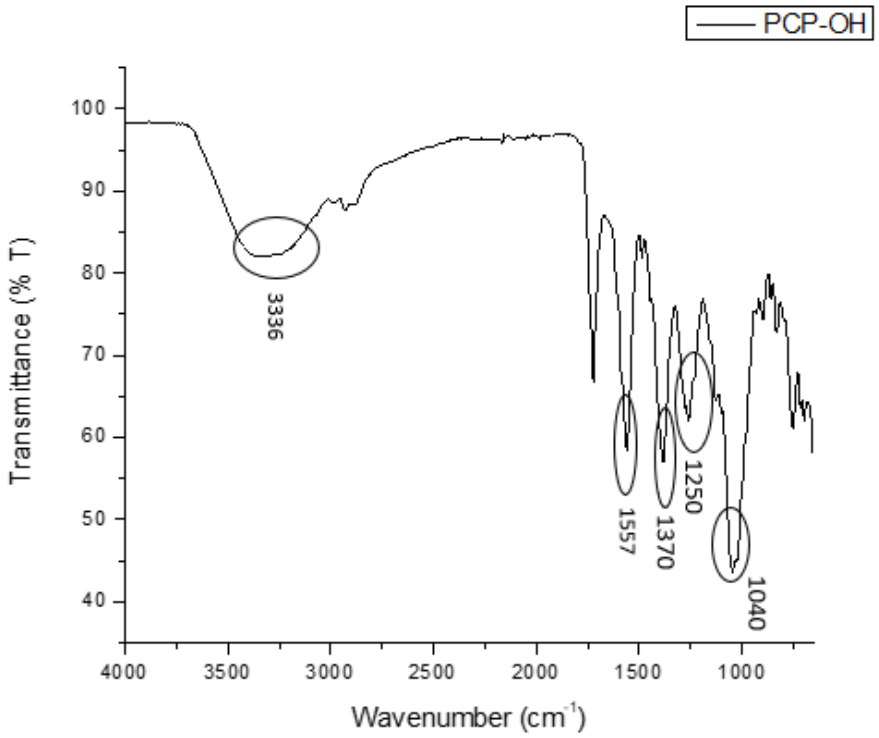


Figure 4.9 FTIR spectra showing the change in chemical structure due to the functionalization of the scaffold through hydrolysis

Hydrolysis also proved to have the desired effect of functionalization. A very clear and characteristic OH bond is seen at ~3336 cm^{-1} and supported by the presence of the peak at ~1370 cm^{-1}. A C-O bond is also present and shown at ~1250 cm^{-1}. The band at ~1040 cm^{-1} denotes the presence of a primary alcohol, which directly supports the success of the hydrolysis process.

The proposed reaction and chemical structure are depicted in Figure 4.10 below

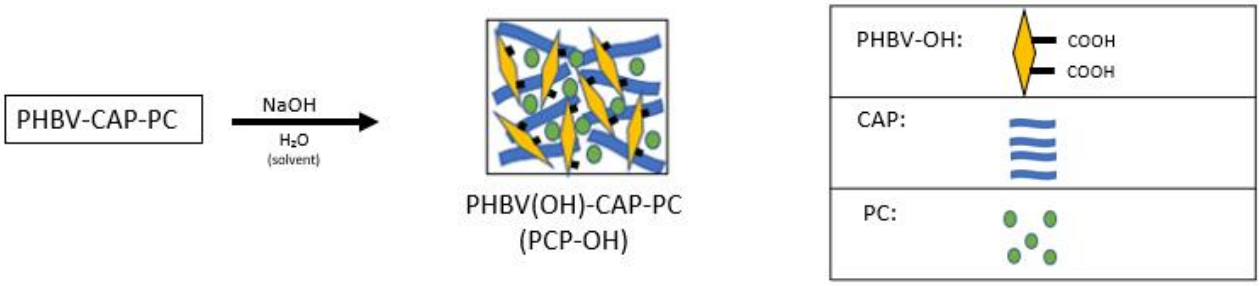


Figure 4.10 Diagram depicting the proposed reaction and chemical structure of the hydrolysis-modified scaffold

As such, these functionalizations were not only successful in terms of changing the chemical structure, but desirable functional groups were also introduced which can now be analyzed for their effects on the properties of the scaffolds, as well as potentially exploited for further use.

4.3.2.2 Thermal Transitions Associated with Hydrolysed 3D Bioprinted Scaffolds

As explained previously, thermograms are particularly important in observing the effects of modifications, especially in cases where these modifications take place after printing, as it is necessary for the thermal profile to remain stable before and during clinical application.

The thermogram below (Figure 4.11) reflects thermal changes as a result of basic hydrolysis. The analysis was done on crushed 3D bioprinted and subsequently functionalized fibers.

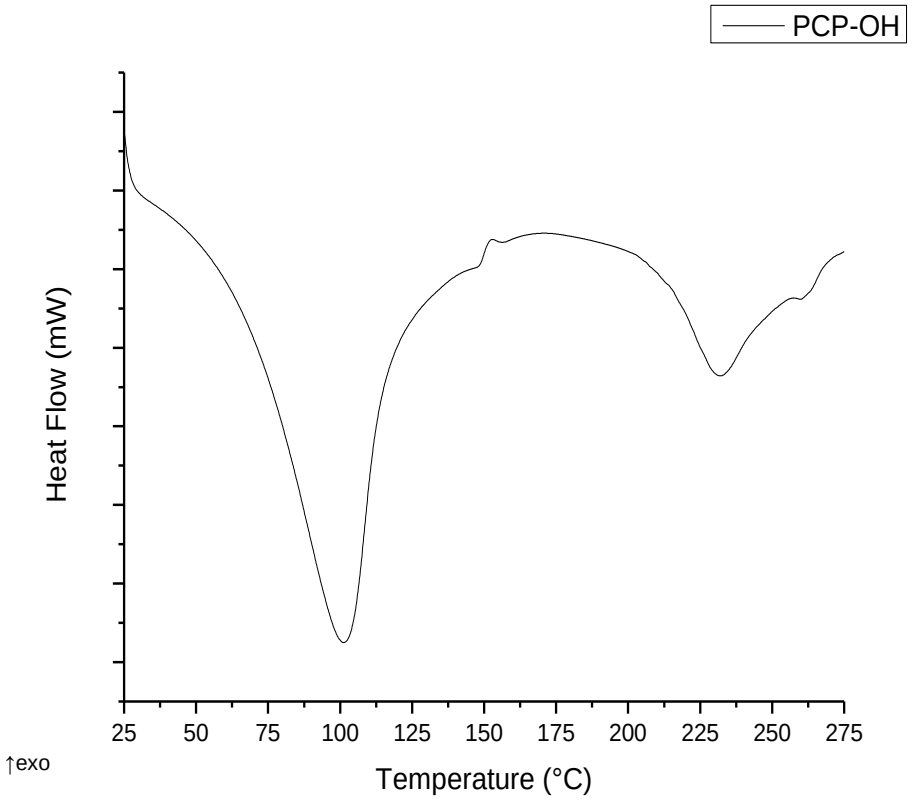


Figure 4.11 DSC thermogram showing the effect of hydrolysis-based functionalization on the thermal behaviour of the scaffold

As with aminolysis, hydrolysis did not have a particularly adverse effect on the thermal profile of the scaffold. However, it has drastically decreased the melting point to 101°C, with an exothermic crystallinity peak at 152°C and decomposition starting at 232°C. These changes, while still permittable due to the nature of the construct's biomedical application, do still limit the potential processing window for any future modifications, and this does need to be considered should further modifications under harsher conditions be required.

4.3.2.3 Evaluation of Mechanical Properties of Hydrolysed 3D Bioprinted Scaffolds

As mentioned previously, load-bearing is an important aspect to consider when evaluating mechanical properties of scaffolds. Figure 4.12 shows the difference in tensile strength between PC-PC and the hydroxy-functionalized scaffold - PCP-OH, while Figure 4.13 compares the compression strength of PCP-OH to that of PC-PC.

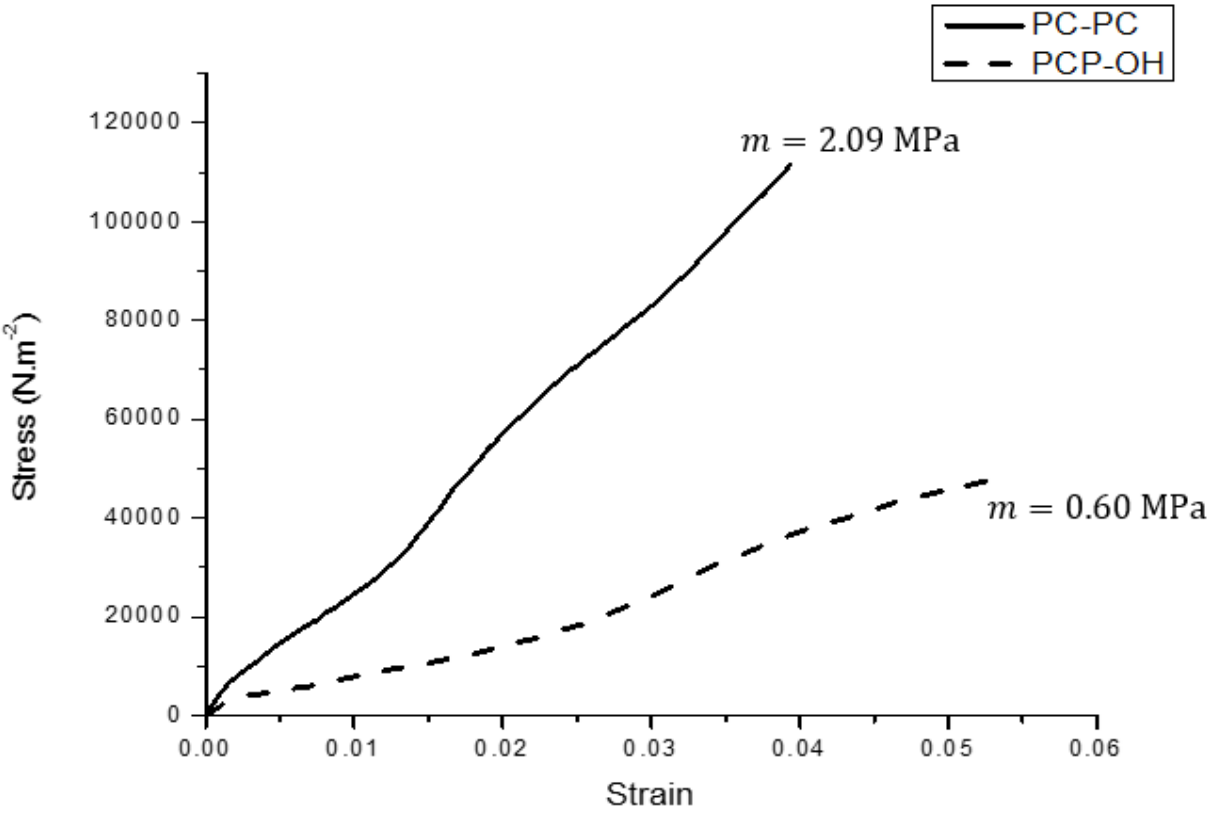


Figure 4.12 A stress-strain curve comparing the tensile properties of a hydroxy-functionalized scaffold (PCP-OH) to that of previously characterized PC-PC (Strain SD: <0.1)

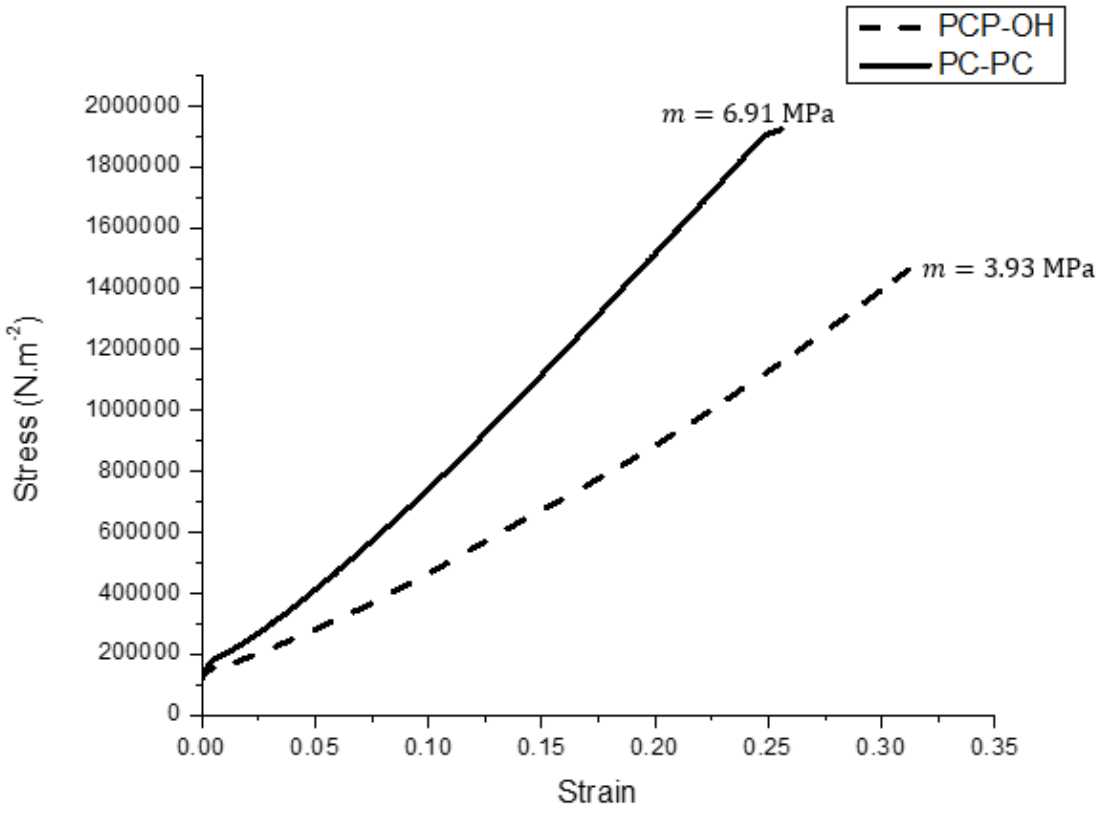


Figure 4.13 A stress-strain curve comparing the compression properties of hydroxy-functionalized scaffolds (PCP-OH) when compared to the previously characterized PC-PC (Strain SD <0.1)

When compared to PC-PC, the presence of hydroxyl groups also improved the flexibility of the scaffold with a tensile Youngs modulus of ~0.60MPa. This is also useful to compare to that of the amine-functionalized results (depicted in Figure 4.14a), as hydroxyl groups appear to still contribute more positively towards mechanical strength than amine-functionalities, even though the process of hydrolysis is harsher and requires more monitoring. In terms of compressive strength, the Young's modulus which, although lowered to ~3.93MPa when compared to PC-PC, is still higher than that of amine-functionalized scaffolds (depicted in Figure 4.14b), as well as the previously characterized glycerol plasticized scaffold (PC-G), and that of the non-plasticized scaffold (PC). This is useful, because not only does the construct display relatively impressive

resistance to deformation, but also proves that chemical modifications are a promising avenue to alter mechanical properties.

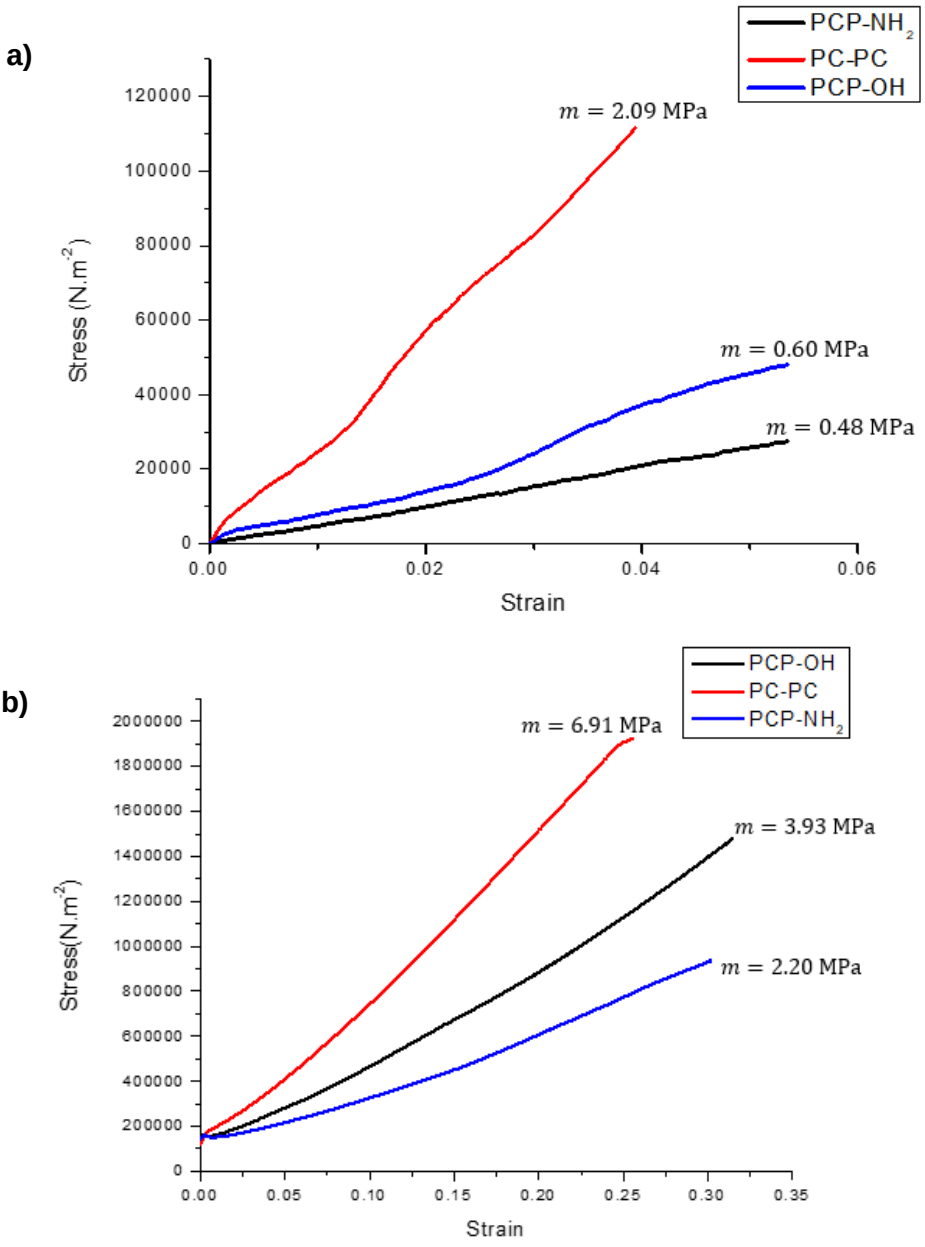


Figure 4.14 Graphs comparing the a) tensile properties of PC-PC, PCP-NH_2 and PCP-OH (Strain SD<0.1), b) the compressive properties of PC-PC, PCP-NH_2 and PCP-OH (Strain SD <0.2)

The hydroxy-modified scaffolds can potentially be utilized for a variety of clinical purposes, as shown in Table 4.2, depending on mechanical requirements. This proves that post-printing chemical modifications contribute positively towards the versatility of the 3D bioprinted construct.

Chemical Modification	**Potential Application**	**Reference**

PCP-OH	• Skin
	• Reproductive System
	  ➢ Uterus
	  ➢ Ligaments (uterosacral, cardinal)
	  ➢ Vagina
	• Nasal Cartilage:
	  ➢ Septal cartilage
	• Bone:
	  ➢ Mandible without cortical layer
	  ➢ Tibia
	  ➢ Radius
	  ➢ Vertebra
	• Femoral cartilage
		(Baah-Dwomoh *et al*., 2016, Serup *et al*., 2006, Griffin *et al*., 2016b, Lakatos *et al*., 2014, Vidal-Lesso *et al*., 2014)

Table 4.2 Potential clinical applications for the amine-modified scaffolds as per their elastic modulus found in literature

4.3.2.4 Mapping of Surface Morphology of Hydrolysed 3D Bioprinted Scaffolds

SEM micrographs are important in comparisons, so as to ascertain structural changes as a result of modifications. The micrograph below (Figure 4.15) reflects the changes observed in a scaffold as a result of hydroxy-functionalization

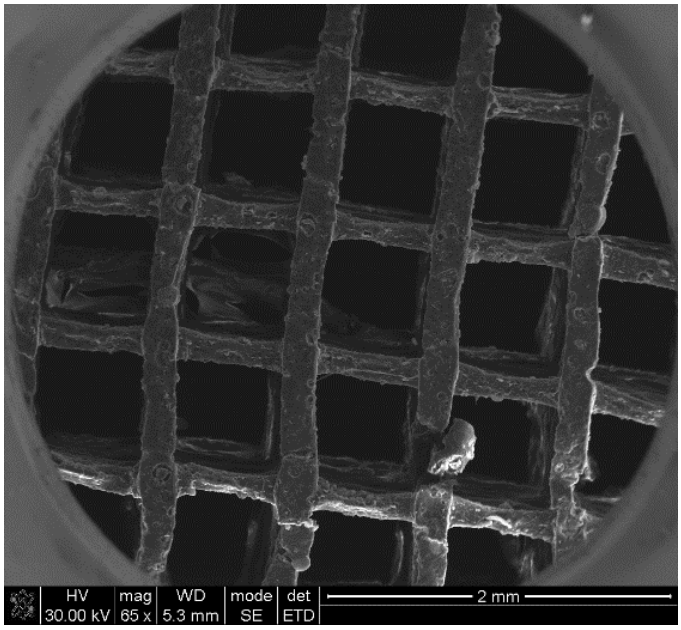


Figure 4.15 SEM image showing the change in structure and morphology of the scaffold post-hydrolysis functionalization (mag: 65x)

It must be noted that the processing conditions of hydrolysis are harsh on the scaffold structure. This is evidenced by the visibly larger pores, when compared to the other scaffolds. This could prove advantageous when nutrient, cellular and waste diffusion is considered, as larger pores improve the transport system. This could assist in cellular growth, due to the abundance of nutrients that would be able to access a larger surface area. However, it could also retard cellular growth due to the need for cellular growth to span across what is essentially ‘dead space’, and this could result in cellular growth taking longer due to the lack of support structure in these spaces.

4.3.2.5 Evaluation of Biodegradation Behaviour of Hydrolysed 3D Bioprinted Scaffolds

As previously mentioned, it is important to assess the degradation behaviour of scaffolds used in tissue engineering, because biodegradation is an essential criterion of scaffolds. The degradation behaviour of hydroxyl-functionalized scaffolds is particularly interesting to note due to the nature of the functional groups which actively contribute in the form of hydrolytic degradation. It is therefore important to assess the degradation of hydroxyl-functionalized scaffolds compared to the previously characterized PC-PC so as to observe the effect of adding and exploiting hydroxyl groups on the scaffolds surface. Figure 4.16 shows the *in vitro* degradation behaviour of the hydroxy-functionalized scaffolds.

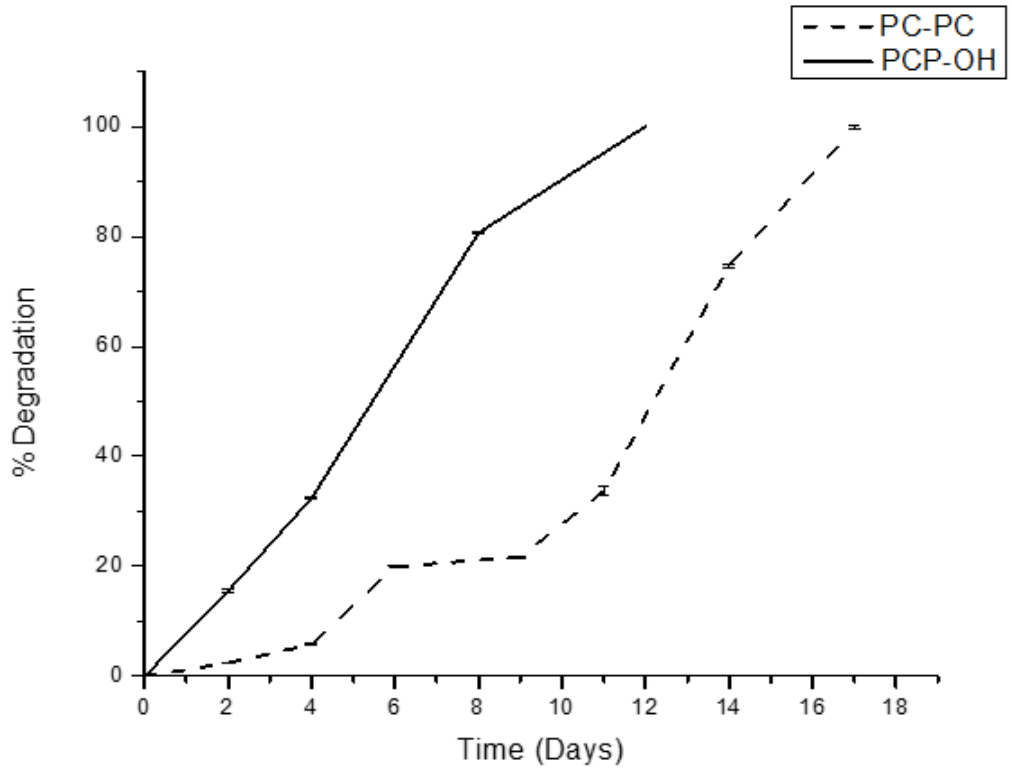


Figure 4.16 Graphical comparison of the degradation behaviour of hydroxy-functionalized scaffolds to PC-PC scaffolds (SD <0.8)

PCP-OH degraded sooner than both the PC-PC scaffold and the aminolysed scaffold reported on above (11-days compared to 17- and 14- days, respectively) (Depicted in Figure 4.17). This is an

expected conclusion due, firstly, to the presence of hydroxyl groups which are known to degrade structures faster, as well as the basicity of the solution used – which has been elaborated upon above with regards to aminolysis. The effect of concentration used in hydrolysis had a similar effect as in aminolysis, and increased concentrations drastically increased the degradation behaviour. Both these factors contributed to the compromised structural integrity of the scaffold as shown in the SEM images, which was also more susceptible to physical manipulation, as well as displaying decreased mechanical properties.

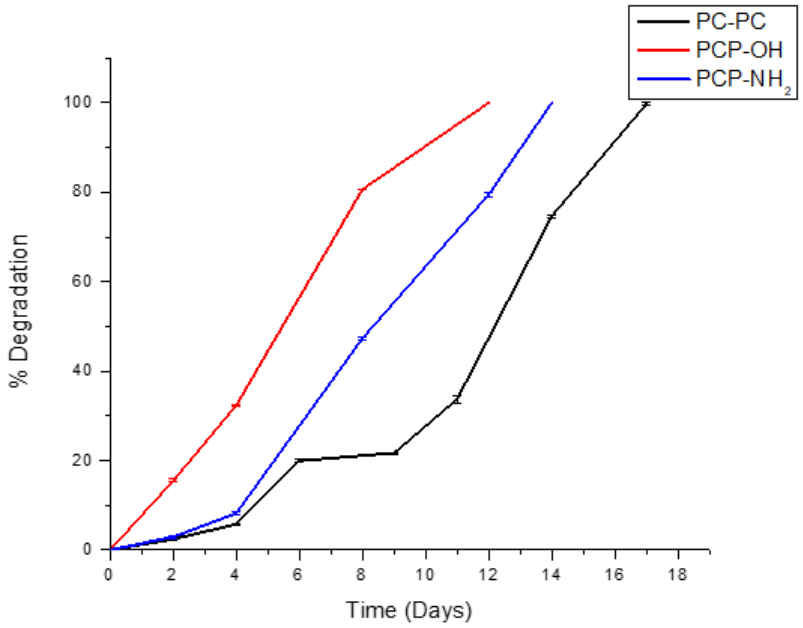


Figure 4.17 Graph comparing the degradation behaviours of PC-PC, PCP-NH_2 and PCP-OH (SD<0.8)

The degradation rate of PCP-OH was also more rapid than that of PC-PC, as expected, as shown in the figure below.

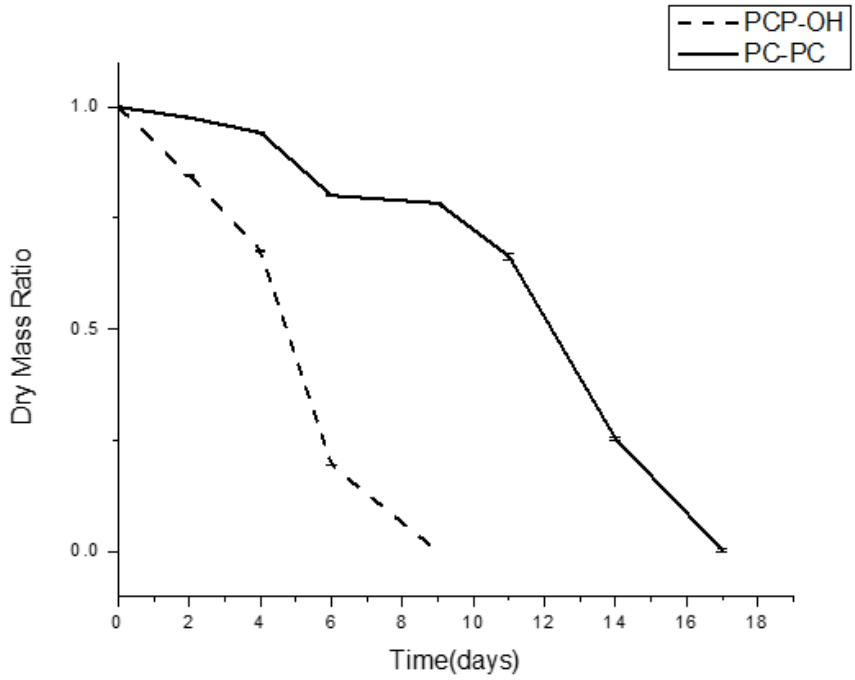


Figure 4.18 Graphical representation of the degradation rate of hydroxy-functionalized scaffolds when compared to PC-PC scaffolds, using dry mass ratio (SD <0.01)

The initial degradation took place at a rate of 0.13 day^{-1} after which it slowed to 0.06 day^{-1} the retardation of which is possibly owing to the removal of the extra hydroxyl groups. The half-life of PCP-OH was also identified as 4.5 days, which is much shorter than the abovementioned half-life of PC-PC which was 12 days. Thus, the addition of hydroxyl groups can be used as a method to hasten the degradation rate in rapidly growing tissues, or as a method of hastening the degradation of slow-degrading polymers. However, the degradation rate of PCP-OH, was inferior to that of PCP-NH_2 (as depicted in Figure 4.19). This proves that the addition of amine groups did not compromise the degradation behaviour of the scaffold as drastically as the addition of hydroxyl groups. The elucidation of this data allows us to conclude that post-printing chemical modifications can be used to tailor the degradation behaviour of the construct, but must be carefully controlled.

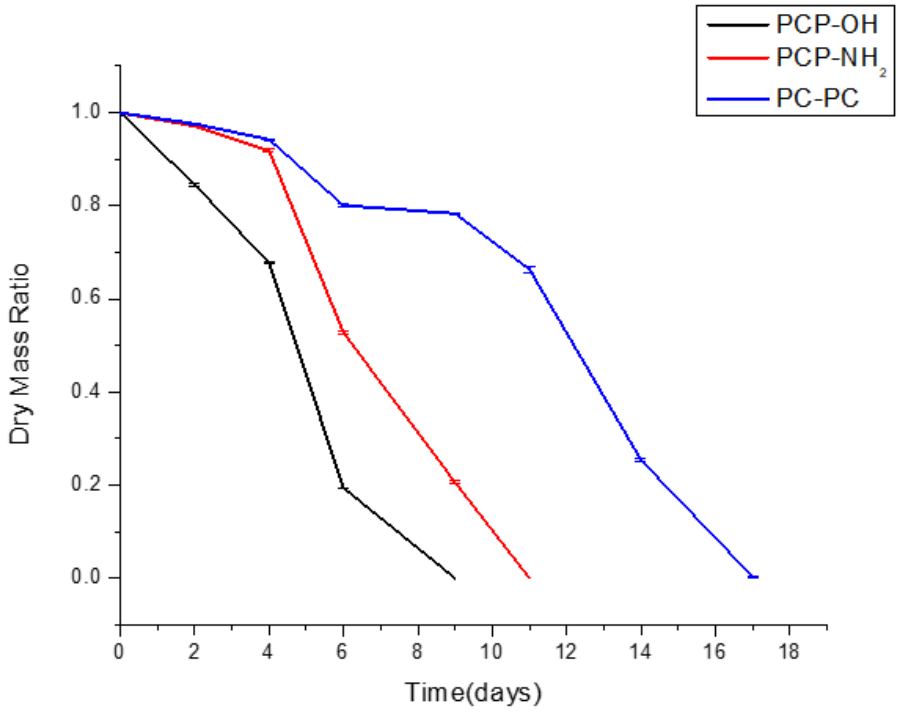


Figure 4.19 Graph comparing the degradation rate of PC-PC, PCP-NH_2 and PCP-OH (SD<0.1)

4.3.3 Biomacromolecular attachment

4.3.3.1 Chemical Transitions of Chemically Modified 3D Bioprinted Scaffolds with Biomacromolecular Attachment

The spectra below show the effect of the hyaluronic attachment on the aminolysed scaffold.

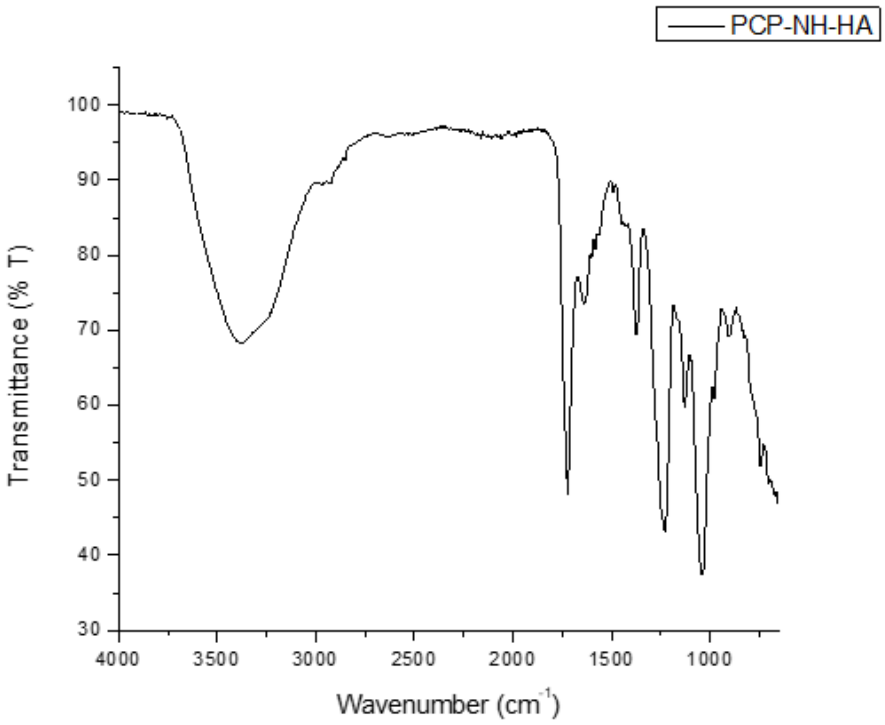


Figure 4.20 FTIR spectra showing the effect of hyaluronic acid grafting onto the PCP-NH_2 backbone

While each component of the system is represented, it must be noted that due to the similarity of chemical groups found in each component's chemical structure, bands often overlap and changes can often only be noticed through change in intensity, shape or wavenumber. This is evidenced by propylene carbonate, which was not well-represented in the observed structure. However, this could be too to its structure, wherein it shares many groups with the other polymers, and as such, just does not have identifiable markers. Table 4.3 shows the various bands that are present, as well as which component of the system they may be attributed to.

Table 4.3 Band assignments for the spectra of Figure 4.20 and componential categorization

PHBV-CAP	**Propylene Carbonate**	**-NH_2**	**Hyaluronic acid**
~3379: -OH stretching	~1378: Methyl groups	~3268: secondary amine	~3379: -OH stretching
~1378: -OH band		~896: N-H wag	~1039: C-O-C stretching
~1717: C=O		~1563: N-H	~1441: C-O group with C=O combination
~1219: ester			~2935: C-H stretching
~2935: H-C-H			~1632: amide
~1441: O-H			~1235: C-O
~1378: Methyl groups			
~1039: C-O-C stretching			

In terms of the -OH band, there is an increase in intensity and shape, as well as a wavenumber shift, as a result of the additive effect of HA. This effect may have led to the overlapping of the amine group. However, the amine is still represented through the band at 896 cm^{-1}. Another overlap takes place at 1039 cm^{-1}, and is evidenced by the increase in intensity and slight narrowing of the peak, due to additional C-O-C bonds. The band at 1378 cm^{-1} may signify -OH, but could also be overlapped by methyl groups present in multiple components of the structure. The proposed reaction and chemical structure are presented in Figure 4.21 below.

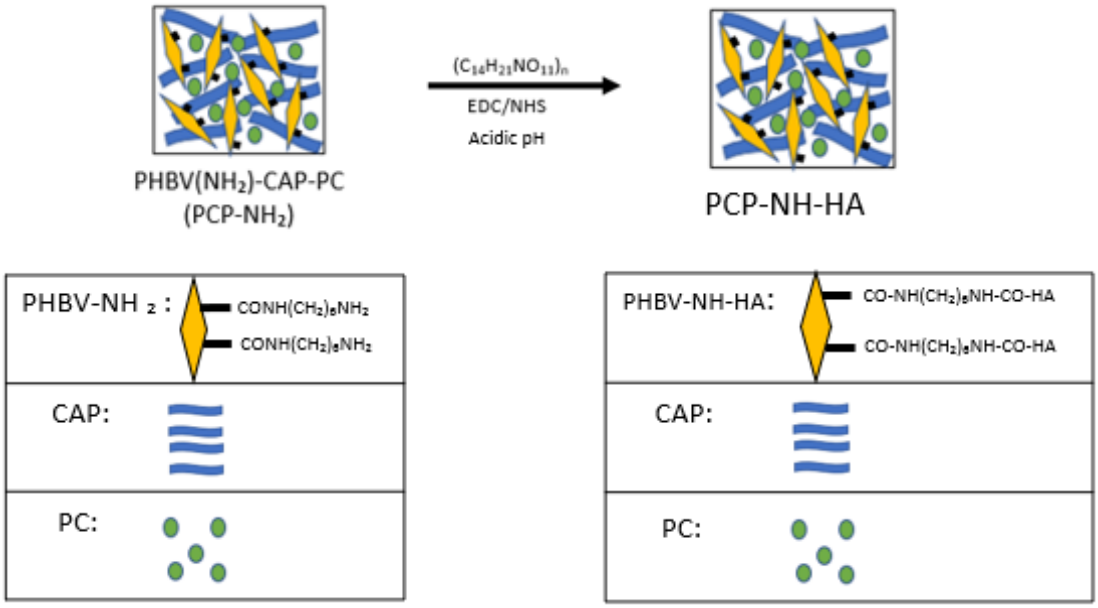


Figure 4.21 Diagram depicting the chemical reaction and proposed structure of PCP-NH_2 modified with hyaluronic acid

Hyaluronic acid was also attached to the PCP-OH scaffold, and this is reflected in Figure 4.22, and the subsequent elaboration.

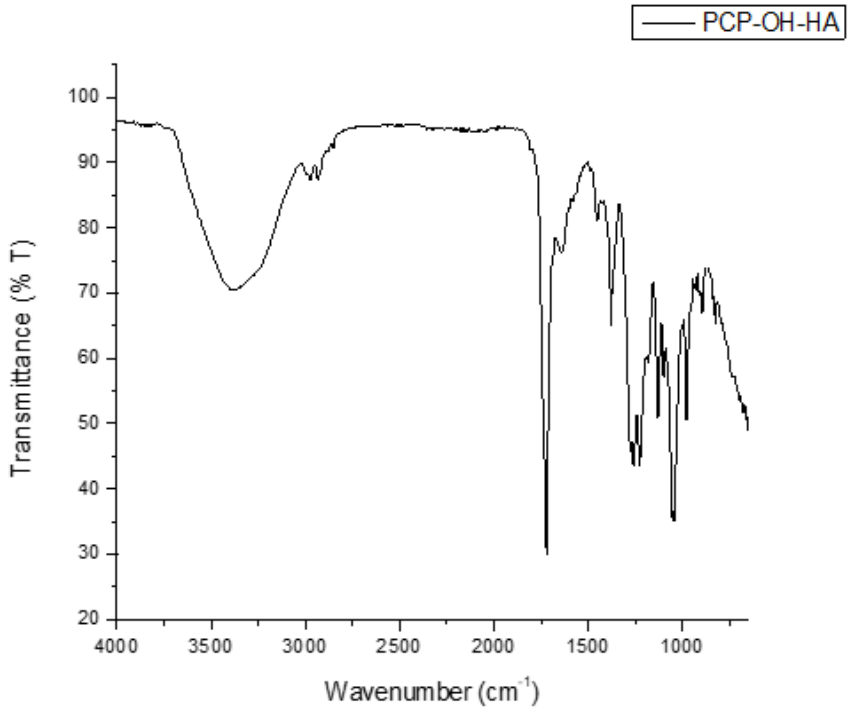


Figure 4.22 The effect of hyaluronic acid grafting onto the PCP-OH backbone

As mentioned previously, there are many bonds overlapping and many additive effects due to identical bonds found in multiple components, as evidenced by changes in shape, intensity and wavenumber. Table 4.4 assigns bands to various components of the system.

Table 4.4 Table elaborating on various bonds found in Figure 4.14 and componential categorization

PHBV-CAP	**Propylene Carbonate**	**-OH**	**Hyaluronic acid**
~3368: -OH stretching	~1373: Methyl groups	~3368: -OH	~3379: -OH stretching
~1373: -OH band		~1441: O-H	~1044: C-O-C stretching
~1717: C=O		~1250: C-O	~1441: C-O group with C=O combination
~1219: ester			~2935: C-H stretching
~2935: C-H stretching			~1643: amide
~1441: O-H			~1235: C-O
~1373: Methyl groups			
~1044: C-O-C stretching			

As explained above, there are also many overlapping bonds in this structure, which does not permit equal representation of all components (propylene carbonate, is once more, not adequately viewed in the structure). However, the FTIR reflects a conclusive interaction between the hyaluronic acid and the PCP-OH backbone. The proposed reaction and chemical structure can be observed in Figure 4.23 below.

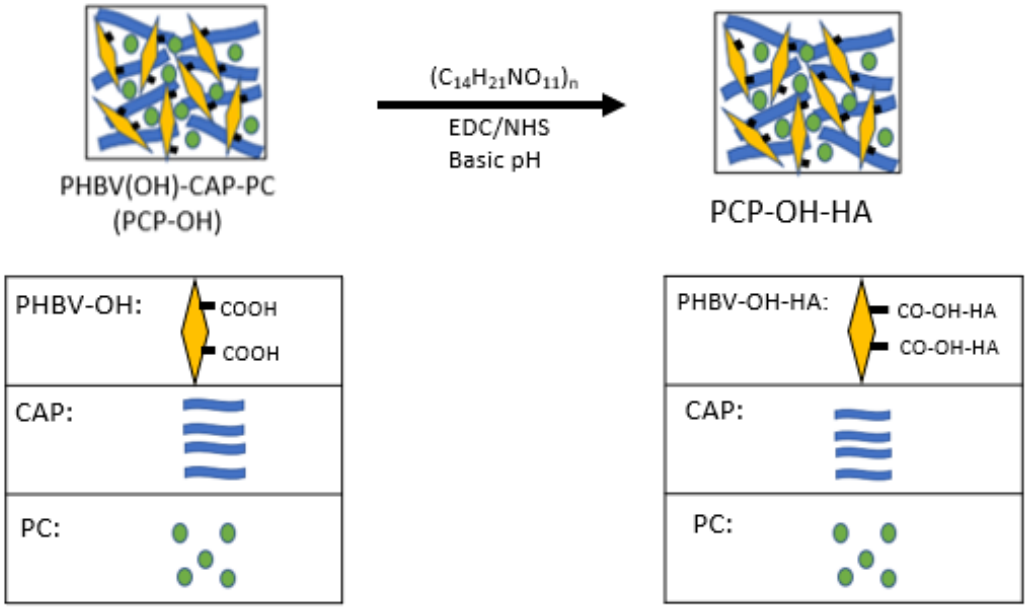


Figure 4.23 Diagram depicting the reaction and proposed chemical structure of PCP-OH modified with hyaluronic acid

It is thus observed that the scaffold structure can indeed be chemically modified post-printing in order to alter mechanical properties, as well as serve as a backbone for a secondary polymer to be attached to the surface of the scaffold.

4.4 Concluding Remarks

Chemical functionalization of scaffolds post-printing has proven to be an effective manner of altering mechanical properties, as elaborated upon above. The conditions used for chemical post-processing are easy to manipulate, and various methods are available, depending on resources as well as desired outcomes.

While the results of both aminolysis and hydrolysis functionalization could not supersede the unmodified scaffold, they proved the concept that the mechanical properties of scaffolds can be dictated by their surface chemistry which is easily manipulatable post-printing. The results also

showed that these methods can be used to customize scaffolds for specific applications, depending on the mechanical requirements of the native tissue, as elaborated upon above.

Various considerations must still be made in order to optimize the process for individual materials. An example of this is the degradation rate exhibited above, which may not be therapeutically appropriate, but which does show that post-printing chemical modifications do successfully alter many properties including the degradation rate – which can even be advantageous in terms of engineered tissues which heal quickly and must be processed by the body rapidly.

Ultimately, the purpose of assessing the effects of these functionalizations was to obtain a proof of the concept that post-printing chemical modifications can be used in order to alter the physicomechanical properties of already-printed structures, according to various requirements including tensile and compression strength, as well as degradation rate requirements based on tissue growth patterns. This was done successfully for future work to build off, and consider further evaluation and quantification of the effects of other chemical groups.

References

Baah-Dwomoh, A., Mcguire, J., Tan, T. & De Vita, R. 2016. Mechanical Properties of Female Reproductive Organs and Supporting Connective Tissues: A Review of the Current State of Knowledge. *Applied Mechanics Reviews,* 68**,** 060801-060801-12.

Bose, S. V. S. & Bandyopadhyay, A. 2013. Bone tissue engineering using 3D printing. *Mater Today,* 16.

Burdick, J. A. & Prestwich, G. D. 2011. Hyaluronic acid hydrogels for biomedical applications. *Advanced materials,* 23**,** H41-H56.

Griffin, M. F., Premakumar, Y., Seifalian, A. M., Szarko, M. & Butler, P. E. M. 2016. Biomechanical Characterisation of the Human Auricular Cartilages; Implications for Tissue Engineering. *Annals of Biomedical Engineering,* 44**,** 3460-3467.

Griffin, M. F., Premakumar, Y., Seifalian, A. M., Szarko, M. & Butler, P. E. M. 2016. Biomechanical characterisation of the human nasal cartilages; implications for tissue engineering. *Journal of materials science. Materials in medicine,* 27**,** 11-11.

Jia, J., Richards, D. J., Pollard, S., Tan, Y., Rodriguez, J., Visconti, R. P., Trusk, T. C., Yost, M. J., Yao, H. & Markwald, R. R. 2014. Engineering alginate as bioink for bioprinting. *Acta biomaterialia,* 10**,** 4323-4331.

Ke, Y., Liu, C., Zhang, X., Xiao, M. & Wu, G. 2017. Surface Modification of Polyhydroxyalkanoates toward Enhancing Cell Compatibility and Antibacterial Activity. *Macromolecular Materials and Engineering,* 302**,** 1700258.

Kesti, M., Müller, M., Becher, J., Schnabelrauch, M., D'este, M., Eglin, D. & Zenobi-Wong, M. 2015. A versatile bioink for three-dimensional printing of cellular scaffolds based on thermally and photo-triggered tandem gelation. *Acta biomaterialia,* 11**,** 162-172.

Lakatos, E, Magyar, L., Bojtar, I. 2014. Material Properties of the Mandibular Trabecular Bone. *Journal of Medical Engineering,* 2014**,** 7.

Lannutti, J., Reneker, D., Ma, T., Tomasko, D. & Farson, D. 2007. Electrospinning for tissue engineering scaffolds. *Materials Science and Engineering: C,* 27**,** 504-509.

Müller, M., Becher, J., Schnabelrauch, M. & Zenobi-Wong, M. 2015. Nanostructured Pluronic hydrogels as bioinks for 3D bioprinting. *Biofabrication,* 7**,** 035006.

Necas, J., Bartosikova, L., Brauner, P. & Kolar, J. 2008. Hyaluronic acid (hyaluronan): a review. *Veterinarni medicina,* 53**,** 397-411.

Ouyang, L., Highley, C. B., Rodell, C. B., Sun, W. & Burdick, J. A. 2016. 3D Printing of Shear-Thinning Hyaluronic Acid Hydrogels with Secondary Cross-Linking. *ACS Biomaterials Science & Engineering,* 2**,** 1743-1751.

Panwar, A. & Tan, L. P. 2016. Current status of bioinks for micro-extrusion-based 3D bioprinting. *Molecules,* 21**,** 685.

Schante, C., Zuber, G. & Vandamme, T. 2011. Chemical modifications of hyaluronic acid for the synthesis of derivatives for a broad range of biomedical applications. *Carbohydrate Polymers,* 85**,** 469-489.

Serup, J., Grove, G. L. & Jemec, G. B. 2006. *Handbook of non-invasive methods and the skin*, CRC press.

Shih, Y. C. 2015. Effects Of Degradation On Mechanical Properties Of Tissue-Engineering Poly (glycolic Acid) Scaffolds.

Suntornnond, R., An, J., Yeong, W. Y. & Chua, C. K. 2015. Biodegradable polymeric films and membranes processing and forming for tissue engineering. *Macromolecular Materials and Engineering,* 300**,** 858-877.

Vidal-Lesso, A., Ledesma-Orozco, E., Daza-Benítez, L. & Lesso-Arroyo, R. 2014. Mechanical Characterization of Femoral Cartilage Under Unicompartimental Osteoarthritis. *Ingeniería mecánica, tecnología y desarrollo,* 4**,** 239-246.

Wang, L.-Y., Wang, Y.-J. & Cao, D.-R. 2009. Surface Modification of Poly(3-hydroxybutyrate-co-3-hydroxyvalerate) Membrane by Combining Surface Aminolysis Treatment with Collagen Immobilization. *Journal of Macromolecular Science, Part A,* 46**,** 765-773.
Wysocki, B., Idaszek, J., Szlązak, K., Strzelczyk, K., Brynk, T., Kurzydłowski, K. J. & Święszkowski, W. 2016. Post Processing and Biological Evaluation of the Titanium Scaffolds for Bone Tissue Engineering. *Materials,* 9**,** 197.
Zhao, J., Griffin, M., Cai, J., Li, S., Bulter, P. E. M. & Kalaskar, D. M. 2016. Bioreactors for tissue engineering: An update. *Biochemical Engineering Journal,* 109**,** 268-281.
Zong, X., Bien, H., Chung, C. Y., Yin, L., Fang, D., Hsiao, B. S., Chu, B. & Entcheva, E. 2005. Electrospun fine-textured scaffolds for heart tissue constructs. *Biomaterials,* 26.

CHAPTER 5

THE *IN VIVO* ASSESSMENT OF BIODEGRADATION BEHAVIOUR AND IMMUNE RESPONSE OF THE SCAFFOLDS IN A RAT MODEL

5.1 Introduction

Although the materials being researched have been characterized individually for their *in vitro* biocompatibility (Shrestha *et al*., 2016, Sundaramurthi *et al*., 2013), they have not been evaluated as potential engineered tissue and as such, have not been subjected to *in vivo* studies. *In vivo* evaluations are necessary for performance, safety and regulatory reasons (Khorramirouz *et al*., 2018). Since biomaterials for tissue engineering require good biocompatibility, it is vital that we assess and compare the inflammatory reactions provoked by various implanted biomaterials *in vivo* (Khorramirouz *et al*., 2018). In addition to the tissue response, it is also necessary to evaluate the degradation behaviour of the engineered scaffolds in a biological environment, comparable to that of humans. Subcutaneous implantation in an animal model has shown to be useful in evaluating immune reactivity (Neethling *et al*., 2010). The subcutaneous implantation in an animal model also enables the evaluation of biocompatibility by assessing potential sensitization, irritation and inflammation, toxicity, carcinogenicity and biodegradation (including the processing of the degradation products) (Wang *et al*., 2005, Modulevsky *et al*., 2016).

5.1.1 Selection of Appropriate Animal Model for In Vivo Studies

The field of biomedical research, and specifically tissue engineering, relies on animal models to provide evidence of success – whether it is with regards to biocompatibility, actual tissue growth, novel biomaterial evaluation or investigating healing and tissue responses. However, the use of animals in research still remains a controversial issue, and is highly regulated when permitted. Humane treatment, reduction of suffering, as well as the reduction of the number of animals required to produce statistical significance should all be adhered to. An appropriate animal model

should also be selected, so as to obtain the most appropriate and significant data, and avoid unnecessary suffering and irrelevant data.

The most commonly used lab animal are rats as they are inexpensive, easy to house and, because they have been used extensively, they are well-understood and characterized animal models (Liebschner, 2004). The rat model for subcutaneous implantation has been widely used, especially when testing for biocompatibility (Standardization, 2007, Standardization, 1997) and tissue responses, of which the information is necessary to provide direction in the tissue engineering realm.

5.2 Materials and Methods

5.2.1 Preparation of 3D Bioprinted Scaffold for In Vivo Implantation

The scaffold discussed in previous chapters (PC-PC), as well as its chemically modified counterparts (PCP-NH_2, PCP-OH), were prepared for *in vivo* assessment in order to evaluate the biodegradability, biocompatibility and tissue response. Prior to use, the scaffolds were washed extensively in order to remove any free chemical groups, as well as to remove any solvents from within the structure. The scaffolds were then sterilized under UV overnight, and hydrated with sterile Phosphate Buffered Saline before use.

5.2.2 Surgical Protocol for Implanting Scaffolds into Rat Model

Upon weaning and appropriate weight, the rats were habituated for at least a week to facilitate behavioural, physical and temperament monitoring, which would ensure effective post-surgical monitoring for changes. It was decided that a pilot study would not be relevant because it would simply be a replication of the actual study, and would thus be time-consuming, as well unnecessarily subjecting more animals to the surgical process. The study was thus designed to utilize the least number of animals required for statistical significance which resulted in five animals being used for the two chemically-modified experimental groups (PCP-NH_2 and PCP-

OH), three being used for PC-PC, and two animals being used as sham controls per time point (2- and 7- days). This allowed for statistical relevance across the experimental groups (n=3), but also left room for untimely and unrelated morbidity in the chemically-modified experimental groups. The rats were anaesthetized, as per the approved protocol, with ketamine (80mg/kg) and xylazine (10mg/kg) prior to the surgery (Kumbhar et al., 2017). The surgical incision site (the upper-middle back) was shaved to prepare for the surgery. Anesthesia was maintained with 2% Isoflurane in 100% oxygen. In a sterile field, a dorsal incision was made 1cm away from the spine. A subcutaneous pocket was thereafter created, via blunt dissection. The pocket was created just large enough to fit the scaffold, so as to ensure that it would remain in place without any fixing or suturing. The scaffold was placed into the pocket, and thereafter the incision site was sutured. Sham surgeries were used as controls, with the incision and subcutaneous pocket made, and sutured without inserting a scaffold. The rats were then induced out of anesthesia and placed in a warm environment in order to facilitate recovery. Buprenorphine (0.3mg/kg) was administered as a post-surgical pain reliever in order to combat pain, whilst not inhibiting inflammatory responses as those were necessary potential observations in the study. Following the surgical procedure, the rats were allowed to recover, under careful monitoring, and given food and water ad libitum until euthanasia.

Euthanasia was performed at certain time points (2 days and 7 days) through an overdose of sodium pentobarbital. Once euthanized, initial observations of the surgical site were made in order to identify any visible signs of adverse tissue responses. After this, the incision site was re-opened, macroscopic observations were made, and the tissue, as well as any remaining scaffold was excised and stored in 10% neutral buffered formalin until analysis. In cases where there were scaffold remnants, these were also removed and stored for analysis. Tissue samples from sham controls were also excised and stored for analysis in order to assess the biological response to the surgical procedure.

5.2.3 Immunohistological Protocol for Analysis

After sufficient fixation of the collected specimens in 10% buffered formalin, the tissues were cut according to standard operating procedure (IdexxSA-AP-SOP-26) and processed according to routine histological tissue processing in an automated tissue processor with standard operating procedures (IdexxSA-AP-SOP-27). Following tissue processing, sections were cut of 5-6µm (IdexxSAAP- SOP-30) and the slides produced stained in an automated Haematoxylin and Eosin tissue stainer (IdexxSA AP-SOP-205) before histological evaluation.

The staining was used to observed immune responses into the tissue according to semi-quantitative scaling (Lin *et al*., 2015):

- Minimal to Mild: <5 mononuclear inflammatory cells in a 10x10 grid
- Moderate: Mononuclear inflammatory cells scattered through the tissue, but background tissue still clearly visible
- Severe: Mononuclear inflammatory cells densely infiltrating the tissue

5.3 Results and Discussion

5.3.1 Surgical procedure of Implanting the Scaffolds in the Rat Model

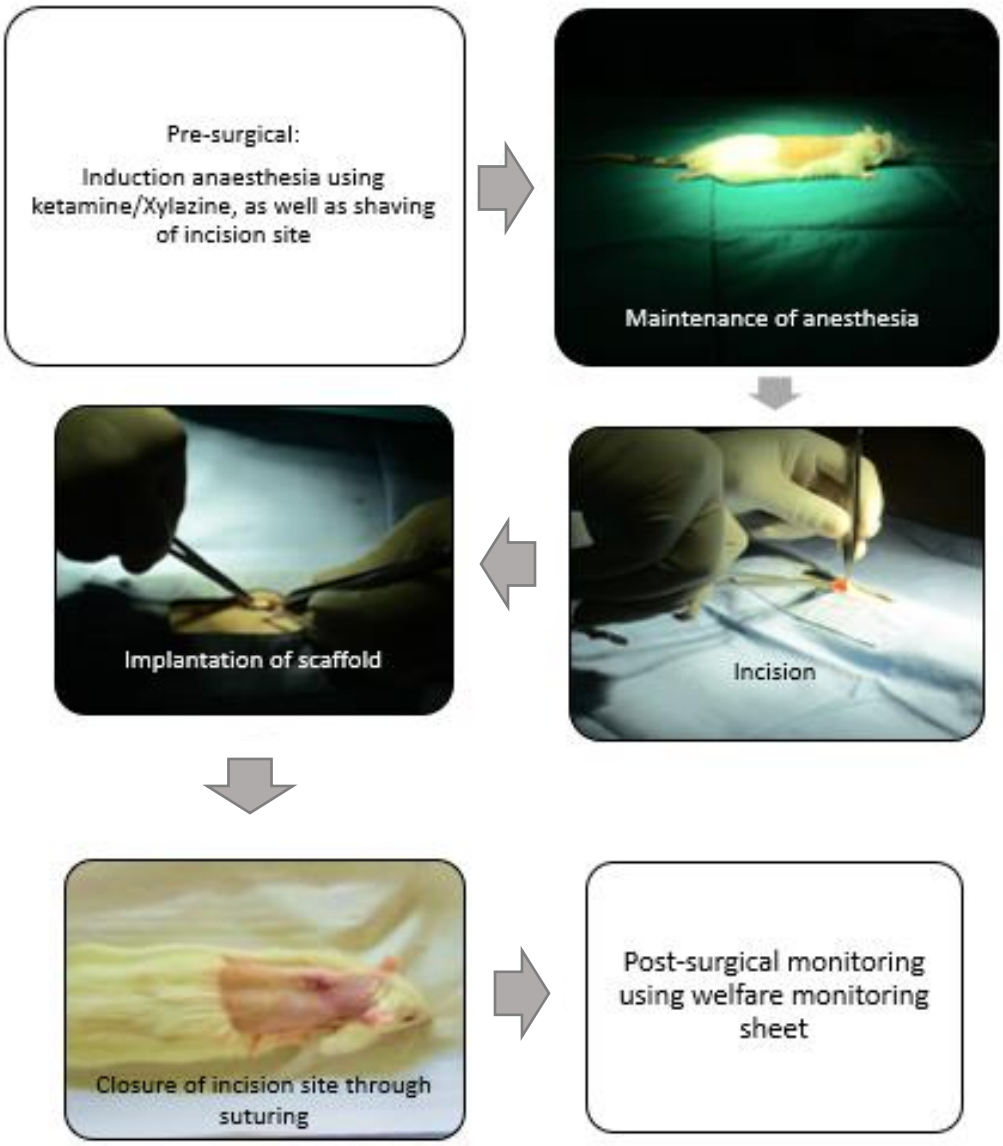


Figure 5.1 Flow chart showing the surgical procedure used to conduct *in vivo* studies

5.3.2 In Vivo Analysis

5.3.2.1 Biodegradation Behaviour Assessed In Vivo

The degradation rate of the scaffolds *in vivo* was significantly faster than that observed in *in vitro* studies and all three specimen types of scaffolds had completely degraded by seven days. The

initial reasoning can be attributed to CAP's inherent properties which result in its degradation in neutral to more basic environments – which is the physiological environment. PHBV has been proven to degrade faster *in vivo* than during *in vitro* hydrolysis under the same temperature and pH conditions (Williams and Martin, 2002). This can be attributed to nonspecific esterase and lysozyme enzymes, which are secreted by the body's immune system, and catalyze the degradation process (Sultana and Khan, 2012).

An increase in degradation rate is a well-documented phenomenon (Tamariz and Rios-Ramírez, 2013) and can be attributed to parameters which are not mimicked in *in vitro* studies, such as the presence of oxidation and enzyme factors, metabolism, activity and immune response (Tamariz and Rios-Ramírez, 2013).

The degradation behaviour itself is highly susceptible to immune response. When foreign materials are exposed to the body, they are immediately engulfed by proteins which form a complex and a system for phagocytic cells (Paul, 2013). This form of innate immunity results in different kinds of leukocytes (neutrophils, monocytes, macrophages and dendritic cells) engulfing the foreign material. Once this has occurred, enzymes and oxidative processes work to destroy the foreign body. As such, the degradation rate can be explained in part, by the immune response, as it would facilitate the rapid degradation of the scaffold in order to expel its presence.

5.3.2.2 Tissue Immune Response of the Animal Model to the Scaffold Implantation

5.3.2.2.1 Macroscopic Observations

It is first important to observe the rats for signs of rejection or discomfort during the monitoring period. Stress signs as a result of the surgery presented in a small number of subjects (approximately 3-4) after each surgery but faded within a few hours. Bi-daily check-ins found all of the subjects presenting as well and in good health. All of them displayed increases in weight at their weekly weigh-ins, and were energetic and unhampered by the presence of the scaffold.

There was no visible inflammation on any of them, as well as an absence of other infection markers such as edematous swelling or pus at the incision site.

It is also important to observe tissue response for visible signs of foreign body reactions, and to assess the severity of these reactions. As such, after the subjects were euthanized, visual images (Table 5.1) were taken of the surgical area immediately upon removal of sutures and opening the incision.

Table 5.1 Visual depiction of the macroscopic tissue response to the implantation of various scaffold types, as well as the sham surgery control, upon termination at two different time points (two days and seven days)

	Day 2		Day 7	
Sham Control				
PC-PC				
PCP-OH				
PCP-NH_2				

In terms of the two-day study, overall results obtained showed little adverse reaction to the scaffold's presence. There was no visible edema, no fluid build-up or swelling, no excessive

bleeding or pus and no signs of visible internal inflammation. This was a common observation across all specimen types. There was, however, presence of a visible pocket wherein the scaffolds had been placed and this could have been attributed to the body's immune response to a foreign object.

The seven-day study yielded similar visible results with no visible edema or inflammation amongst the PCP-NH_2 and PCP-OH groups, but slight fluid build-up upon opening the incision site of those rats implanted with PC-PC scaffolds. As per the two-day study, there was a pocket visible, confirming the body's response to a foreign object.

Tissue samples were excised and subjected to immunohistological analysis in order to further quantify the immune response.

5.3.2.2.2 Immunohistological Results

The tissues that were immunohistologically analysed presented with varying results depending on the scaffold type, as well as the day the tissue was extracted. As the scaffolds were implanted in a living model, it is also useful to note that the wound healing process induces an inflammatory response and would expose the scaffold to the immune system. As such, we would expect to see neutrophils arrive at the incision site and within a few days, monocytes, macrophages and lymphocytes could be expected to arrive and facilitate a chronic inflammatory response. If the inflammatory process and the scaffold persist, multinucleated cells would invade as part of a foreign body reaction to form a fibrotic capsule around the scaffold.

5.3.2.2.3 Results Obtained from Tissue Extracted on Day Two after Surgical Implantation

The overall histological observation was that a central cavity (sometimes collapsed) can be observed visibly (the subcutaneous pocket made to house the scaffold). This cavity was analysed and contained fibrin, intact neutrophils as expected, and foreign material (scaffold). Neutrophils were also visible along the periphery of the cavity. The surrounding subcutaneous tissue

contained interstitially infiltrated inflammatory cells (a mixture of neutrophils, macrophages, lymphocytes and plasma cells). There was also varied infiltration of these cells into surrounding muscle bundles. The fibroblasts, together with the inflammation, extended variably along the peripheral septa between the adipose lobules. The table below elaborates on the degree of immune response at two-days post implantation according to the scaffold type.

Table 5.2 The varying immune responses at two-days post-implantation according to the scaffold type

	PCP-OH	**PCP-NH_2**	**PC-PC**
Central Exudate	Mostly severe	Moderate	Mostly severe
Granulomatous Inflammation	None	None	None
Mixed Interstitial Reaction	Moderate	Moderate	Moderate
Peripheral Septal Inflammation	Mild-Moderate	Mild	Mild
Stromal Reaction	Mild-Moderate	Mild	Mild
Muscle Infiltration	Mild	Mild	Mild

The images below (Figure 5.2) illustrate the *in vivo* immune responses to the implantation of the various scaffold type, as elaborated upon above.

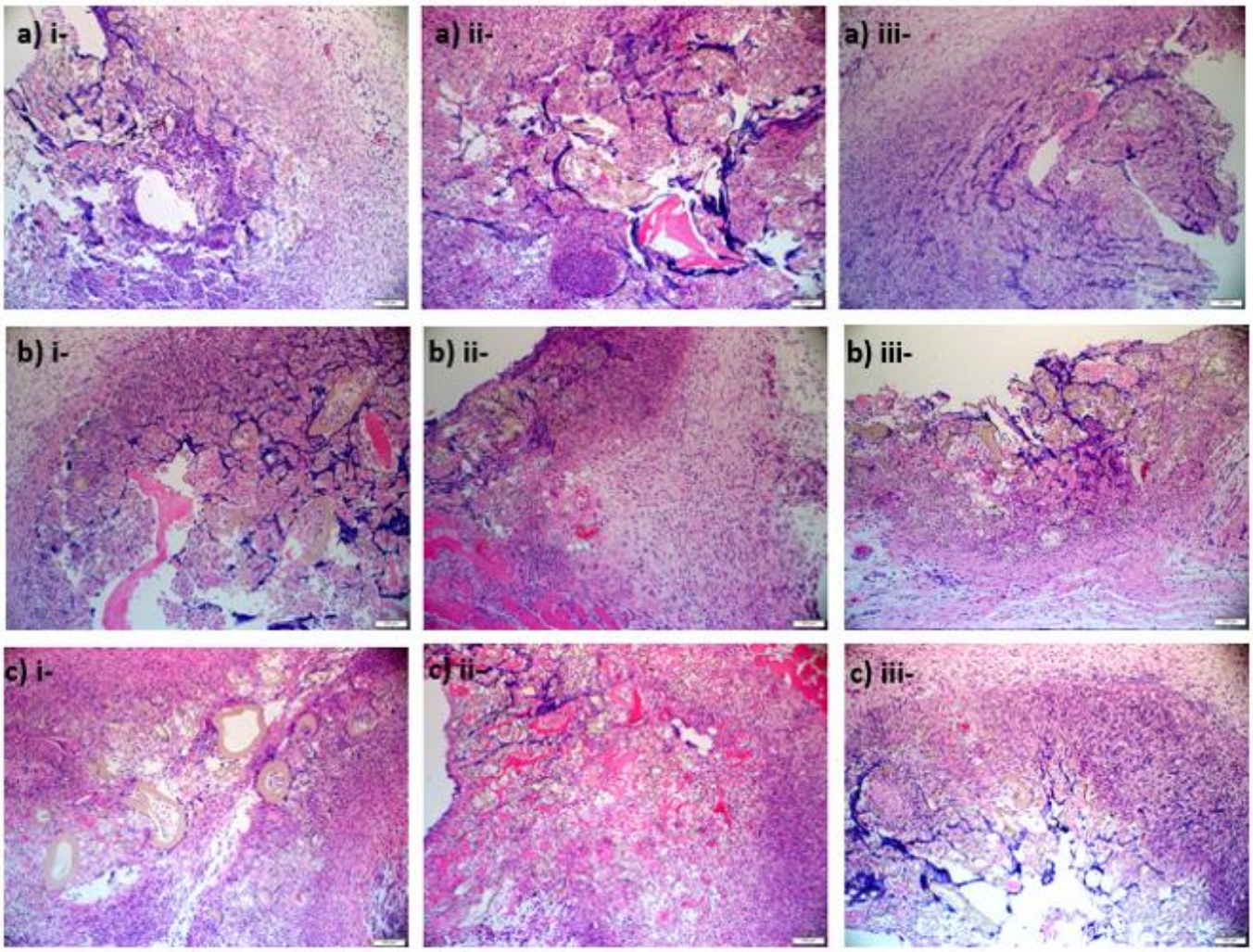


Figure 5.2 Immunohistological images showing the two-day immune response displayed during in vivo studies in response to implantation of various scaffold types a) (i-iii) PCP-OH, b) (i-iii) PCP-NH_2, c) (i-iii) PC-PC (magnification for all: x10)

As can be observed from the table and figures above, PCP-OH performed poorly in comparison to the other two scaffold types, eliciting a more severe immune response. However, the above immune responses are overall expected in relation to acute immune responses to foreign bodies.

Scaffold samples from PCP-NH_2 (Figure 5.3a) and PC-PC (Figure 5.3b) were also identified and removed for analysis. The scaffold for PC-PC was particularly well-maintained and the grid-like structure could be observed clearly, while PCP- NH_2 formed irregular fragments with some areas exhibiting a linear arrangement. Both PCP-NH_2 and PC-PC presented with fibrinopurulent

exudate, in varying degrees, which is consistent with the surrounding tissue response. The predominant component of the PCP-NH_2 exudate was observed to be neutrophils mostly intact, with a few degenerates, while in the PC-PC scaffold, fibrinous material was more prominent than neutrophils. There were no inflammatory markers for either scaffold type - with regards to the scaffold itself, but the tissue around the scaffold did exhibit a mild response, also consistent with the above results. There were also indications of mild neovascularization, with blood vessels showing interspersed connective tissue where some neutrophils, lymphocytes, plasma cells and macrophages are visible. No scaffold for PCP-OH could be recovered, leading to the conclusion that the hydrolytic process significantly affects the degradation rate of the scaffold *in vivo.*

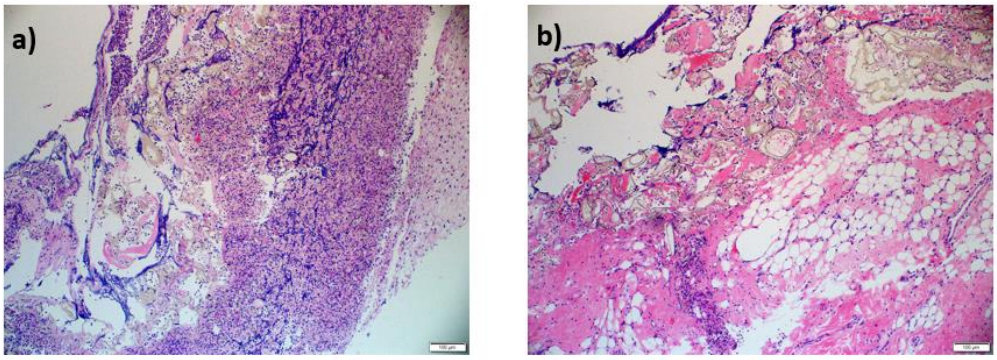


Figure 5.3 Images showing the immunohistological analysis of two scaffold types, after a two-day *in vivo* implantation period a) PCP-N H_2, b) PC-PC (magnification for both: x10)

5.3.2.2.4 Results Obtained from Tissue Extracted on Day Seven after Surgical Implantation

In the seven-day batch of samples, the lesions appear similar to those described in the two-day batch, but present with granulomatous inflammation in varying degrees which results in a thick reactive layer around the central cavity. This reaction consists of macrophages (most appearing epithelioid), as expected as part of the immune response, arranged around foreign scaffold material. There are also variable numbers of multinucleate giant cells, sometimes showing small phagocytosed foreign material fragments. Lymphoplasmacytic cells and neutrophils are scattered

throughout the reaction, mostly in small numbers. The table below elaborates on the degree of immune response at seven-days post implantation according to the scaffold type.

Table 5.3 The immune response at seven days elicited by the various scaffold types

	PCP-OH	**PCP-NH_2**	**PC-PC**
Central Exudate	Moderate	Mild- Moderate	Moderate
Granulomatous Inflammation	Moderate	Moderate	Severe
Mixed Interstitial Reaction	Mild	Mild	Mild
Peripheral Septal Inflammation	Mild	-	Mild
Stromal Reaction	Mild	Mild	Mild
Muscle Infiltration	Mild	Mild	Mild

The table above shows that PC-PC presents with the most severe granulomatous inflammatory response, possibly indicating chronic inflammation. Thus, it can be concluded that the chemical modifications may result in less chronic inflammation than the unmodified scaffold, and this implies improved biocompatibility.

The images below (Figure 5.4) illustrate the *in vivo* response to the implantation of each scaffold type, elaborated upon above.

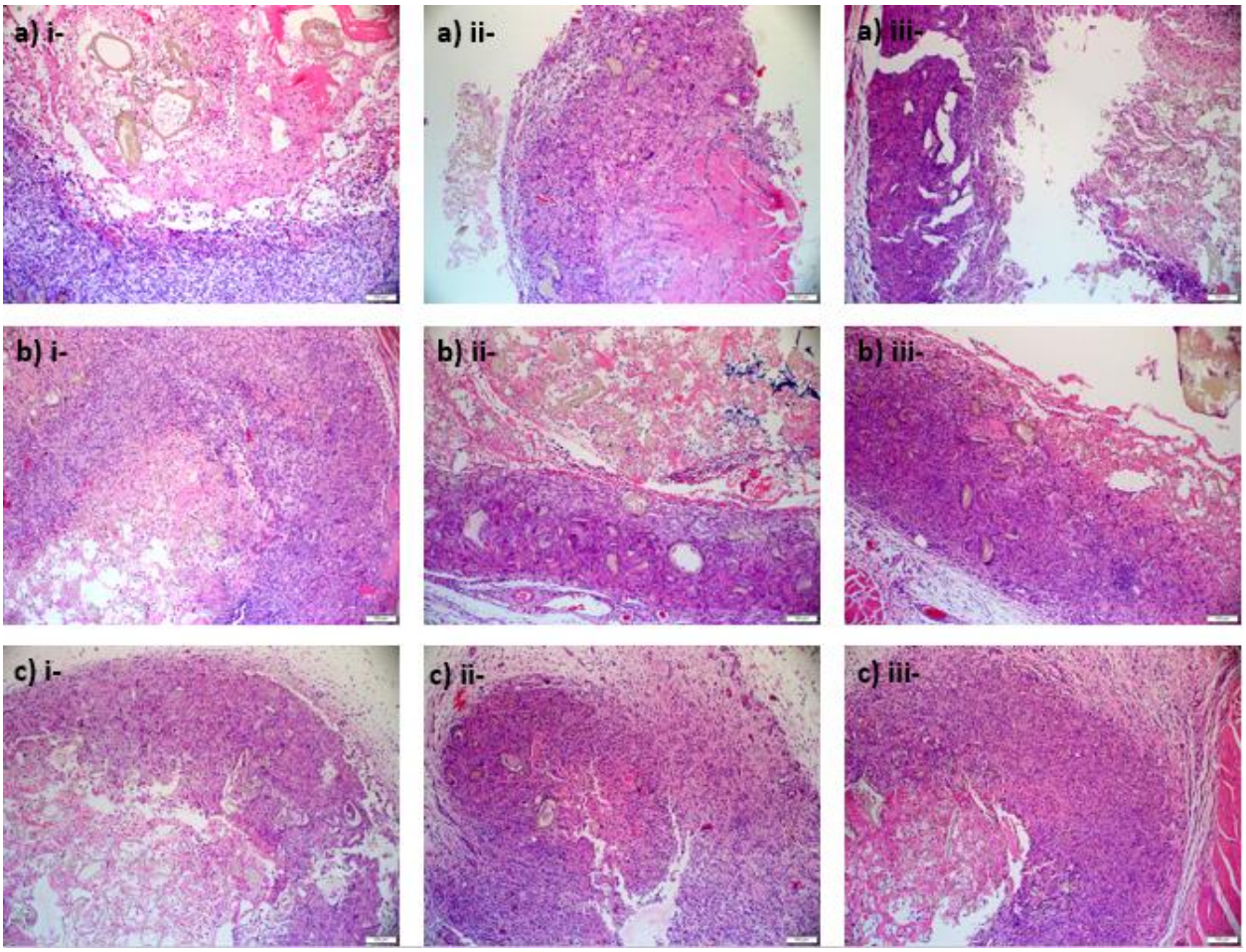


Figure 5.4 Immunohistological images showing the seven-day immune response displayed during *in vivo* studies in response to implantation of various scaffold types a) (i-iii) PCP-OH, b) (i-iii) PCP-NH_2, c) (i-iii) PC-PC (magnification for all: x10)

5.3.2.2.5 Discussion of Results from In Vivo Study

It is useful to use the tissues removed from the sham controls for comparison. The tissues removed as part of the sham control two-day batch (Figure 5.5) presented with no exudate and minimal inflammation, as expected from scaffold-free subjects, and presented with adipocytes, poorly cellularised attached fibrous connective tissue and a few mononuclear leukocytes which is considered normal post-surgery. The stromal connective tissue appeared mildly increased – a

chronic and reactive change – and the skeletal tissue also showed minimal changes consisting of interstitial fibroplasia causing minimal fiber degeneration.

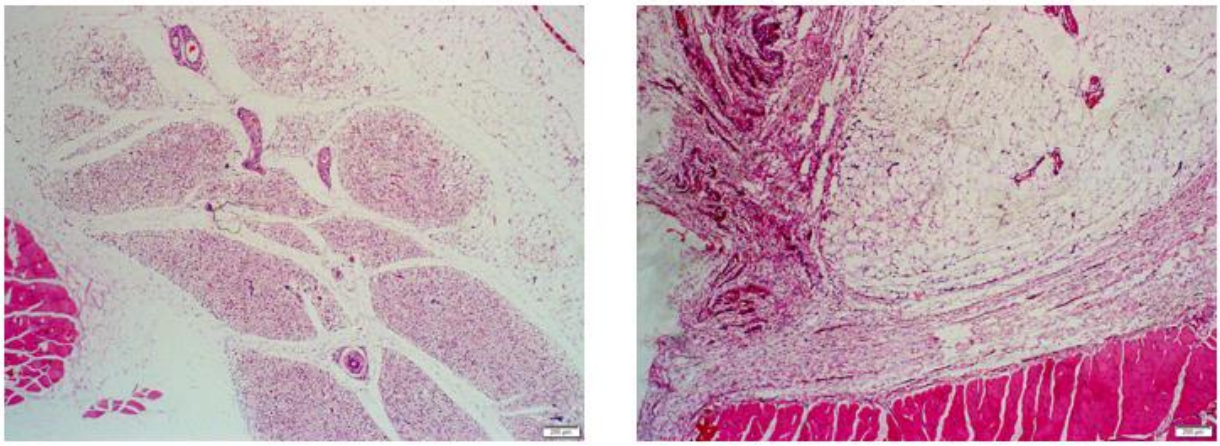


Figure 5.5 Immunohistological images showing the two-day immune response towards sham surgeries which were used as a control, wherein surgical interventions were conducted, but no scaffold was implanted (magnification: x4)

In the scaffold implantation two-day batch, the lesions presented as acute which could be due to surgical recovery. The central cavities themselves contain foreign material from the scaffold with exudate surrounding this material – implying that the scaffold is the reason for the exudate, which is an expected reaction as the scaffold is treated as a foreign body. As mentioned above, there are varying degrees of inflammation. However, the extension of the inflammatory reaction into surrounding tissues, along with the mesenchymal stromal reaction, is overall minimal to mild which indicates that the reason is localized to the area of implantation. This is advantageous in that the scaffold is treated as a foreign body with the immune system reacting as such, but none of the immune response spreads to the rest of the body indicating a localized reaction which can be controlled in future studies. The recovered scaffolds from this batch also presented with areas exhibiting mild neovascularization. In terms of sample superiority, PCP-NH_2 and PC-PC perform better than PCP-OH with regards to the amount of exudate surrounding the scaffold, implying that PCP-OH causes a more severe acute immune response than the other samples.

The tissue removed from the sham control seven-day batch (Figure 5.6) contained odd sites of neutrophils, but was otherwise considered to be relatively normal. Compared to the scaffold-containing tissues, it can be observed that the scaffold did trigger an immune response. This can, however, be considered a normal immune response to the presence of a foreign body.

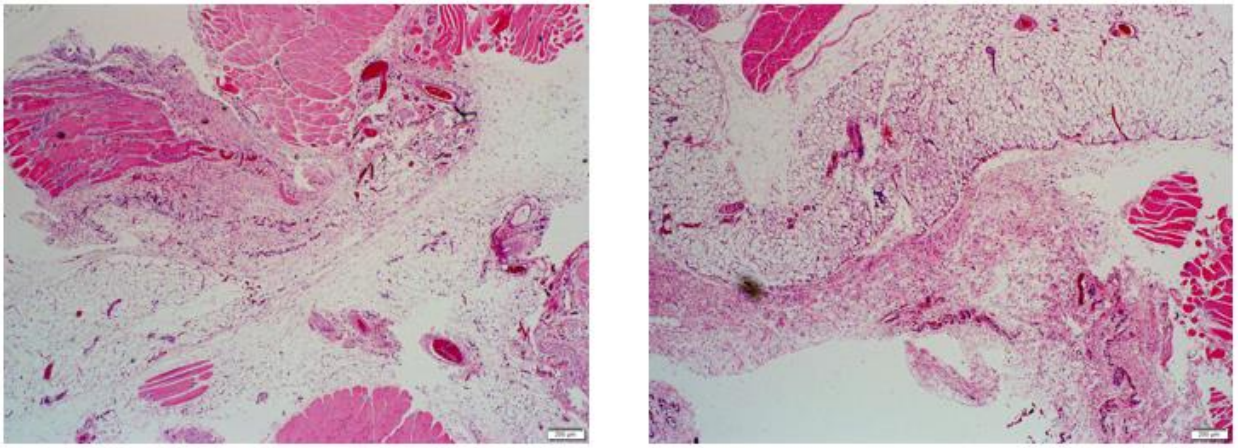


Figure 5.6 Immunohistological images showing the seven-day immune response towards sham surgeries which were used as a control, wherein surgical interventions were conducted, but no scaffold was implanted (magnification: x4)

In the scaffold implantation seven-day batch, the reaction appears to be more chronic, with inflammation still active in varying degrees as elaborated upon above. While the exudate is still present, there are less neutrophils present. Macrophages and multinucleate giant cells are however still predominantly present. As per the two-day batch, the surrounding interstitial inflammatory reaction does not extend to surrounding tissues and is concluded to be localized. The mesenchymal stromal reaction is similar to the two-day batch but is less associated with inflammation. In this group, the response to PCP-OH and PCP-NH_2 was far more desirable than the response to PC-PC which presented as moderate to severe in terms of exudate and inflammation. Thus, the overall response was a chronic, but localized immune response. It can also be noted that over the longer period of time, the chemically modified scaffolds presented with less of an immune response, possibly indicating higher biocompatibility.

5.4 Concluding Remarks

The *in vivo* studies were used to assess the biodegradation behaviour in an animal model, compared to the behaviour identified in *in vitro* studies. As explained above, the *in vivo* model was found to have a faster degradation rate, which could be attributed to a variety of causes including enzymes and oxidative factors, as well as characteristics of the animal model itself such as its activity level and subsequent metabolism, and most importantly – the immune response

All of the samples tested resulted in some form of immune response, which is expected, as elaborated upon above. However, it was useful to note that the chemical modifications used improved the biocompatibility and resulted in less severe immune responses. It would be useful, going forward, to focus on reducing the deleterious effects of the immune response, and to improve the biocompatibility, as well as the degradation behaviour.

References

Khorramirouz, R., Go, J. L., Noble, C., Jana, S., Maxson, E., Lerman, A. & Young, M. D. 2018. A novel surgical technique for a rat subcutaneous implantation of a tissue engineered scaffold. *Acta Histochem,* 120**,** 282-291.

Kumbhar, J. V., Jadhav, S. H., Bodas, D. S., Barhanpurkar-Naik, A., Wani, M. R., Paknikar, K. M. & Rajwade, J. M. 2017. In vitro and in vivo studies of a novel bacterial cellulose-based acellular bilayer nanocomposite scaffold for the repair of osteochondral defects. *International Journal Of Nanomedicine*, 12, 6437-6459.

Liebschner, M. A. K. 2004. Biomechanical considerations of animal models used in tissue engineering of bone. *Biomaterials,* 25**,** 1697-1714.

Lin, H. C., Lee, H. S., Chiueh, T. S., Lin, Y. C., Lin, H. A., Lin, Y. C., Cha, T. L. & Meng, E. 2015. Histopathological assessment of inflammation and expression of inflammatory markers in patients with ketamine-induced cystitis. *Molecular medicine reports,* 11**,** 2421-2428.

Modulevsky, D. J., Cuerrier, C. M. & Pelling, A. E. 2016. Biocompatibility of Subcutaneously Implanted Plant-Derived Cellulose Biomaterials. *PLoS One,* 11**,** e0157894.

Neethling, W. M., Glancy, R. & Hodge, A. J. 2010. Mitigation of calcification and cytotoxicity of a glutaraldehyde-preserved bovine pericardial matrix: improved biocompatibility after extended implantation in the subcutaneous rat model. *J Heart Valve Dis,* 19**,** 778-85.

Paul, W. E. 2013. *Fundamental immunology,* Philadelphia, Wolters Kluwer Health/Lippincott Williams & Wilkins.

Shrestha, R., Palat, A., Punnoose, A. & Paul, S. 2016. Electrospun cellulose acetate phthalate nanofibrous scaffolds for 3D culture of primary chondrocytes and neurons. Tissue Cell, 48(6):634-643

Standardization, I. O. F. 1997. *Dentistry: Preclinical Evaluation of Biocompatibility of Medical Devices Used in Dentistry (test Method for Dental Materials*, International Organization for Standardization.

Standardization, I. O. F. 2007. 10993-6: Biological evaluation of medical devices--Part 6: Tests for local effects after implantation. *Geneva, Switzerland: International Organization for Standardization*.

Sultana, N. & Khan, T. H. 2012. *In Vitro* Degradation of PHBV Scaffolds and nHA/PHBV Composite Scaffolds Containing Hydroxyapatite Nanoparticles for Bone Tissue Engineering. *Journal of Nanomaterials,* 2012**,** 12.

Sundaramurthi, D., Krishnan, U. M. & Sethuraman, S. 2013. Biocompatibility of poly(3-hydroxybutyrate-co-3-hydroxyvalerate) (PHBV) nanofibers for skin tissue engineering. *J Biomed Nanotechnol,* 9**,** 1383-92.

Tamariz, E. & Rios-Ramírez, A. 2013. Biodegradation of medical purpose polymeric materials and their impact on biocompatibility. *Biodegradation-Life of Science Croatia: Intech***,** 1-29.

Wang, Z., Wang, S., Marois, Y., Guidoin, R. & Zhang, Z. 2005. Evaluation of biodegradable synthetic scaffold coated on arterial prostheses implanted in rat subcutaneous tissue. *Biomaterials,* 26**,** 7387-7401.

Williams, S. F. & Martin, D. P. 2002. Applications of PHAs in medicine and pharmacy. *Biopolymers,* 4**,** 91-127.

CHAPTER 6

CONCLUSIONS AND RECOMMENDATIONS

6.1 Conclusions

The dynamic and rapidly advancing realm of tissue engineering has led to numerous innovations, the most recent and exciting of which is 3D bioprinting. The 3D bioprinting industry has revolutionized tissue engineering by integrating chemistry, biology, medicine and technology. It is at this intersection that we hope to be able to improve and expand on the success of tissue engineering. Unfortunately, we still face limitations with the concept of 3D bioprinting, owing to its recency. These limitations include technological limitations of printing equipment to handle tissue micro-architecture, as well as issues relating to cost, scaling-up of products, and a lack of available standards regarding tissue standards.

One of the biggest problems, however, relates to the limited available biomaterials for use in tissue engineering. Many biomaterials were not originally developed with 3D printing in mind, and as such, are not printable and do not exhibit shear-thinning behaviour. Oftentimes, materials also do not exhibit effective solidification mechanisms once printed, and this results in constructs that lack structural fidelity as well as resolution, which compromises the potential for tissue engineering. There are other issues relating to mechanical properties, bioactivity, degradation, cell compatibility, etc. And although there are ways to overcome these issues, ‘ideal’ properties have not been identified in a singular biomaterial for use in 3D bioprinting.

Furthermore, the body is a complex and dynamic system. Many efforts have been made to understand its complexities, but it is difficult to mimic. This is especially in the case of tissues that require angiogenesis, vasculature, heterogenous cellular development etc.

This dissertation therefore aimed to address the lack of available biomaterials which exhibit desirable properties by developing a conceptual method of chemically modifying 3D printed

constructs to induce or imbue characteristics different to those expressed by the native material, of which the focus was on mechanical properties. This would allow a singular material which possesses good printability to undergo printing, and thereafter undergo chemical modifications in order to present with desired mechanical properties. This was ascertained through the evaluation of two methods of chemical functionalization – namely aminolysis and hydrolysis. Aminolysis introduces an amine-functionality onto the surface, while hydrolysis introduces a hydroxyl.

The first component of this system was the development of a novel-combination bioink which was optimized and printed into the desired geometry. This was the culmination of exhaustive preliminary studies which identified appropriate polymers, methods, quantities and concentrations, and also sought to evaluate the effect of plasticizers on the system. Thereafter, the produced constructs (scaffolds) were subjected to the above-mentioned chemical functionalizations.

Extensive characterization observed the chemical transitions, thermal transitions, mechanical properties and *in vitro* degradation characteristics of native materials, as well as scaffolds prior and post- plasticizer, as well as scaffolds prior and post-chemical functionalization.

Subsequent to these characterizations, scaffolds were subjected to *in vivo* analysis in a rat model. The *in vivo* analysis assessed biodegradation behaviour which was observed to be much more rapid than the *in vitro* studies had shown. This could be attributed to a number of factors elaborated upon above, but would need to be researched further in order to improve clinical applicability. Results also indicated that the scaffolds caused localized inflammation in varying degrees, but that the chemically modified scaffolds caused less overall inflammation, thus it can be concluded that post-printing chemical modifications have shown to improve biocompatibility which is an essential characteristic of 3D bioprinted constructs.

In conclusion, the developed bioink was an effective novel combination bioink which was characterized for its response to plasticization, which had a positive effect on the scaffold properties. Thereafter, proposed chemical modifications ultimately proved that conceptually, desirable properties, including mechanical properties as well as biocompatibility, can be imbued or enhanced in scaffolds post-printing. This facilitates and encourages versatility and improved scaffold properties, independent of the native material properties, which allows for customizable and optimized scaffolds to be created post-printing, and also allows for a wider variety of tissue applicability.

6.2 Recommendations

The process of chemical modification is complicated and relies on many variables to evaluate and ensure its success. While the above study showed the qualitative success of the assessed chemical modifications through the use of FTIR, and focused on the effect of such modifications on the properties of the scaffold, more work should be done to elaborate on the purity of such obtained compounds, as well as how different degrees of chemical modifications could potentially affect the properties discussed in this work. Such a recommendation applies to the process of biomacromolecular attachment as well, the process and results of which should also be monitored and assessed using other methods of characterization and analysis, so as to elaborate on the chemical synthesis, and its results, in order to ensure success and enhance reproducibility.

Subsequent to the success of the developed formulation and its chemical modifications, it is recommended that further studies be undertaken for various other chemical modifications, so as to create a standard of functionalities that can be used to alter specific properties such as mechanical strength, hydrophilicity, degradation rate and porosity. Other forms of modifications can also be studied in order to enhance application, such as the attachment of drugs or peptides, which would be evaluated for their effect on the properties of the scaffold, but could also provide other functionalities.

As *in vivo* studies showed varying degrees of inflammation, with the lowest relating to specific chemical modifications, it is important that future research focus on elucidating the biocompatibility of the scaffold. It is also recommended that cell studies – including toxicity studies - be done in order to ascertain bioactivity, as well as the potential for toxicity, which could further quantify the biological effects of the novel bioink combination, as well as the potential for advancement in realm of post-printing chemical modifications. It would also be useful, as part of the *in vivo* study to identify and analyse the degradation products/metabolites, so as to ascertain the toxicity of these products on the animal model.

APPENDIX

STRICTLY CONFIDENTIAL

ANIMAL ETHICS SCREENING COMMITTEE (AESC)

CLEARANCE CERTIFICATE NO. 2018/09/44/B

APPLICANT: Ms A Parak

SCHOOL: Pharmacy
DEPARTMENT:
LOCATION:

PROJECT TITLE: Evaluation of the vivo biodegradability of 3-D printed biomaterial scaffolds in a rat model

Number and Species

68X 235-280g male Sprague-Dawley rats

Approval was given for the use of animals for the project described above at an AESC meeting held on 2018/09/25. This approval remains valid until 2021/01/15.
Unreported changes to the application may invalidate the clearance given by the AESC
An annual progress report must be provided

The use of these animals is subject to AESC guidelines for the use and care of animals, is limited to the procedures described in the application form and is subject to any additional conditions listed below:

The researcher requires a veterinary surgeon listed as a co-worker or as the responsible vet.

Signed: _____ (Chairperson, AESC) Date: 22/01/2019

I am satisfied that the persons listed in this application are competent to perform the procedures therein, in terms of Section 23 (1) (c) of the Veterinary and Para-Veterinary Professions Act (19 of 1982)

Signed: _____ (Registered Veterinarian) Date: 16 January 2019

cc: Supervisor: Prof V Pillay, Prof Y Choonara, Dr P Kumar and Prof L Dutoit
Director: CAS

Works 2000/lain0015/AESCCert.wps